UNIVERSIDADE FEDERAL DO CEARÁ
CENTRO DE CIÊNCIAS
PROGRAMA DE PÓS-GRADUAÇÃO EM QUÍMICA

WESLEY DOS SANTOS GALVÃO

SYNTHESIS OF NANOPARTICLES FOR BIOLOGICAL APPLICATIONS: DRUG DELIVERY AND KINETIC RESOLUTION OF DRUG PRECURSORS

FORTALEZA
2018

WESLEY DOS SANTOS GALVÃO

SYNTHESIS OF NANOPARTICLES FOR BIOLOGICAL APPLICATIONS: DRUG DELIVERY AND KINETIC RESOLUTION OF DRUG PRECURSORS

Tese de Doutorado apresentada ao Programa de Pós-graduação em Química da Universidade Federal do Ceará como requisito para obtensão do título de Doutor em Química. Área de concentração: Química Inorgância.

Orientador: Prof. Dr. Pierre Basílio Almeida Fechine.

FORTALEZA

2018

Dados Internacionais de Catalogação na Publicação
Universidade Federal do Ceará
Sistema de Bibliotecas
Gerada automaticamente pelo módulo Catalog, mediante os dados fornecidos pelo(a) autor(a)

G173s Galvão, Wesley dos Santos.
Synthesis of nanoparticles for biological applications : drug delivery and kinetic resolution of drug precursors / Wesley dos Santos Galvão. – 2018.
117 f. : il. color.

Tese (doutorado) – Universidade Federal do Ceará, Centro de Ciências, Programa de Pós-Graduação em Química, Fortaleza, 2018.
Orientação: Prof. Dr. Pierre Basílio Almeida Fechine.

1. Drug delivery. 2. Nanoparticles. 3. Enzyme immobilization. 4. Kinetic resolution. I. Título.
CDD 540

WESLEY DOS SANTOS GALVÃO

SYNTHESIS OF NANOPARTICLES FOR BIOLOGICAL APPLICATIONS: DRUG DELIVERY AND KINETIC RESOLUTION OF DRUG PRECURSORS

Tese apresentada ao Programa de Pós-Graduação em Química da Universidade Federal do Ceará, como requisito parcial à obtenção do título de Doutor em Química. Área de concentração: Química Inorgância.

Aprovada em: 06 / 12 / 2018.

BANCA EXAMINADORA

_____
Prof. Dr. Pierre Basilio Almeida Fechine (Orientador)
Universidade Federal do Ceará (UFC)

_____
Prof. Dr. Adonay Rodriguês Loiola
Universidade Federal do Ceará (UFC)

_____
Prof. Dr. Jeanlex Soares de Sousa
Universidade Estadual do Ceará (UFC)

_____
Prof. Dr. Josimar de Oliveira Eloy
Universidade Federal do Ceará (UFC)

_____
Prof. Dr. José Cleiton Sousa dos Santos
Universidade da Integração Internacional da Lusofonia Afro-Brasileira (Unilab)

To the glory of the Great Architect of the Universe.

ACKNOWLEDGMENTS

The recognition of this thesis is a tribute to all the people who made this academic journey of knowledge, advanced science, culture and wisdom. Firstly, I would like to express my sincere thanks to my Advisor Prof. Dr. Pierre Fechine for his friendship, advice, patience, motivation and for providing guidance and feedback during all this project. This endeavor would also not have been possible without the collaboration and guidance of my advisors in Germany, Prof. Dr. Med. Volker Mailander and Dr. Mark Bannwart. Thanks for all the help and support during the internship at the Max Planck Institute of Polymer Research in the city of Mainz, Germany, from March to October 2017. I can't help but thank my wonderful wife Marina Galvão for all her support and for being by my side during my time abroad, sacrificing her studies at the State University of Ceará (UECE).

I would also like to thank the following people, without whom I would not have been able to complete this research. To the professors Dr. Marcos Carlos de Matos, Dr. José Cleiton S. d. Santos, Luciana R.B Golçalves, Valder Nogueira Freire, Dr. José Marcos Sasaki, for all support and collaboration. My thanks to researchers Rayanne M. Bezerra and Nathalia S. Rios from Chemical engineering from Federal University of Ceará - UFC. My deepest thanks to my friend Civil Engineer Dr. Eduardo Façanha and the WhatsApp group “Doutorado Sanduíche Alemanha” for all their help during my studies in Germany.

Furthermore, I would like to thanks the Federal University of Ceará (UFC), the National Council for Scientific Development (CNPq) and the Max Planck Institute for all their help, collaboration and support.

Finally, I express my heartfelt gratitude to my friends who have been my pillars of strength and special to all the members of the Advanced Materials Chemistry Group – GQMAT. Thanks in particular to Dr. Rafael Freire, Dr. Davino Machado and Dr. Victor Moreira.

“Before you heal someone, ask if the person is willing to give up the things that made him sick” (Hippocrates).

ABSTRACT

This work aims the development new nanohybrids materials and used them for the first time to the kinetic resolution of secondary alcohols. The first nanobiocatalyst was composed by lipase from *Pseudomonas fluorescens* immobilized on superparamagnetic nanoparticles (SPMNPs). This system was used for the kinetic resolution of *rac*-indanol, rac-1-phenylethanol (*rac*-1), *rac*-1-(3-bromophenyl)-1-ethanol (*rac*-2), *rac*-1-(3-methylphenyl)-1-ethanol (*rac*-3) and rac-1-methyl-2-(2,6-dimethylphenoxy)ethyl acetate. The high thermal stability is mainly related to the covalent bonding between enzymes and support. Immobilized lipase on magnetic support proved to be a robust biocatalyst in the kinetic resolution, leading to (S)-indanol with high selectivity (*e.e*. > 99%, E > 200) in 1.75 h at 50 ºC, being reused five times without significant loss of the activity and selectivity. The kinetic resolution of *rac*-1, via acetylation reaction led to (R)-acetate with enantiomeric excess > 99% and to the remaining (S)-alcohol with enantiomeric excess of 94%, conversion of 49% and E > 200, after 48 h of reaction at 40 ºC. Under the same reactions conditions, *rac*-2 and *rac*-3 were slightly less reactive, since the corresponding (R)-acetates were obtained with conversion values of 44%, but with high enantioselectivity (*e.e*. > 99%, E > 200). The second biocatalyst was formed by lipases from *Thermomyces lanuginosus* (TLL) immobilized on different support. The biocatalyst was used for the kinetic resolution of *rac*-1-methyl-2-(2,6-dimethylphenoxy)ethyl, obtained 50%(maximum conversion) and the $e.e_p$ of 99%. Besides that, a second study was conducted in order to the development of styrene nanoparticles (STNPs) for the controlled drug delivery via folate receptor. Initially, studies were performed in order to synthesize STNPs via miniemulsion polymerization reaction using the polymer F127 as surfactant. The hydrophobic initiator V59 was introduced into the organic phase to prevent nucleation of hydrophilic monomers in the water phase. After that, In order to evaluate the FA influence on the uptake of STNPs in cells, folic acid (FA) was covalently linked to the F127 and the modified polymer (F127-FA) was used as surfactant during the polymerization reaction of styrene. In this case, five samples were prepared by increasing the percentage of F127-FA in the aqueous phase (ST@F127 – FA 0%, ST@F127 – FA 1 %, ST@F127 – FA 3 %, ST@F127 – FA 5 % and ST@F127 – FA 10 %). Cytotoxicity assays were conduct and no toxicity was founded for all the samples.

Keywords: drug delivery; nanoparticles; enzyme immobilization; kinetic resolution.

RESUMO

Este trabalho tem como objetivo o desenvolvimento de novos materiais nanohíbridos e seu uso pela primeira vez para a resolução cinética de álcoois secundários. O primeiro nanobiocatalisador foi composto por lipase de Pseudomonas fluorescens imobilizada em nanopartículas superparamagnéticas (SPMNPs). Este sistema foi usado para a resolução cinética do rac-indanol, rac-1-feniletanol (rac-1), rac-1-(3-bromofenil)-1-etanol (rac-2), rac-1-(3-metilfenil)-1-etanol (rac-3) e rac- 1-metil-2-(2,6-dimetilfenoxi)acetato de etila. A alta estabilidade térmica está relacionada principalmente à ligação covalente entre as enzimas e o suporte. A lipase imobilizada em suporte magnético mostrou-se um biocatalisador robusto na resolução cinética, levando ao (S)-indanol com alta seletividade (e.e. > 99%, E > 200) em 1,75 h à 50 ºC, sendo reutilizado cinco vezes sem perda significativa da atividade e seletividade. A resolução cinética do rac-1, via reação de acetilação, levou ao (R)-acetato com excesso enantiomérico > 99% e ao (S)-álcool restante com excesso enantiomérico de 94%, conversão de 49% e E > 200, após 48 h de reação à 40 ºC. Sob as mesmas condições de reação, rac-2 e rac-3 foram ligeiramente menos reativos, uma vez que os (R)-acetatos correspondentes foram obtidos com valores de conversão de 44%, mas com alta enantiosseletividade (e.e. > 99%, E > 200). O segundo biocatalisador foi formado por lipases de Thermomyces lanuginosus (TLL) imobilizadas em diferentes suportes. O biocatalisador foi usado para a resolução cinética de rac-1-metil-2-(2,6-dimetilfenoxi)etil, obteve 50% (conversão máxima) e e.ep. de 99%. Além disso, um segundo estudo foi conduzido para o desenvolvimento de nanopartículas de estireno (STNPs) para a administração controlada de fármacos via receptor de folato. Inicialmente, estudos foram realizados para sintetizar STNPs via reação de polimerização em miniemulsão, usando o polímero F127 como surfactante. O iniciador hidrofóbico V59 foi introduzido na fase orgânica para prevenir a nucleação de monômeros hidrofílicos na fase aquosa. Depois disso, para avaliar a influência do FA na captação de STNPs nas células, o ácido fólico (FA) foi covalentemente ligado ao F127 e o polímero modificado (F127-FA) foi usado como surfactante durante a reação de polimerização do estireno. Neste caso, cinco amostras foram preparadas aumentando a porcentagem de F127-FA na fase aquosa (ST@F127 – FA 0%, ST@F127 – FA 1%, ST@F127 – FA 3%, ST@F127 – FA 5% e ST@F127 – FA 10%). Ensaios de citotoxicidade foram conduzidos e nenhuma toxicidade foi encontrada para todas as amostras.

Palavras-chave: administração de medicamentos; nanopartículas; imobilização de enzimas; resolução cinética.

LIST OF FIGURES

LIST OF TABLES

LIST OF ABBREVIATIONS AND ACRONYMS

APTES	3-aminopropyl-triethoxisilane
DCI	Carbonyldiimidazole
CMC	Critical micelle concentration N,N'-
DCC	Dicyclohexylcarbodiimide
DMSO	Dimethylsulfoxide
DNA	Deoxyribonucleic acid
DKR	Dynamic kinetic resolution
DLS	Dynamic Light Scattering
E	Enantioselectivity
e.e.	Enantiomeric excess
EPC	Enantiomerically pure compounds
EPR	Enhanced permeability and retention Enzyme Enzyme
Enz	Triethylamine
Et3N	Folic acid
FA	Fluorescence activated cell sorter Food
FACS	and Drug Administration
FDR	Fourier transform infrared spectroscopy Glutaraldehyde
FT-IR	Glutaraldehyde
GLU	Gel Permeation Chromatography
GPC	Hexadecane
HD	International Centre for Diffraction Data
ICDD	International Union of Biochemistry and Molecular Biology
IUBMB	Kinetic resolution
KR	Moaminoxidase
MAO	Multidrug resistance
MDR	Nanoparticle
NP	Nuclear Magnetic Resonance N-
NMR	Hydroxysuccinimide
NHS	Poly(propylene oxide)
PPO	

PD	Parkinson's disease
PEI	Polyethylenimine
PEO	Poly(ethylene oxide)
pNPB	p-Nitrophenyl butyrate
PTX	Paclitaxel
Rac	Racemic
RNA	Ribonucleic acid
SEM	Scanning Electron Microscopy
SP	Polystyrene
SPM	Superparamagnetic
SPMNPs	Superparamagnetic nanoparticles
ST	Styrene
STNPs	Styrene nanoparticles
TGA	Thermogravimetric analyzes Thin
TLC TLL	Layer Chromatography
VSM	*Thermomyces lanuginosus*
V59	Vibrating Sample Magnetometer
U.K	2,20-azobis(2-methylbutyronitrile)
UV	Unit Kingdom
	Ultraviolet

SUMMARY

1 INTRODUCTION

1.1 Overview

According to ISO Technical Specification 80004, a nanoparticle (NP) is defined as a nano-object with all three external dimensions in the nanoscale, i.e, between 1 and 100 nm [1]. Nanoclusters for example, have at last one dimension in the nanometric size. Nanometer-sized single crystals, in turn, are generally refers as nanocrystals. The term nanoparticle is not applied to individual molecules, but is generally used to refer to a broad class of inorganic or organic particulate materials. NP synthesis and development have grown significantly over the last decade [2,3], due to the outstanding properties of these materials. When the size of a particle decreases until the nanometric dimension, the percentage of the surface in relation to the volume of a material becomes significant [4]. This large surface-ratio gives to the nanoparticles important biological applications by providing a wide area of contact of a drug in the body at the same concentration [4]. Furthermore, the nanometric size of the NP can facilitate its passage through the plasma and cells membranes, besides enabling the immobilization of biological structures such as antibodies, DNA, enzymes, drugs and viruses on its surface.

The NP can also present interesting and sometimes unexpected physio-chemical, optical or magnetic properties [13]. This not occurs with bulk material for example, that present constant properties regardless of its size. Because of that, the NPs are considered a bridge between bulk materials and atomic or molecular structures, with important applications in the scientific research [13].

The possibility of miniaturization of devices and materials has enabled the development of new products with high added value for food, paint, coatings, catalysts, information technology, pharmaceuticals and industry in general. At the nanoscale, the materials have higher physical properties such as mechanical, electrical, optical, temperature tolerance and chemical properties, such as high chemical and catalytic reactivity, due to the high surface area ratio.

Because they have dimensions in the order of biological structures such as hemoglobins and bacteria, the NP have also been widely used for biomedical purposes, making up one of the most promising areas of contemporary medicine called nanobiomedicine [67]. Among the medicinal applications of nanomaterials, its possible to mention the drug delivery [68,69], hyperthermia [70,71], nuclear magnetic resonance (NMR) images [72,73], biosensors and sensors for DNA detection (genosensers) [74,75]. As an example of nanomaterials for biological purposes, we can

mention: quantum dots [76], carbon nanotubes [77], gold nanoparticles [78] and nanoparticles of metallic oxides [70].

This thesis is divided in seven chapters and presents the results obtained for the synthesis of NP for biological applications. Chapters 1 and 4 are introductory and give depth to the research topics developed in this paper.

The first chapter introduces concepts such as enzymatic kinetic resolution and enzyme immobilization on magnetic nanoparticles. The second and third chapters bring the experimental results obtained for enzymatic kinetic resolution of drug precursors. The results were obtained using enzymes from *Pseudomonas fluorescens* immobilized on magnetic NP. This system was used for the first time to the kinetic resolution of *rac*-indanol, according general procedure showed in the figure 1.

Figure 1. General procedure for the kinetic resolution of *rac*-indanol.

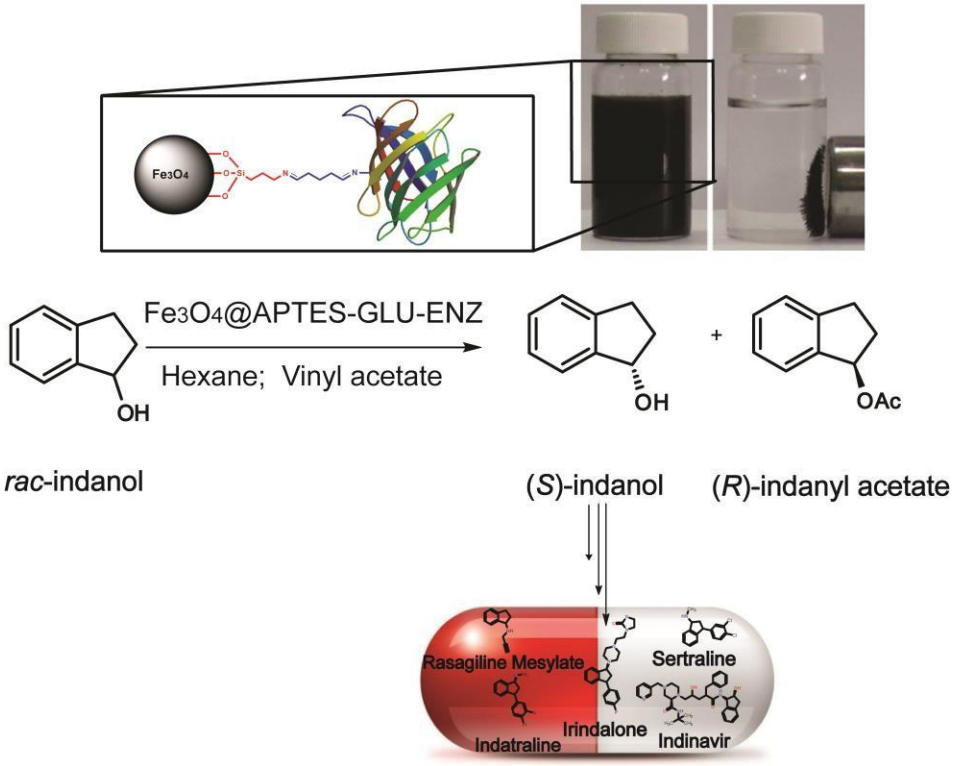

Source: Author

The fourth chapter introduces topics such as drug delivery for the treatment of cancer and the fifth chapter brings the experimental results. The results were obtained during the six months of exchange abroad to the Max Planck Institute of Polymer in Mainz – Germany. During the internship, it was sought the synthesis of a polymeric nanocarrier for hydrophobic cancer drugs. Finally, chapter

6 presents the general conclusions and perspectives for the works, ending with the bibliographical references in the chapter 7.

1.2 Enantiomeric pure compounds

Stereochemistry is a branch of chemistry that studies the spatial arrangement of atoms in a molecule, and this arrangement may interfere with the reactivity of the compound [1]. Bulky binders, for example, may difficult the contact of some groups with a given spatial orientation or generate attraction or repulsion, depending on the chemical environment to which it is inserted. In this sense, the stereochemistry can be used to estimate the stability of a compound and its physicochemical properties [2].

Molecules that are mirror images of each other and are not superposable, either by rotation or translation, are called enantiomers [3]. Most enantiomers have similar physical and chemical properties in an achiral environment, with the exception of plane rotation of polarized light. Enantiomers of the same compound deviate the plane of polarized light, in the same magnitude, but in opposite directions [4].

The first scientist to study the phenomenon of chirality was the French chemist Louis Pasteur in 1848 [5]. Pasteur was interested in the study of crystallography and began his work from the separation of the two isomers of sodium ammonium tartrate from wine by crystallization. The different salts obtained in the recrystallization had the same physical properties in the achiral environment, but deviated the planes of polarized light in opposite directions [5]. This fact led the researcher to consider asymmetry in all of nature. Today, it is known that all amino acids, proteins, carbohydrates, nucleosides, and a number of alkaloids and hormones are chiral compounds [6]. In this case, given the chiral nature of many living beings, its possible to predict that pairs of enantiomers should present different interactions with biological structures and thus, may present different biological properties.

Because of the chirality of cell receptors in the body, only one of the enantiomeric forms of a racemate can bind to a particular receptor site (chiral recognition). This means, that the pairs of enantiomers will bind to different receptors, and the biological result may be unpredictable. Figure 2 shows how the different interactions of enantiomers in the body occurs.

Figure 2. Different interaction of enantiomers in the body.

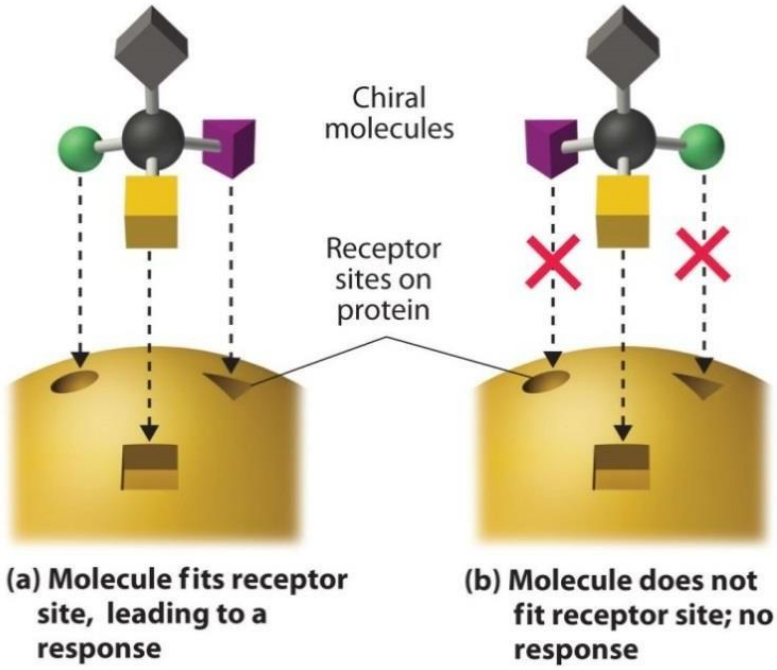

Source [7]

An enantiomer, for example, may have a therapeutic effect, while the other may be inactive or have a beneficial or undesirable side effect. In addition, one of the enantiomers may simply antagonize the action of its stereoisomers, negating any possible therapeutic action [8].

One of the most emblematic cases with respect to different properties of enantiomers in humans has been known as Thalidomide syndrome [9]. In the late 1950s, German industry developed a sedative and anxiolytic drug known as thalidomide, which consisted of the racemic mixture of the enantiomeric pairs of an active ingredient. The drug quickly became popular, being marketed in several countries and prescribed even to pregnant women. A few years after the beginning of its commercialization, numerous cases of congenital malformation in newborns were reported, reaching a mark of 12,000 cases at the end of 1962. Studies revealed that only one enantiomeric form of the thalidomide (R-isomer) had the desired pharmacological activity [9]. The (S) isomer, in this case, was responsible for the teratogenic effect (Fig. 3).

Figure 3. Enantiomers of Thalidomide.

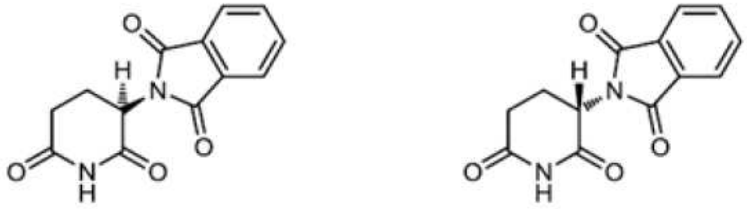

Source: Author

There are many other examples of enantiomers with adverse biological properties. Ketamine (S), for example, has an anesthetic effect, while its (R) isomer has a hallucinogenic effect [3]. Ethambutol (S, S), on the other hand, has been used for the treatment of tuberculosis, while the (R, R) isomer can cause blindness [10, 11]. Table 1 provides another examples of chiral compounds and effects related to their enantiomeric forms:

Table 1. Effects of enantiomers in the body.

Entry	Drug	Effect
1	Penicillin	Isomer S: Anti-arthritis. Isomer R: Extremely toxic.
2	Albuterol	*l*-Isomer is a bronchodilators used in the treatment of asthma. *d*- isomer is inactive [12]
3	L-DOPA	Isomer S: used in the treatment of parkinsonian syndromes. Isomer R: It is not metabolized in the liver and its accumulation can be harmful [10, 11].
4	Verapamil	The *l* -isomer is 20-30 times more active than the *d*-isomer [14, 15]
5	Hexobarbital	Hypnotics or sedative used in psychiatric treatment. *l*-Isomer is active whereas *d*-isomer is inactive [17]
6	Naproxen	Naproxen: (*S*)-(+)-naproxen act as analgesic and used to treat arthritis pain, but (*R*)-(–)-naproxen causes side effects such as liver poisoning [11].

7	Methadone	Analgesic for treatment of opiate dependence and cancer 8pain. *l*- Isomer is 25-50 times more potent than *d*-isomer [18].
8	Methorphan	l-methorphan is a active opioid analgesic, while d methorphan is suppress cough actively [11].
9	Propranolol	d-isomer reduces plasma concentrations of T3 cells and used to treat hyperthyroidism while l-isomer is β-blocking drug used as antihypertensive [18, 19].
10	Propoxyphene	d-Propoxyphene (Darvon) is painkiller, whereas the l-propoxyphene (Novrad) is a cough suppressant [17].
11	Bupivacaine	Local anaesthetic. l-Bupivacaine is less toxic than d-isomer [21]

In view of the foregoing, its possible to see how the production of enantiomerically pure compounds (EPC) are of extreme importance for pharmaceutical industries and, for this reason, much efforts have been devoted to the production of these products.

The production of (EPD) requires a great effort and planning for its execution. The main strategy for EPD production consists of the use of an optically pure compound as the starting reagent (chiral blocks) [22]. The choice of the starting compound should take into account the obtained product. In addition, it is important that the chiral block is not consumed during the synthesis process [22].

Chiral alcohols have stood out among the numerous chemical intermediates used in the synthesis of pharmaceutical, food and agricultural products. Beyond of the great versatility of this organic function, in many cases, the alcohols are present in the chemical structure of the desired product [22, 23]. For example, chiral 1-phenylethanol is an overusage chemical intermediate as ophthalmic preservative, solvatochromic dye, inhibitor of cholesterol absorption and a mild floral fragrance. The chiral alcohol 1-(2,6-dimethylphenoxy)propan-2- ol is a chemical intermediate for the to the formation of enantiomerically pure drug (R)- Mexiletine[(2R)-1-(2,6-dimethylphenoxy)propan-2-amine], an antiarrhythmic agent. The chiral indanol is another important chiral block which has a hydroxyl group capable of being transformed into an amino group, leading to key intermediates for production of drugs such as (+)-Indatraline, Irindalone, Indinavir, (+)-Sertraline and Rasagiline mesylate [24, 25].

Specifically, the last one is used as an active pharmaceutical ingredient for treatment of Parkinson's Disease [26, 27] (Fig.4).

Figure 4. Example of use of indanol for the synthesis of innumers pharmaceutical ingredients.

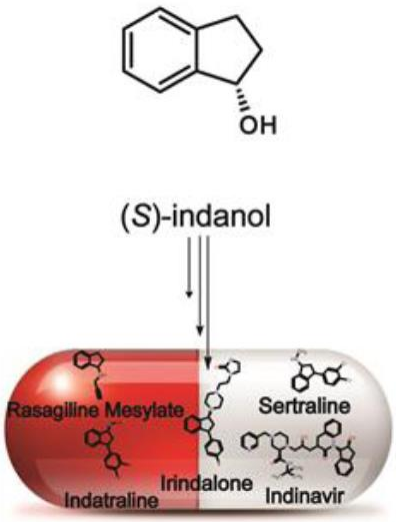

Source: Author

Parkinson's disease (PD) is a degenerative disease of dopaminergic motor neurons of the midbrain, where the cell bodies are located in the black substance of the brain. The black substance is formed by dark brain cells and it is responsible for the production of dopamine, a neurotransmitter responsible for the contraction and relaxation of the muscles [29]. Some authors have also described the loss of non-dopaminergic neurons such as serotonin and this fact may explain other symptoms related to Parkinson's disease such as the autonomic dysfunction and sleep abnormalities [29, 30]. In this way, the phases of PD can be categorized from the appearance of motor and non-motor symptoms. The initial or non-motor phase is characterized by olfactory problems, constipation, depression and rapid disturbance of ocular movements [32]. The motor phase is indicative of a progressive stage of the disease and presents as symptoms: resting tremor, rigidity or stiffness, bradykinesia, and postural instability. MAO-B inhibitors (moaminoxidase B) as the drugs selegiline and rasagiline mesylate have been used to treat the disease during the motor phase [33].

The possibility of synthesis of EPCs has made grow the drugs sales from these compounds, reaching USD 57.79 billion in 2019 and is predicted to reach USD 150.64 billion by 2030 with a compound annual grow rate at 9.1% from 2020-2030, [34, 35]. Figure 5 shows the ratio of chiral, achiral, and racemic mixtures approved by the FDA during the period from 2010 to 2020. The large difference between the quantity of pure components approved in relation to racemic mixtures is noticeable.

Figure 5. Percentage of approved new chemical entities worldwide.

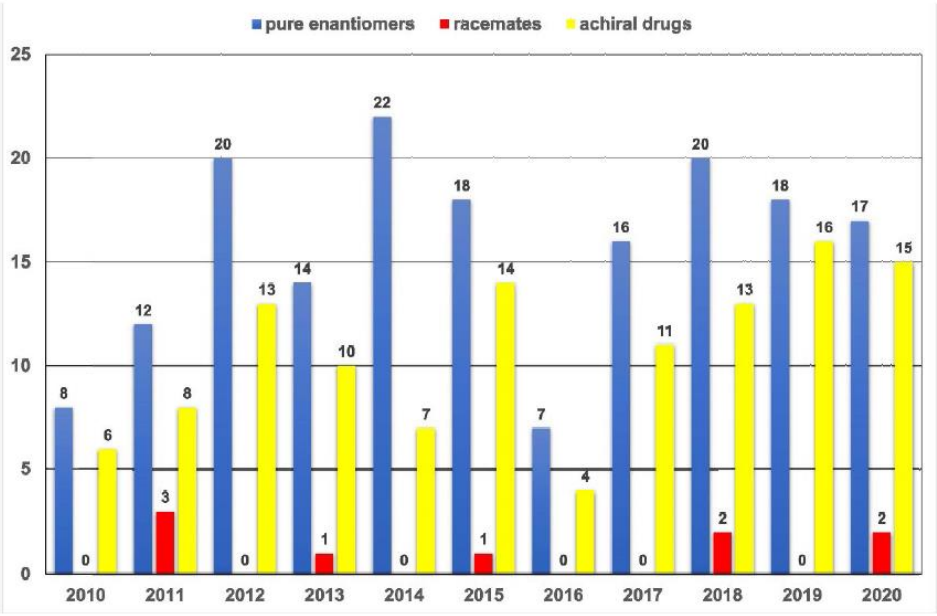

Source [36]

Despite the increasing effort to producion of EPCs, many drugs are still marketed in the form of racemates, and this is mainly due to the difficulty and high costs involved in the production of the pure drugs. To solve this problem, it is so important the development and improvement of techniques for the synthesis and separation of enantiomers [6].

1.3 Enzymes

The chemical reactions that occur inside of all cells should occur slowly due to their enormous complexity and the environment conditions (Temperature around 37 ºC and pH 7.4). However, this does not occur, and it leads us to imagine that cells must have some biocatalysts to accelerate the rate of the reactions. These efficient biocatalysts are called enzymes and can increase the rate of a reaction by a factor of 105 to 1017 times. The enzyme orotidine-5'-phosphate decarboxylase, for example, has reduced the reaction time from 78 million years to 25 milliseconds [37].

The modern history of enzymes began in the late 17th century, when the French chemists Anselme Payen and Jean-François Persoz isolated a substance capable of transforming starch in glucose [37, 38]. It was the first time that an enzyme had been isolated and, as the substance was able to separate the starch in its fundamental units, they called it "diastase" (from the Greek "to separate") [38, 39]. Already in century XIX, Louis Pasteur concluded that the transformation of the sugar in alcohol by the yeasts was realized by ferments [41]. According to him, this phenomenon was

due to the biological structures present in cells, not as a result of the decomposing matter, as the chemist Justus von Liebig believed. In 1897, the German chemists Eduard Buchner and Hans Buchner performed the alcoholic fermentation from an extract of cell-free yeasts [42]. Thereafter, it was discovered that the cells produced the enzymes and the enzymes performed the reactions.

Enzymes are solid organic substances, mostly of a protein nature, and formed by tens or thousands amino acid residues [43]. Enzymes are produced from instructions contained in the DNA in the nucleus of cells. The gene for enzyme synthesis is driven by mRNA to be translated into ribosomes, where protein synthesis occurs [43].

As the amino acid units bind to each other through peptide bonds, the amino acid strands formed are folded together so as to leave an open cavity (active site). The active site is a microenvironment with high electron and geometric specificity capable of forming the enzyme-substrate complex (Fig. 6). The high affinity of the enzymes for the transition state between the substrate and the product, leads to the decrease of the activation energy and consequent reduction of the reaction speed [43].

Figure 6. Biological process of enzyme action.

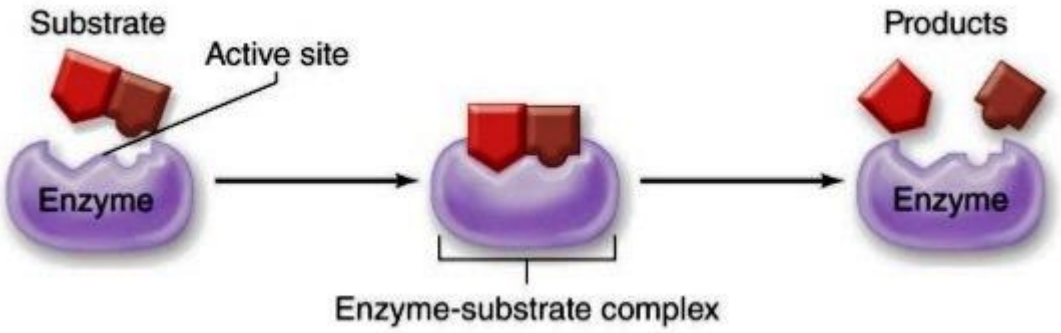

Source [43]

The speed of the enzymatic reactions depends on some factors such as: enzyme concentration and substrate, temperature and the pH of the reaction medium [44]. As enzymes have ionizable chemical groups in the side chains of their amino acids, a change in pH can cause a change in the electric charges, generating forces of attraction or repulsion that can alter the three-dimensional structure of the enzyme and result in the loss of its activity. The increase in temperature can cause breakage of the peptide bonds that hold the amino acid chains together, modifying its three-dimensional structure and the catalytic site, resulting in the loss of its enzymatic capacity [43].

Enzymes can be designated from common names, whose rule is divided, in most cases, in two forms. The first rule is the use of the suffix -ase to the name of the substrate on which the hydrolysis is performed [40]. For example, the enzyme that hydrolyzes urea is called urease; the amido, the amylase; phosphate esters, phosphatases, and so on. Others are designated by the type of catalytic action they perform, such as carbonic anhydrase; D-amino oxidase; lactate dehydrogenase. Some have common names such as trypsin and pepsin.

Knowing that all the chemical reactions that occur in the organism are catalyzed by enzymes, it is possible to imagine the amount of enzymes that exist in living beings [40]. For this reason, *the International Union of Biochemistry and Molecular Biology* (IUBMB) decided to divide them into six large groups depending on the type of reaction they catalyze [40]:

(1) Oxidoreductases (Oxidation and reduction: Transfer of electrons - hydride ions or H atoms).
(2) Transferases (Transfer of chemical groups).
(3) Hydrolases (promote breakage of bonds by the addition of water).
(4) Liases (Addition of functional groups to double bond or formation of double bond by removal of groups).
(5) Isomerases (internal rearrangement of atoms or isomerization).
(6) Ligases (junction of two or more molecules).

The six large groups represent the classes to which the enzymes belong. These groups can be further subdivided, progressively increasing the specificity. Thus, each enzyme receives an "E.C" classification number proposed by the Enzyme Commission of the IUBMB. This number is formed by 4 digits separated by dots (E.C W.X.Y.Z), which represent [40]:

(1) Class.
(2) Sub-class.
(3) Chemical groups that participate in the reaction.
(4) Specific for each enzyme.

The enzyme Glucose phosphotransferase for example, has the classification number E.C 2.7.1.1. That is:

(2) It is an enzyme that transfers groups.

(7) The group to be transferred is a phosphate.

(1) Transfers phosphate groups using a hydroxyl group as acceptor.

(1) Indicates D-glucose as the substance receiving the phosphate group.

Due to the high catalytic capacity, selectivity and efficiency, enzymes have been widely used in industrial catalytic processes. Because they are natural catalysts, they do not require the use of chemical compounds that can generate damages to the environment. The enzymes in this case, can be considered as an important option for the green chemistry.

1.4 Resolution of racemates and kinetic resolution

Chiral blocks for the production of enantiomerically pure drugs can be obtained directly from nature as amino acids and carbohydrates and are subsequently chemically modified by the transformation of their functional groups. It may also be obtained by asymmetric synthesis, wherein an achiral or prochiral center present in the molecule is transformed into an asymmetric center enantioselectively. A third way is through the resolution of racemates.

The resolution consists in the separation of enantiomers in a racemic mixture, from the difference in the reaction rate of one of the enantiomers with a chemical or enzymatic catalyst, or from the difference between the interaction of the substrate and a carrier. The main disadvantage of this technique is due to the maximum yield obtained of 50% [45]. In all cases, the choice of the catalyst needs to be evaluated. There are some methods available to perform the resolution of enantiomers, as in the use of chiral stationary phase chromatography. This method consists in the chromatographic separation of the racemate through its passage by a chiral support. As the enantiomers have different spatial arrangements, it is likely that one of the configurations has a greater or lesser affinity for the stationary phase of the chromatographic column. The difference in the affinity between the enantiomers and the support will result in different migration speeds.

Chemical catalysts are suitable for the kinetic resolution for adverse conditions such as high temperatures and pH control. Fajans and Bredig in 1908 [46], were pioneers in performing the decarboxylation of camphor-3-carboxylic acid performed with chiral alkaloids. Later in 1981 [47], Sharpless efficiently performed the separation of racemates from Ti $(OiPr)_4$ / tartrate ligand / tert-butylhydroperoxide as efficiently as possible. However, the use of chemical compounds has some disadvantage such as the use of toxic compounds and the necessity of process in several steps, resulting in high cost. Enzymes have high efficiency, they are environmentally correct and present

the main types of selectivity. In this sense, the enzymatic kinetic resolution has been the most used technique in industrial scale to obtain pure enantiomers in the last two decades [45].

The enzymatic kinetic resolution allows the separation of the enantiomeric pairs in a racemic mixture, but for this, it is needed that the constants of velocity of the reaction forn the conversion of the R and S isomers in the mixture are be different ($k_R \neq k_S$). If the rate of reaction of a given enzyme by the R-enantiomer is much higher than the S-enantiomer ($k_R >> k_S$), for example, only the first is converted to the product, obtaining the isomer S in 50% yield (Fig. 7).

Figure 7. Ideal kinetic resolution with $k_R >> k_S$.

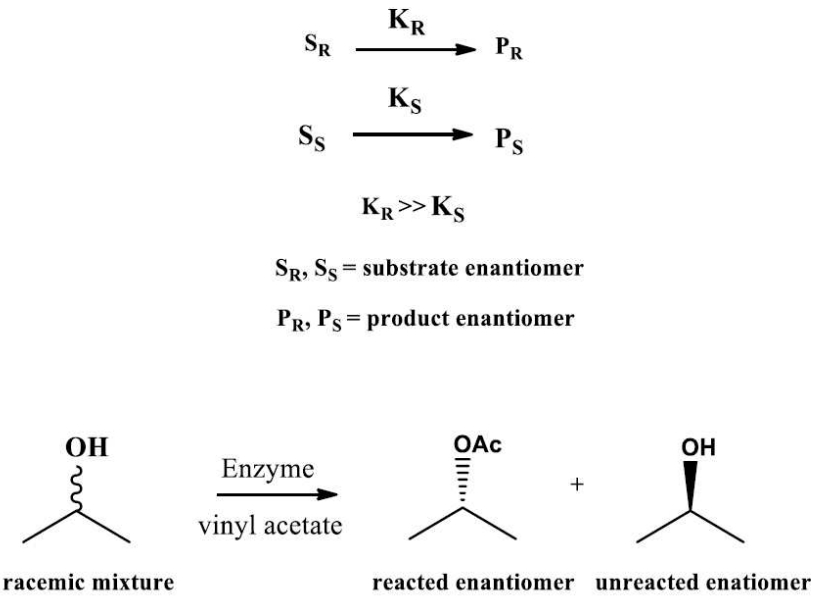

Source: Author

For a reaction to be catalyzed, the activation energy must be lowered to form the substrate-product transition state. Figure 8 demonstrates how the formation of the enzyme-substrate

complex promotes the decrease of the activation energy, resulting in the reduction of the reaction rate. "Enz" represents the enzyme, A and B are the enantiomers of a racemate to be solved, P and Q are the two possible products, $\Delta G \ddagger$ is the difference between the activation energy and [EnzA] ǂ and [EnzB] ǂ are the diastereoisomeric complexes.

Figure 8. Diagram of the energy variation of a biocatalyzed reaction.

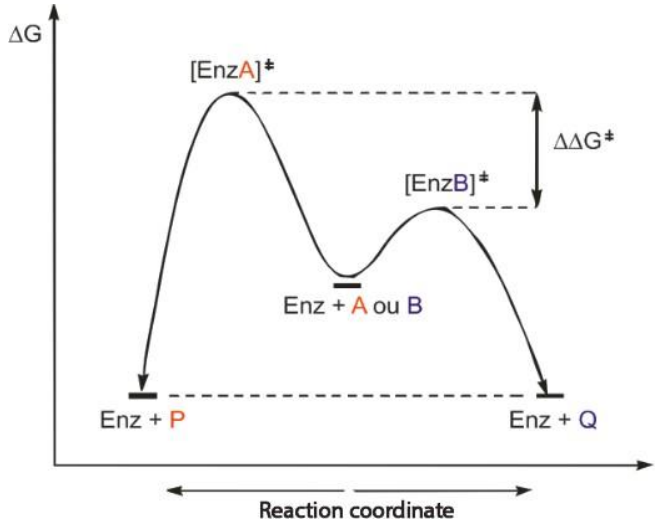

Source: Author

During the enzymatic kinetic resolution, the racemate enantiomers A and B may interact distinctly with the enzyme (Enz), to form the transition states [EnzA] ǂ and [EnzB] ǂ. The greater is the enantioselectivity (E) of the enzyme, the greater its ability to distinguish between the enantiomers pairs and the higher will be the difference between the free energy values of Gibbs (ΔG) the enzyme-substrate complexes of A and B. Figure 8 shows that the isomer B will react more quickly, because it has a smaller value of ΔG for the enzyme- substrate complex. In this case, the higher the difference between the free energy values of Gibbs (ΔG) for the enzyme-substrate complexes, the higher the difference in the reaction rate of the enantiomers [48].

Once the enzymatic kinetic resolution is complete with the total conversion of enantiomer B into product, its necessary that the reaction be interrupted to avoid that the enzyme also converses the other enantiomer. The reaction will reach the maximum conversion of 50%, with only one substrate being transformed into product. The conversion time for reaction interruption can be obtained from the retention times of each substrate and products, previously synthesized. Finally, the separation of the compounds in the mixture will become easier, given the difference between the chemical functions of the substrate and the product formed. During the enantioselective oxidation of alcohols, for example, occurs the formation of a ketone and an alcohol which can be easily separated through a chromatographic column.

The preference of an enzyme for a given substrate is expressed by the enantioselectivity (E) [49]. The value of E is calculated from one of three experimental tests: 1) enantiomeric excess (e.e) of the unreacted substrate [e.e (S)]; 2) e.e of the product [e.e (P)]; 3) conversion by the reaction. To

evaluate the enantioselectivity of a reaction (E), it is generally used the excess enantiomeric of the product ($e.e_p$). However, when using a racemic substrate, the enantiomeric excess of the product, as well as that of the substrate, change depending on the conversion (c). Logarithmic calculations are used for $e.e_s$ and conversion values obtained from experiments and even small conversion values generate a large error. Because of that, it is used values of E values above 200 [50].

1.5 Lipases

Lipases belong to a class of hydrolases (triacylglycerol hydrolases, E.C. 3.1.1.3) and they are the most used enzymes either in industrial or in research laboratories. This class of enzymes has been used for the preparation and resolution of chiral alcohols, carboxylic acids and esters through the hydrolysis reaction. The fact is that lipases accept a wide variety of different substrates, with high regio-, chemo- and enantioselectivities [33, 34]. Lipases can catalyze various reactions of industrial interest such as alcoholysis, esterification, transesterification, interesterification, hydrolysis of esters [35, 36]. In addition, lipases are quite resistant in various reaction media, e.g. organic solvents, ionic liquids or supercritical fluids [55] . The high stability of the lipases in organic solvents makes this class of enzymes prominent in industrial biocatalyze, considering that many of the substrates used are organic compounds insoluble in water. Besides that, lipases have a specific catalytic mechanism, so-called interfacial activation, with a lid covering the active center in homogenous medium (closed form) in equilibrium with a form where the active center is exposed to the medium (open form) [38, 39].

Lipases have at their catalytic site three amino acid residues specially developed for the hydrolysis of triacylglycerols, the corresponding fatty acids and glycerol. These residues are formed by serine, histidine and aspartic acid, which together make up the catalytic triad of the enzyme [58, 59]. There are two main methodologies for kinetic resolution of racemates using lipases: Transesterification of alcohols in the presence of an acyl donor (non-aqueous medium) and hydrolysis of esters (aqueous medium).

In the first case, the spatial arrangement of the catalytic triad facilitates the stabilization of the hydroxyl of the serine, making possible the nucleophilic attack of carbonyl ester from vinyl ester, which will act with an acyl donor [58, 59] (Fig. 9).

Figure 9. First stage of transesterification reaction of alcohols in the catalytic site of lipase.

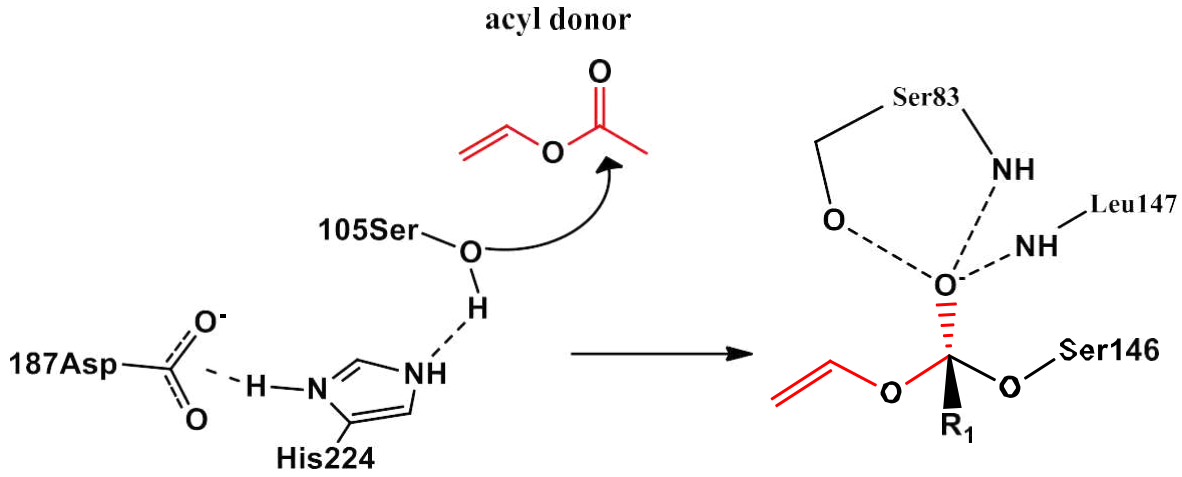

Source: Author

The negative charge generated on the oxygen after the nucleophilic attack is stabilized from the hydrogen bonds present in residues Ser83 and Leu147. In a second moment, the electron pair of the oxygen will restore the double bond, while the oxygen of the acyl group captures the hydrogen of the histidine residue, resulting in the output of the enol group and the formation of the intermediate acyl enzyme (Fig. 10). The enol group formed in the process is readily tantalized to the corresponding aldehyde (acetaldehyde), which is more stable and volatile. This strategy is important so that there is no competition with the substrate, which is also alcohol.

Figure 10. Second stage of transesterification reaction of alcohols in the catalytic site of lipase. Source: Author

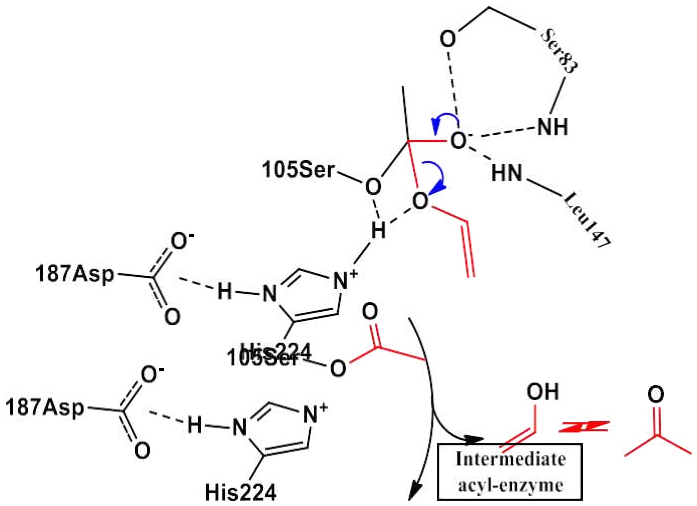

Finally, the acyl-enzyme intermediate receives the nucleophilic attack of one of the enantiomers of the alcohol present in the racemic mixture, resulting in the formation of the acetylated product (Fig. 11). The (R)-Indanol is been used as example.

Figure 11. Third stage of transesterification reaction of alcohols in the catalytic site of lipase.

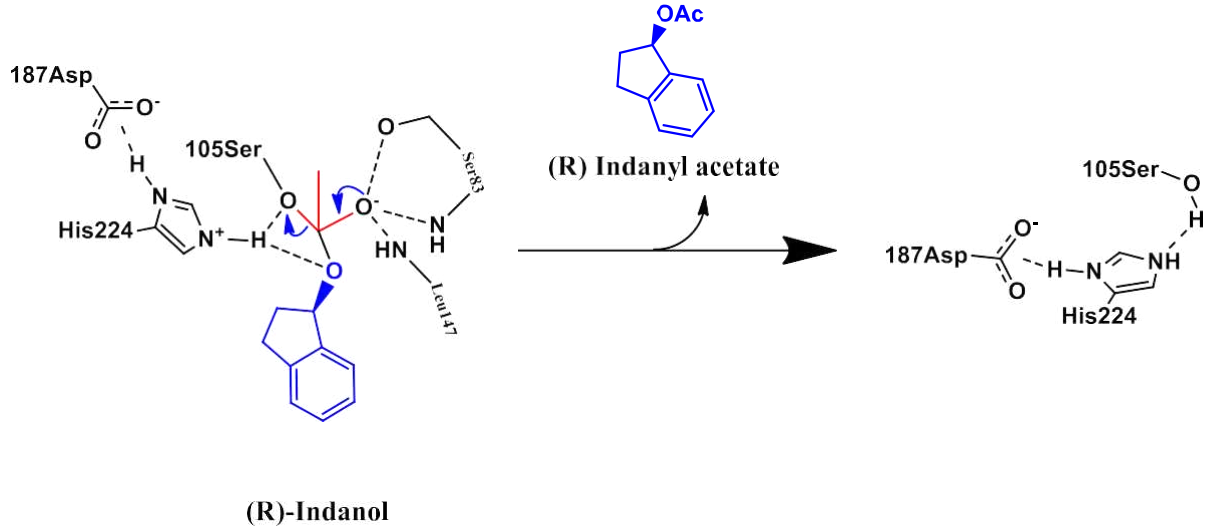

Source: Author

A disadvantage of this process consists in the need for high concentrations of acylating agent so that the reaction achieves a high conversion (c). In addition, high concentration of the acyl donating agent may lead to the formation of side products which may influence the reaction, or even interfere with the separation of substrates.

From the understanding of the mechanism of action of the catalytic triad of lipase in organic solvents, it is now easy to understand its action in aqueous medium. In this second case, the hydroxyl group of the serine residue starts to attack the carbonyl of the ester. The formation of the double bond will allow this time the exit of alcohol. It is possible to observe that, in the absence of water, it has a reversible process, with the transesterification of alcohol to ester formation (Fig. 12)

Figure 12. General scheme for the hydrolysis of esters in the catalytic site of lipase.

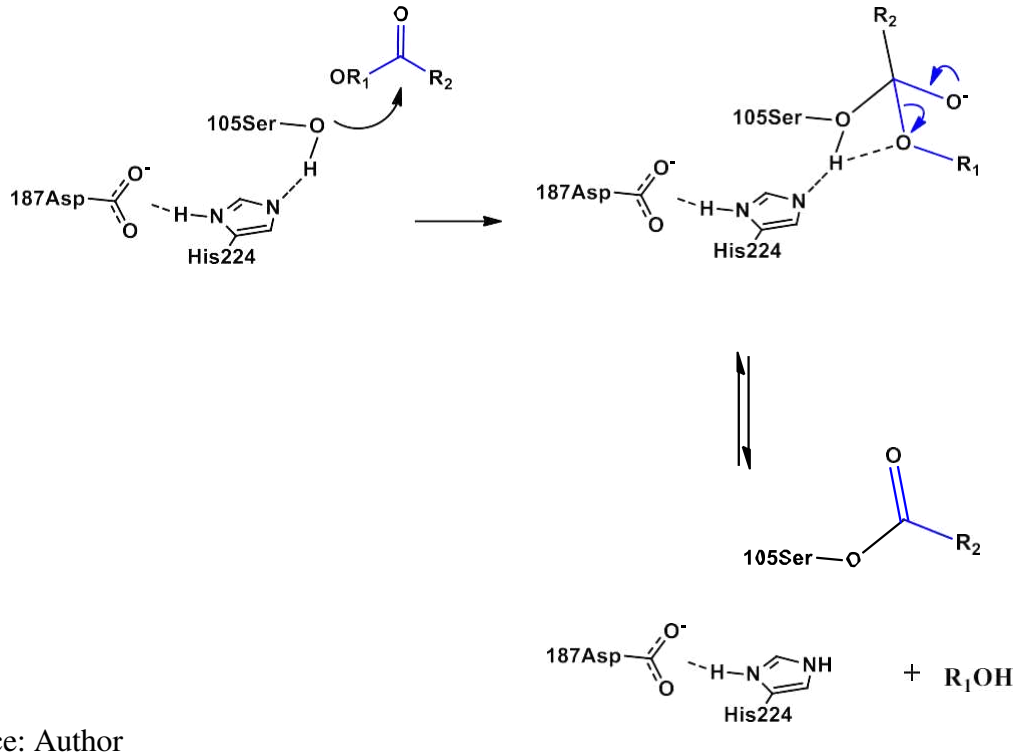

Source: Author

There is still one last question to elucidate the transesterification and hydrolysis mechanism performed by lipase, that is, which of the enantiomers in the racemate will have preference in the reaction with the enzyme.

Many enzymes have high selectivity, and this means that only one of the enantiomers in a racemic mixture may be the substrate of the enzyme. Chymotrypsin, for example, incorporates L-peptides only at the enzyme-substrate binding site to form enzyme-substrate complex [49]. Lipases and stereases, in turn, have a lack chiral recognition and both enantiomers may be incorporated into the enzyme to form the enzyme-substrate complex. In the case of secondary alcohols, one of the most accepted empirical rules for the preference by the enzyme and for the substrate was described by Kazlauskas [60]. According to the author, the preference for one of the enantiomers is due to better accommodation of the substrate molecule in the pockets of the active site of the enzyme (Fig. 13).

Figure 13. Accommodation of the substrate molecule according Kazlauskas.

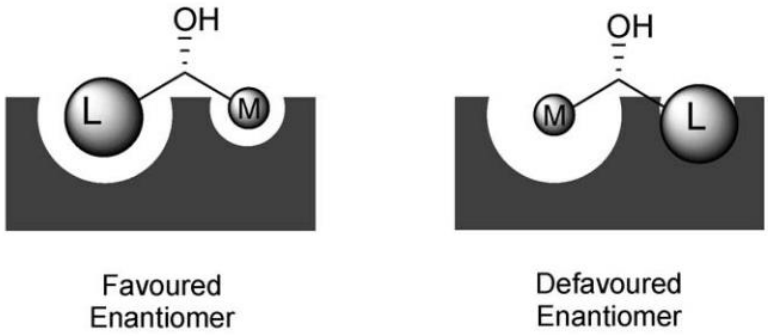

Source [61]

The molecule that presents the best orientation of its groups, so as to present better accommodation to the active center of the enzyme, will react more quickly. Kazlauskas performed a study of enantioselectivity of lipases in ester hydrolysis reactions [60]. Figure 14 summarizes the results obtained in his empirical works.

Figure 14. General scheme for the hydrolysis and transesterification reaction according Kazlauskas.

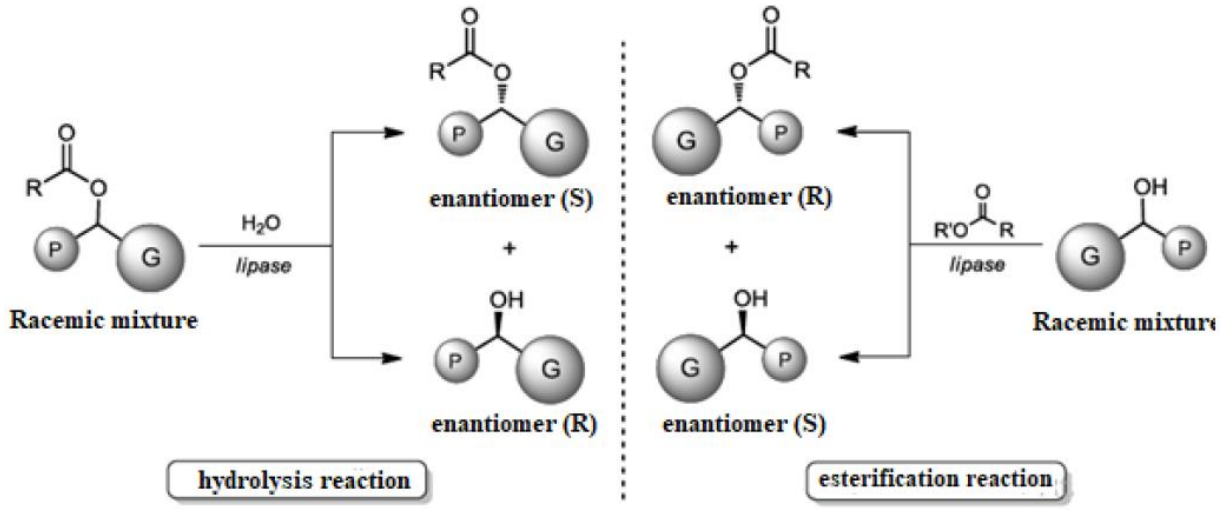

Source [62].

Despite all these advantages, the enzymes may have some drawbacks for industrial catalyst, such as its poor stability and their high solubility in aqueous solutions that makes difficult the enzyme recovering and reuse [63]. An effective approach to circumvent these problems is to conduct an appropriate enzyme immobilization strategy.

The enzyme immobilization on supports provides a series of catalytic advantages compared with the free enzyme [64], such as convenient procedures for the separation of medium, the possibility of reuse, increase in the thermal mechanical resistance, improvement of the catalytic efficiency, decrease in the limitation of substrate and product diffusion [64]. These set of factors may provide remarkable cost-benefit ratio for the industrial use of immobilized enzyme [28]. Moreover, the enzyme immobilization via covalent bonding has been proved to be more effective, leading to a more stable biocatalyst [65]. De Souza et al. used lipase B from *Candida antarctica* expressed in *Aspergillus niger*, covalently immobilized on cashew apple bagasse to evaluate the chemoenzymatic synthesis of (*R*)-indanol [66]. According to the authors, the nanohybrid system led to conversion values of 50% and e.e. > 99%. Souza et al. also promoted the enzymatic kinetic resolution of racemic indanol in the presence of lipase from *Thermomyces lanuginosus* covalently immobilized on immobead-150 [66]. The authors evaluated the reaction in different organic solvents, obtaining the best results using hexane.

1.6 Ferrites

Some metal oxides have been prominent among the nanomaterials due to the possibility of being attracted by an external magnetic field, allowing their vectorization to a specific target. An example of these materials are the ferrites [34], a ceramic material which have attracted many attentions due to their nanometric size, physic stability and magnetic properties [79]. According to its crystal structure and magnetic properties, ferrites are classified as spinel ($REFe_2O_4$, where RE = Mn, Fe, Co, Ni, Co, Zn.), garnet ($RE_3Fe_5O_{12}$, where RE = rare earth cations), hexaferrite ($SrFe_{12}O_{19}$ and $BaFe_{12}O_{19}$) and orthoferrite ($REFeO_3$, RE = rare earth cations) [79]. The chemical formulation of spinel ferrite can be represented by MB_2O_4, where A and B represent octahedral and tetrahedral sites respectively. Oxygen atoms is divided between the both sites, while Fe^{+3} atoms occupy a preferential position. Depending on the position of the M^{+2} and Fe^{+3} cations in the structure, the ferrites can be classified as normal type, inverse spinel or mixed [79]. In the normal type, the tetrahedral sites are occupied by cations + 2, whereas the cations of Fe^{+3} occupy the octahedral sites [79]. The $ZnFe_2O_4$ ferrite is an example of normal spinel ferrite. The inverse ferrite in turn, the cations Fe^{+3} are equally distributed in the both sites, while the M^{+2} occupies the octahedral sites. Fe_3O_4 and $NiFe_2O_4$ are common examples for inverse spinel ferrite. Mixed ferrites are formed by the randomly occupation of both sites by the cations with different oxidation state. $MnFe_2O_4$ is a typical example of mixed spinel ferrite [79].

The spinel structure was determined through independent works of Bragg and Nishikawa in 1915 [80]. The crystalline arrangement of the spinel ferrites is presented in the Figure 15.

Figure 15. Schematic representation of spinel ferrite structure.

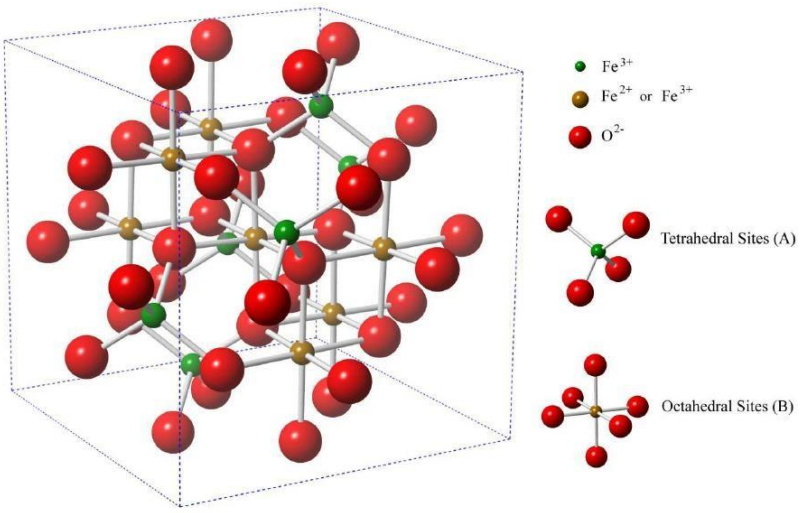

Source [79].

The magnetism of ferrites is due to the arrangement of the atoms in the unitary cell. In the spinel, for example, the electron spins of the Fe^{+3} ions in octahedral interstices are aligned antiparallel to those in tetrahedral interstices and thus, no net magnetization is observed from these ions [67]. Fe^{2+} ions, in turn, tend to align their spins parallel to the Fe^{+3} ions at adjacent octahedral sites, leading to liquid magnetization. This arrangement of antiparallel spins throughout the solid that do not completely cancel out is called ferrimagnetism [67].

An important magnetic property of ferrites for biological application is the superparamagnetism (SPM). It is called SPM, the presence of magnetism in a material only when it is subjected on the external magnetic field, ceasing its effects, as soon as the field is withdrawn.

The phenomenon of SPM can be demonstrated and quantified from the magnetization curve of the material obtained by the equipment called Vibrating Sample Magnetometer (VSM). In this equipment, a small mass of material is placed on the end of a non-magnetizable horn and placed to vibrate between two powerful magnets (Fig. 16).

Figure 16. Sample during the measurement of its magnetization.

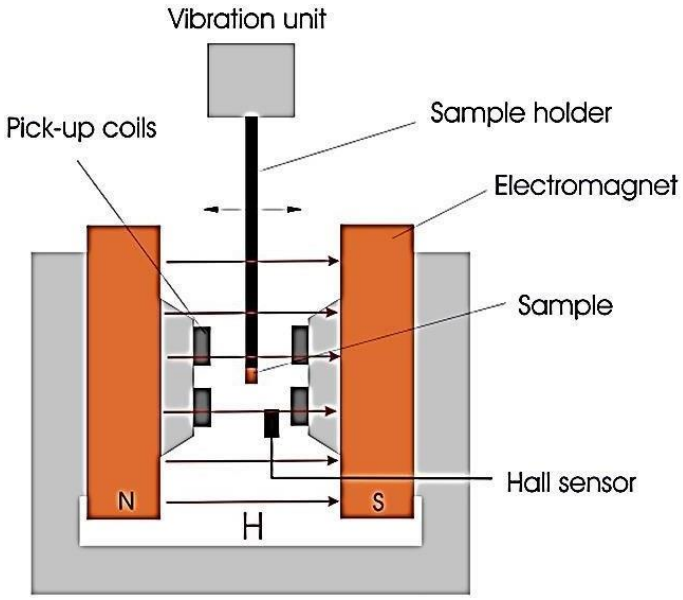

Source [81]

Initially, there is no passage of electric current in the coils and the sample vibrates without the presence of an external magnetic field. It is possible to observe that when the magnetic field

(H) is zero the sample magnetism is also zero (Fig. 16B). As a magnetic field is introduced onto the sample, the spins in the monodomain align it selves in favor or against the field, in an attempt to create a magnetic field of its own that will cease the external magnetism, in accordance with the principle of conservation of energy. To understand this process, initially, its needed to understand the concept of a monodomain. When a magnetic material is formed by regions where the electrons of a neighborhood behave in a similar way, we say that the material presents a magnetic domain. When a ferrite is in the nanometric dimension and below of the critical size, its electrons behave as if they were all belonging to a single domain (magnetic monodomain) (Fig. 17A).

Figure 17. Magnetic curve of SPM ferrite.

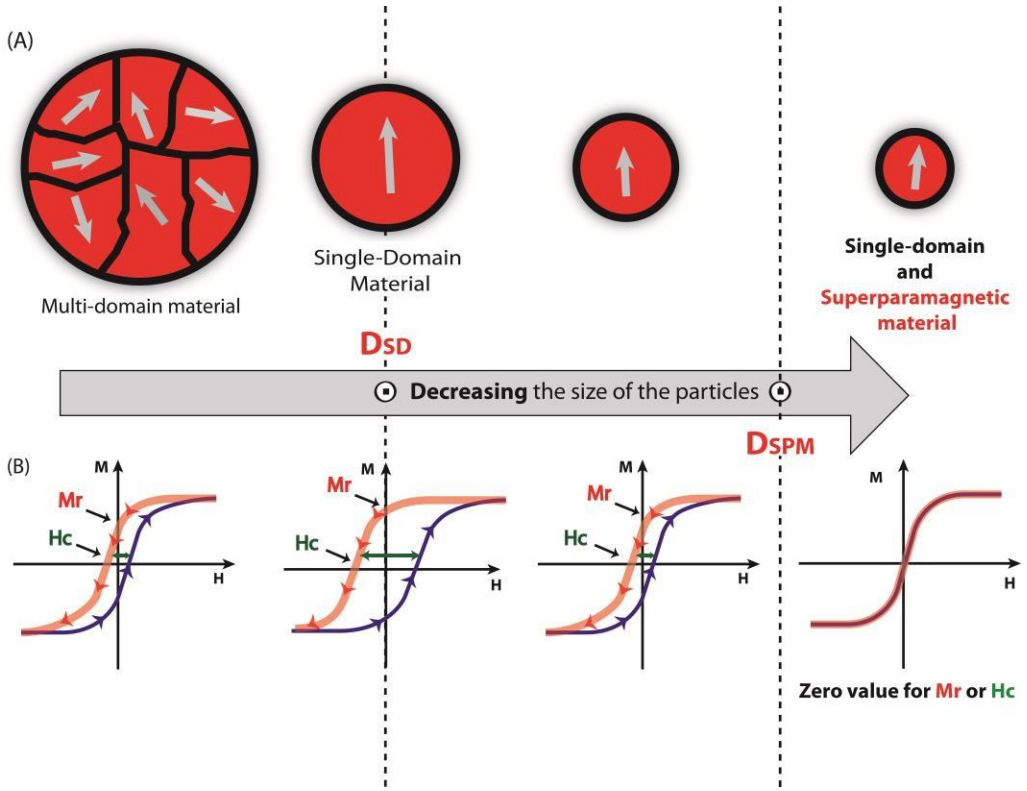

Source [67]

The decrease of the external magnetic field due to the alignment of the spins of the material is recorded and computed as sample magnetism. The external magnetic field gradually increases, followed by the aligning the spins until all the spins in the material are aligned. At this time, the slope of the magnetization curve reaches its maximum value and we obtain the magnetization of saturation of the material. After that, the magnetic field is automatically and gradually inverted, forcing the alignment of the spins in the opposite direction. However, in order for the spin to be inverted, there is a magnetic anisotropy barrier that needs to be overcome. This energy barrier is given by the equation of relaxation time (equation 1).

$$\tau = \tau_o \exp\left(\frac{\mathrm{K}V}{k_B T}\right) \quad (1)$$

For superparamagnetic particles with size distribution in the nanosize range, the magnetic anisotropy barrier (KV) is smaller than the average thermal energy ($k_B T$) of the particles [82].

Due to very small relaxation time (τ), the magnetic moment flips rapidly, so that the effective moment during the time of measurement becomes zero (KV/ k_BT) [82]. This causes the collapse of a multiplet to a superparamagnetic doublet. At room temperature, the thermal energy is sufficient to cause inversion of spin as a function of H. In this case, the ambient temperature at which the experiment is performed is sufficient to provide the thermal energy required for spins inversion. Thus, the magnetization curve shows that the inverse direction of magnetization of the sample passes through the same path, reaching again the value of zero in the absence of the magnetic field. On the other hand, in a sample that does not show the phenomenon of SPM, some of the spins will not completely relax in the absence of the magnetic field and the magnetization curve will show a certain value of residual magnetic field (M_r) [83] (Fig. 17B). A cohesive field in this case (H_c) is applied in order to cause complete relaxation and the final curve will present a profile with hysteresis, that is, a curve discontinuity (Fig. 17B). It is important to mention that the quantification of the SPMs phenomenon depends on the measurement time, the ambient temperature during the experiments and the particle size.

1.7 Magnetite

The inverse spinel structure has achieved prominence among the ferrites due to their excellence magnetic properties and simple chemical composition. The prototype of the ferrites is the spinel magnetite, a chemical compound with formula (Fe_3O_4) [63, 68]. Magnetite is a natural mineral, but can be chemically synthesized in a laboratory with high magnetization value. Its synthesis is fast and of low cost, not requiring high temperatures and pressure [67]. The main method of synthesis is through the co-precipitation of salts containing the Fe^{+2} and Fe^{+3} ions using a base such as NaOH or NH_3OH. Studies have shown, however, that non-magnetic special formation may occur with the use of strong bases such as KOH or NaOH, due to the strong solvation of the cations by the hydroxide ion. The use of a weak soluble base such as ammonium hydroxide has been shown to be more suitable [67].

The magnetic properties of ferrites depend on the size and shape that they present. These, in turn, depend on the crystal nucleation and growth processes that occur during the synthesis process. In this case, in addition to the choice of base, one must be aware of the synthesis conditions as temperature and especially the stirring process. Studies have shown that sonochemical methods are more efficient in the formation of particles of homogeneous size in relation to processes that use mechanical agitation [67].

The discovery of the ultrasound occurred in 1880 from the study of the piezoelectric effect [85]. In 1894, Thornycroft and Barnaby discovered that in the propulsion of missiles launched by vehicles of the type destroyers, they caused implosions of bubbles and / or cavities in the water. This vibration is now known as cavitation [86]. In the cavitation, the waves are transmitted from a series of cycles of compression and rarefaction that affect the molecules of the liquids. When the negative pressure of the rarefaction cycle exceeds the forces of attraction between the molecules of the liquid, a cavity is created [86]. This void in the liquid phase is filled by a small amount of vapor in the solution. There are many thousands of these bubbles in the liquid. Some of them are relatively stable, while others expand to an unstable size. This causes a violent collapse, generating temperatures of around 5000 K and pressures of around 2,000 atm [86]. This rigorous process of agitation during the precipitation of the base in the formation of the magnetite, helps in the complete mixing of the reagents and hinders the growth process of the grains formed after the nucleation, ensuring the formation of monodisperse particles and formed by a single magnetic domain.

Despite the numerous advantages of magnetite in relation to other ferrites as fast and low-cost synthesis, besides the superparamagnetic properties, it presents a disadvantage that would be its oxidation [67]. Unlike of other ferrites using transition metals such as Co, Ba, etc., the Fe^{+2} present in the magnetite tends to oxidize to Fe^{+3}, reducing magnetism and altering the physical stability in solution [82]. This problem can be overcome from of encapsulating or modifying the ferrite surface. One of the main characteristics of ferrites besides magnetism is that they have terminal hydroxyl groups on their surface that can be covalently reacted with numerous compounds and substances in order to give them superior characteristics such as biocompatibility, bioavailability, hydrophobicity, hydrophilicity, etc. Figure 18 presents a series of examples of structures that can be used for this purpose.

Figure 18. Examples of modification process of magnetite surface.

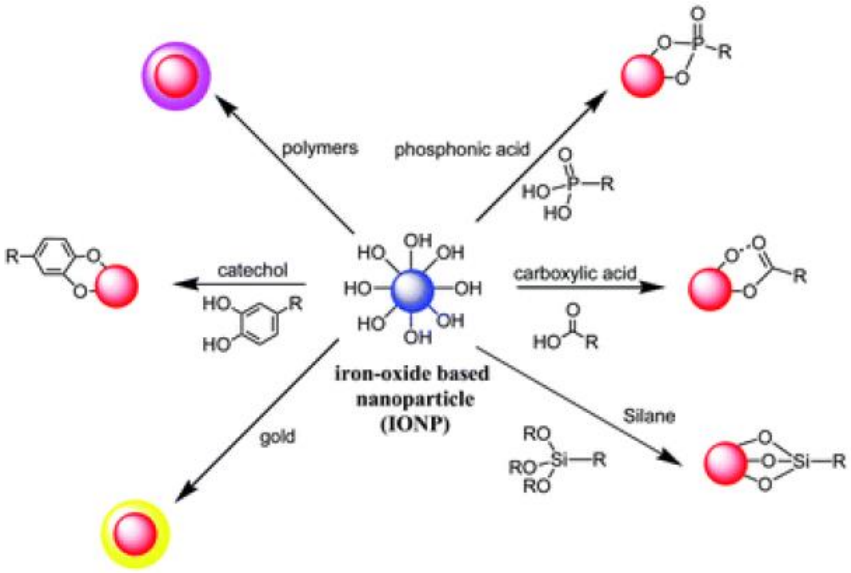

Source [67]

1.8 3-aminopropyl-triethoxisilane

Numerous are the compounds that can be used to the surface modification, such as modified chitosan [40, 41], polyethylene glycol (PEG) [42, 43], poly(NIPAAM) [44], organosilanes [45, 46], among others [47, 48]. The 3-aminopropyl-triethoxisilane (APTES) is an example of organosilane with terminal amino groups [49]. Organosilanes are a class of materials that contain organic and inorganic reactivity in the same molecule and at least one carbon-silicon (Si-C) bond. The organosilane molecule may be represented by XR-Si (OR $'_{)3}$, where X is the organic phase, R'(methyl, ethyl, isopropyl, ...), R represent an aryl or alkyl group, (CH_2)n (with n = 0 , 1 ou 3). (OR ') is a hydrolysable group such as alkoxy (methoxy, ethoxy...). The groups (OR ') may provide the bond with the organic or inorganic phases [2] (Fig. 19). The APTES (3-aminopropyltriethoxysilane) is an example of organosilane having terminal amino (NH_2) groups.

Figure 19 - General image of a silane coupling agent.

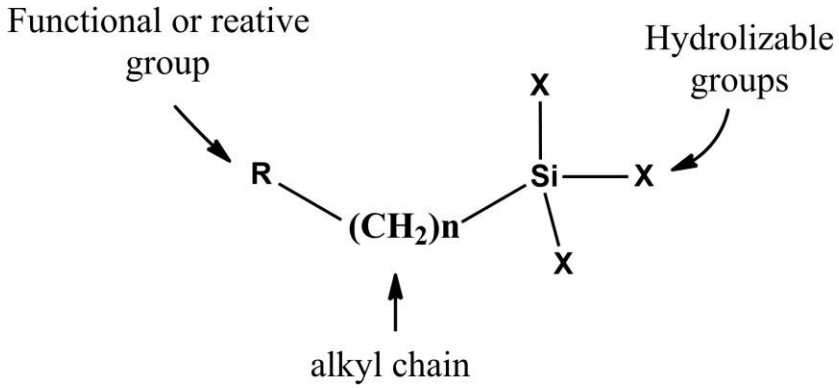

Source: Author

There are several applications for APTES such as cross-linking agents [50], drug delivery [51], biosensors [52] and pre-treatment for coatings. In the last years, the APTES copolymer has received considerable attention due to the possibility of using it as a functionalization agent of different support as silica [53], clay [54] and magnetic support [45].

Some studies have employed APTES-coupling magnetite for enzymes immobilization [55-57]. Li-Shuang Zhang et al. promoted the enzyme immobilization of Protocatechuate 3,4-dioxygenase (P34O) onto (3-aminopropyl) triethoxysilane-modified Fe_3O_4 nanoparticles (NPs) by the glutaraldehyde method [87]. The results showed an increase of thermal stability and enzymatic activity for the immobilized $P_{34}O$ in comparation to the free enzyme. Besides that, the kinetic parameters of the immobilized enzyme were higher than those of the free enzyme, and immobilized $P_{34}O$ on Fe_3O_4 NPs could be reused ten times without a remarkable decrease in enzymatic activity [58].

In this work, nanohybrid biocatalysts composed by lipases immobilized on Fe_3O_4 magnetic nanoparticle were used for the first time to the kinetic resolution of secondary alcohols such as rac-indanol, *rac* -1-phenylethanol (rac-1), *rac* -1-(3-bromophenyl)-1-ethanol (*rac* -2) and *rac*-1-(3-methylphenyl)-1-ethanol (*rac* -3). Besides the promising results in catalysis, our nanohybrid materials present stability in high temperatures and the possibility of reuse due to its magnetic properties.

2 NOVEL NANOHYBRID BIOCATALYST: APPLICATION IN THE KINETIC RESOLUTION OS SECUNDARY ALCOHOLS

2.1 OBJECTIVES

2.1.1 General

- Develop a new nanohybrid material to be used for the kinetic resolution of *rac*- indanol.

2.1.2 Specifics

- Synthesize Fe_3O_4 via co-precipitation method using ultrasound irradiation.
- Performed the surface modification of the Fe_3O_4 by APTES using ultrasound irradiation.
- Activate the terminal amino groups of APTES by glutaraldehyde for enzyme immobilization.
- Characterization of Fe_3O_4 @APTES-GLU support by X-ray powder diffraction (XRPD), FT-IR, Vibrating Sample Magnetometer (VSM), Transmission Electron Microscopy (TEM) and DTG measurements.
- Promote the immobilization of enzyme from Pseudomonas fluorescens on the magnetic support.
- Characterization of the nanohybrid catalyst by XRPD, Vibrating Sample Magnetometer (VSM), Transmission Electron Microscopy (TEM) and DTG measurements.
- Study of the thermal stability essays for the nanohybrid formed and kinetic resolution of *rac*-indanol.

3 EXPERIMENTAL

3.1 Materials

All reagents were commercial chemicals with analytical grade and were used as received without further purification. The chemical Numerous are the compounds reagents for this work were $FeCl_3.4H_2O$ (Dinâmica, 97%), $FeCl_2.H_2O$ (Vetec, 97%) and sodium hydroxide (Cinética Química, 97%). Methanol, hexane, tetrahydrofuran (THF), acetonitrile, ethyl acetate and dichloromethane were purchased from Synth®. Vinyl acetate was acquired from Sigma- Aldrich®. Hexane used in the reaction of biocatalysis was distilled over an adequate desiccant under nitrogen. Lipase from Pseudomonas fluorescens (Amano AK lipase, 22,100.0 U/g) was acquired from Sigma-Aldrich®. The commercial TLL extract (15.83 mg of protein per mL) was obtained from Novozymes (Spain). 6 BCL agarose, 25%(v/v) glutaraldehyde solution and cetyl trimethyl ammonium bro-mide (CTAB) were purchased from Sigma Chemical Co (St. Louis, MO, USA). The commercial preparation of TLL covalently immobilized on immobead-150 (TLL,250 U/g), branched-polyethylenimine (MW 10,000) and 3-amino- propyltriethoxysilane (>98%) were purchased from Sigma-Aldrich. Thin Layer Chromatrography (TLC) analyses were performed on aluminum sheets pre-coated with silica gel 60 F254 (0.2 mm-thick) from Merck®. Flash chromatographies were performed using silica gel 60 (230-240 mesh). Protein concentration was determined using Bradford's method and bovine serum albumin was used as reference [59]. All experiments were performed in triplicate and the results are reported as the mean of this value and the standard deviation (usually under 10%). The synthesis of *rac*-indanyl acetate and *rac*-indanol as well as the calculation of enantiomeric excess and conversion were performed according to the literature [31].

3.2 Methods

3.2.1 Synthesis of Fe_3O_4 SPMNPs

SPMNPs of magnetite (Fe_3O_4) were synthesized via co-precipitation method assisted by ultrasound. 1.16 g of $FeCl_2.H_2O$ and 2.52 g of $FeCl_3.4H_2O$ were dissolved in Mili-Q water and precipitated using 10 mL of the NH_4OH standard solution under ultrasound irradiation at 70% amplitude (Branson sonifier W450 digital, ½ tip) for 10 min, with a pulse of 30s on and 10 s off. Finally, the precipitate was separated magnetically and washed several times with milli-Q water (8

× 30 mL) until the residual solution became neutral. The synthesized SPMNPs were stored in a desiccator until complete remotion of water.

3.2.2 Functionalization of Fe_3O_4 SPMNPs with APTES

The surface of Fe_3O_4 SPMNPs was functionalized with APTES in order to promote the linkage between the enzyme and the support. In this procedure, 100 mg of Fe_3O_4 were added in a Beaker containing 40 mL of a mixture ethanol/toluene (1:1, v/v). Then, 100 µL of APTES was added into the mixture, which remained under ultrasound irradiation during 15 min. Finally, the obtained product (Fe_3O_4@APTES) was washed several times with Milli-Q water (10 × 20 mL) and magnetically separated from the solution by using a NdFeB magnet.

3.2.3 Glutaraldehyde activation

The amino-terminal groups of the Fe_3O_4@APTES nanocomposite were activated with glutaraldehyde in order to promote the covalent linkage between the enzyme and support, via formation of an imine bond. For this purpose, 0.01 g of nanocomposite were suspended in a solution containing 250 µL of a glutaraldehyde solution and 5 mL of a phosphate buffer solution (100 mM, pH 7.0). The mixture was kept under orbital stirring (45 rpm) for 2 h at 25 °C. Finally, the magnetic support (Fe_3O_4@APTES-GLU) was washed (8 × 30 mL) with a 100 mM phosphate buffer (pH 7) to remove the excess of activating agent [60].

3.2.4 Immobilization of lipase from *Pseudomonas fluorescens* on magnetic support (enzymatic nanohybrid catalyst)

The immobilization of lipase from *Pseudomonas fluorescens* under previously activated support was carried out using 1 mL of concentrate extract of enzyme (10 mg/10 mL) inserted directly on 10 mg of the support. The system remained in orbital stirring speed (45 rpm) during 1 h. The immobilized enzyme (Fe_3O_4@APTES-GLU-PF) were removed by magnetic separation and washed (5 × 30 mL) with phosphate buffer solution (100 mM, pH 7.0). The amount of immobilized lipase on the support was determined by measuring the initial and final concentration of enzyme in the immobilization supernatant.

3.2.5 Determination of enzyme activity and protein concentration

The hydrolytic activity of free and immobilized enzyme was determined by hydrolysis of *p*-nitrophenyl butyrate (substrate) and the concentration of formed *p*-nitrophenol was quantified spectrophotometrically at 400 nm with temperature and agitation control [88].

Activity measurements were performed in 25 mM sodium phosphate at pH 7.0 and 25 °C, from the measurement of p-nitrophenol released during the hydrolysis of 0.4 mM *p*-NPB (ε = 10.052 $M^{-1}cm^{-1}$ under these conditions) [89]. To start the reaction, 30-200 µL of lipase solution in suspension was added to 2.5 mL of substrate solution. One international unit of activity (U) was defined as the amount of enzyme that hydrolyzes 1 µmol of *p*-NPB per minute under the conditions described previously. Protein concentration was determined using Bradford's method [90] and bovine serum albumin was used as reference.

3.2.6 Parameters of immobilization

Initially, the immobilization was carried out using 51.4 U/g of support (6 mg of protein per g of wet support) to prevent diffusion limitations that could alter the results. Immobilization yield $IY_{imob}(\%)$ was determined by the difference between the initial activity of the enzyme solution (At_i) and the remaining activity or supernatant (At_f) according to Eq. (6):

$$IY_{imob}(\%) = \frac{At_i - At_f}{At_i} \cdot 100 \quad . \tag{6}$$

The theoretical activity (At_t) of immobilized lipase on the support could be calculated by using the amount of enzyme offered/g of support (At_{off}- U/g support) and the immobilization yield, as it could be seen in Eq. (7). After measuring the activity of the immobilized enzyme (At_d - U/g support), the recovery activity was calculated by using Eq. (8):

$$At_t = IY \cdot At_{off}, \tag{7}$$

$$At_r = \frac{At_d}{At_t} \cdot 100 \tag{8}$$

3.2.7 Thermal inactivation of immobilized enzyme

Thermal inactivation was determined by incubating immobilized enzyme. In this case, 0.1 mg of immobilized enzyme was suspended in 5 mL of 25 mM sodium phosphate buffer (pH 7) at 60 °C in presence of organic solvent (hexane) at 40 °C and 50 °C. Periodically, samples were withdrawn and the remaining activity was measured using the *p*-NPB assay described in the

2.6. The half-life time ($t_{1/2}$) for each immobilized derivative was calculated according to Sadana and Henley model [91] using Microcal Origin version 8.1. With the exponential nonlinear decay model and its parameters, it was possible to determine the half-lives time ($t_{1/2}$) of the derivatives.

3.2.8 General procedure for kinetic resolution of *rac*-secondary alcohols

Vinyl acetate (103 µL, 1.10 mmol) was added into a suspension of the *rac*-alcohol (0.22 mmol) and lipase from *Pseudomonas fluorescens* (Amano AK lipase) immobilized on magnetic nanoparticles (ratio 2:1; lipase: substrate; w/w) in dry hexane (2.2 mL) under nitrogen atmosphere. The reaction was shaken at temperatures ranging from 30 to 50°C and 250 rpm, using an orbital stirrer. Aliquots were regularly analyzed by GC analysis and after the adequate time the reaction was stopped by removing immobilized enzyme by magnetic separation and washed with hexane (30 mL). The hexane was evaporated under reduced pressure. Then, the crude product was purified by flash chromatography on silica gel (5–95% EtOAc/hexane), yielding (*S*)-alcohol and (*R*)-acetate, being their enantiomeric excess determined by GC.

In this work, a nanohybrid material was synthesized for the use in heterogeneous biocatalysis. Fig. 19 shows each step used to obtain the system, while figure 20 presents the chemical reactions in which our biocatalysts (Fe_3O_4@APTES-GLU-PF) were used for kinetic resolution.

Figure 19. The detailed flow chart for the synthesis of the nanohybrid biocatalyst.

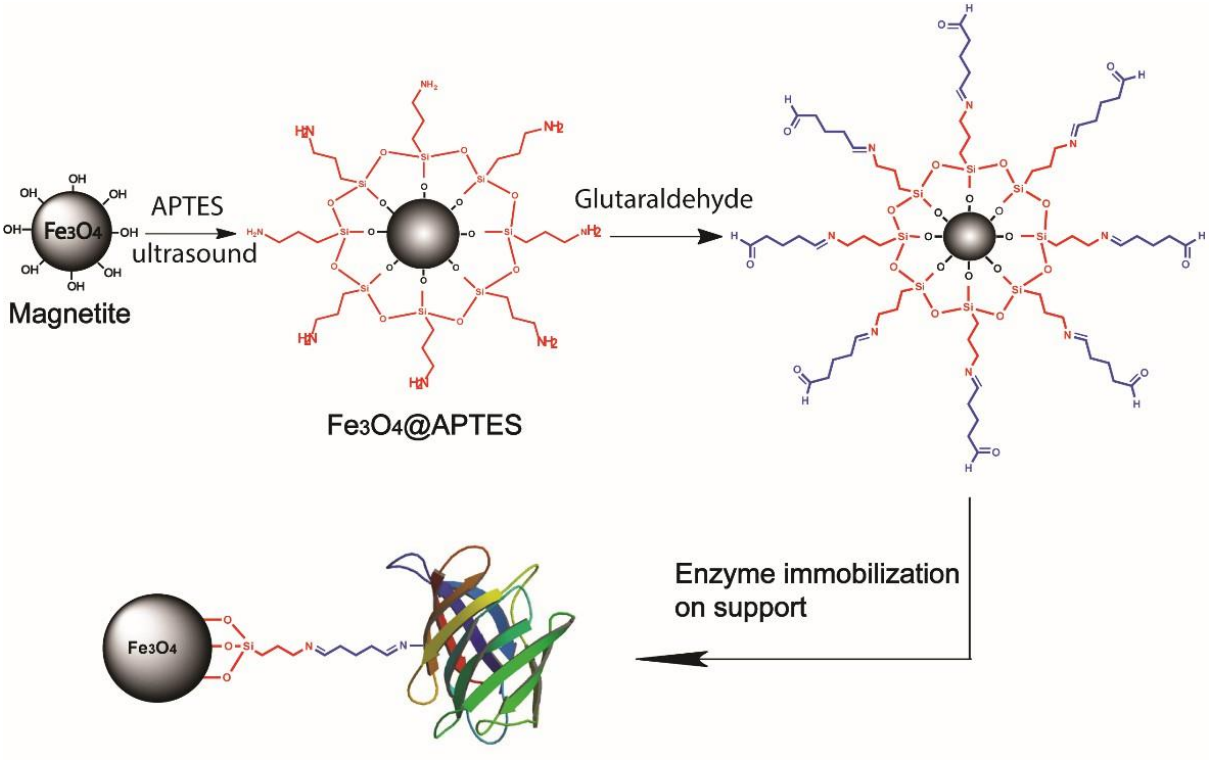

Source: Author

Figure 20. Chemical reactions for kinetic resolution of secondary alcohols.

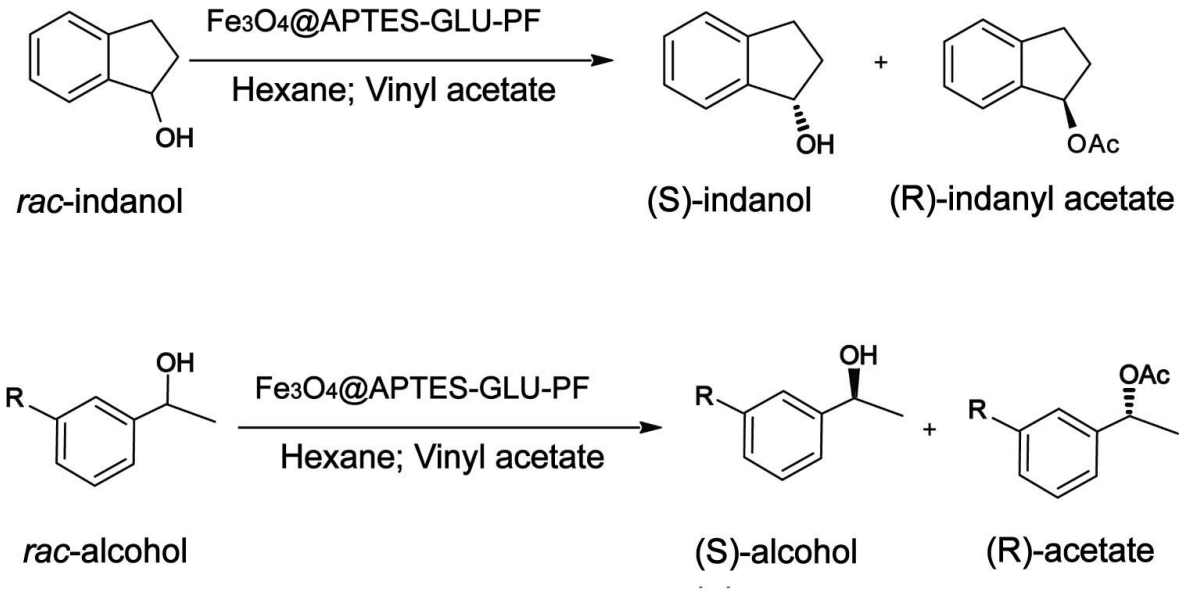

R= H (*rac-1*); Br (*rac-2*); CH_3 (*rac-3*)

3.3 Characterization of the samples

The structural analysis and phase concentrations were obtained by XRPD analysis. The measurement was carried out using Rigaku X-ray diffractometer equipped with CoKα radiation tube (λ = 1.7889 Å) operated at voltage of 30 kV and current of 15 mA. The phase identification analysis was made by comparing powder diffractograms with standard patterns from International Centre for Diffraction Data (ICDD). Rietveld refinement procedure [92] was applied to all diffraction patterns using the DBWS 2.25 [93]. The crystallite size of the samples were calculated from the XRPD data using Scherrer's equation [80].

The magnetic measurements at room temperature were performed using a Lakeshore model 7404 vibrating sample magnetometer, with maximum magnetic field of ±17 kOe. The VSM has been previously calibrated using a pure Ni sample and, after measuring the weight of each sample, provided the magnetization in emu/g.

Fourier transform infrared spectroscopy (FT-IR) experiments were carried out on a Perkin-Elmer Spectrometer in the range 4000-400 cm^{-1}. In recording IR spectra, each of the samples was mixed with potassium bromide (KBr) powder and pressed into pellets. Thermogravimetric analyzes (TGA) were obtained with an equipment Mettler Toledo TGA/SDTA 851 in a temperature range between 50 and 800°C, with heating rate of 10°C/min and nitrogen atmosphere with a flow rate of 50 mL/min, aluminum pan and sample weight of 10 mg.

Transmission Electron Microscopy (TEM) images were acquired with a JEOL JEM 2100 LaB6 operating at accelerating voltage equals 200 kV and equipped with a TV (Gatan ES500W); CCD (TVips– 16MP). The samples were prepared by drop-casting a hexane dispersion of the nanocrystals onto carbon and Formvar-coated copper grids. After deposition, the samples were dried to a temperature of 60 °C overnight prior to obtaining the images. The size distribution was determined by measurement of 100 randomly selected particles in different regions of the expanding TEM images.

Optical rotations were measure with a Jasco P-2000 polarimeter. The enzymatic acetylation was performed in a bench shaker with a chilled incubation of the mark Analítica SI-300R model. GC analysis were carried out in a Shimadzu chromatograph model GC 2010 with a flame ionization detector using a chiral column CP-chirasil-dex (25 m × 0.25 mm × 0.25 m, 0.5 bar N_2).

Determination of the ee by GC analysis of the (*S*) and (*R*)-indanyl acetate; (*S*) and (*R*)- indanol: 110 °C; 0.5 °C/min 130 ºC (hold 15 min); 5.0 °C/min 140 °C (hold 5 min). Retention times were: (*S*)-indanyl acetate = 32.68 min; (*R*)-indanyl acetate = 33.17 min; (*S*)-indanol = 37.95 min; (*R*)-indanol = 38.98 min.

Determination of the ee by GC analysis of the (*S*) and (*R*)-1-phenylethyl acetate; (*S*) and (*R*)-phenylethanol: 80°C (hold 7 min); 10 °C/min 120 ºC (hold 15 min); 4.0 °C/min 140 °C (hold 5 min). Retention times were: (*R*)-1-phenylethyl acetate = 14.01 min; (*R*)-phenylethanol = 15.31 min; (*S*)-phenylethanol = 15.62 min.

Determination of the ee by GC analysis of the (*S*) and (*R*)-1-(3-bromophenyl)-ethyl acetate; (*S*) and (*R*)-1-(3-bromophenyl)ethanol: 100 °C (hold 5 min); 4°C/min 140 ºC (hold 20 min). Retention times were: (*R*)-1-(3-bromophenyl)-ethyl acetate = 19.97 min; (*R*)-1-(3-bromophenyl)ethanol = 27.62 min; (*S*)-1-(3-bromophenyl)ethanol = 28.92 min.

Determination of the ee by GC analysis of the (*S*) and (*R*)-1-(3-methylphenyl)-ethyl acetate; (*S*) and (*R*)-1-(3-methylphenyl)ethanol: 100 °C (hold 5 min); 2 °C/min 140 ºC (hold 20 min). Retention times were: Retention times were: (*R*)-1-(3-methylphenyl)ethanol = 15.73 min; (*R*)- 1-(3-methylphenyl)-ethyl acetate = 19.60 min; (*S*)-1-(3-methylphenyl)-ethyl acetate = 20.18 min.

4 RESULTS AND DISCUSSION

4.1 Characterization of nanohybrid biocatalyst

XRPD analysis was used to confirm the formation of crystalline phase and to provide the structural parameters for Fe_3O_4 (Fig. 21).

Figure 21. XRPD of the samples Fe_3O_4, Fe_3O_4@APTES and Fe_3O_4@APTES-GLU-PF.

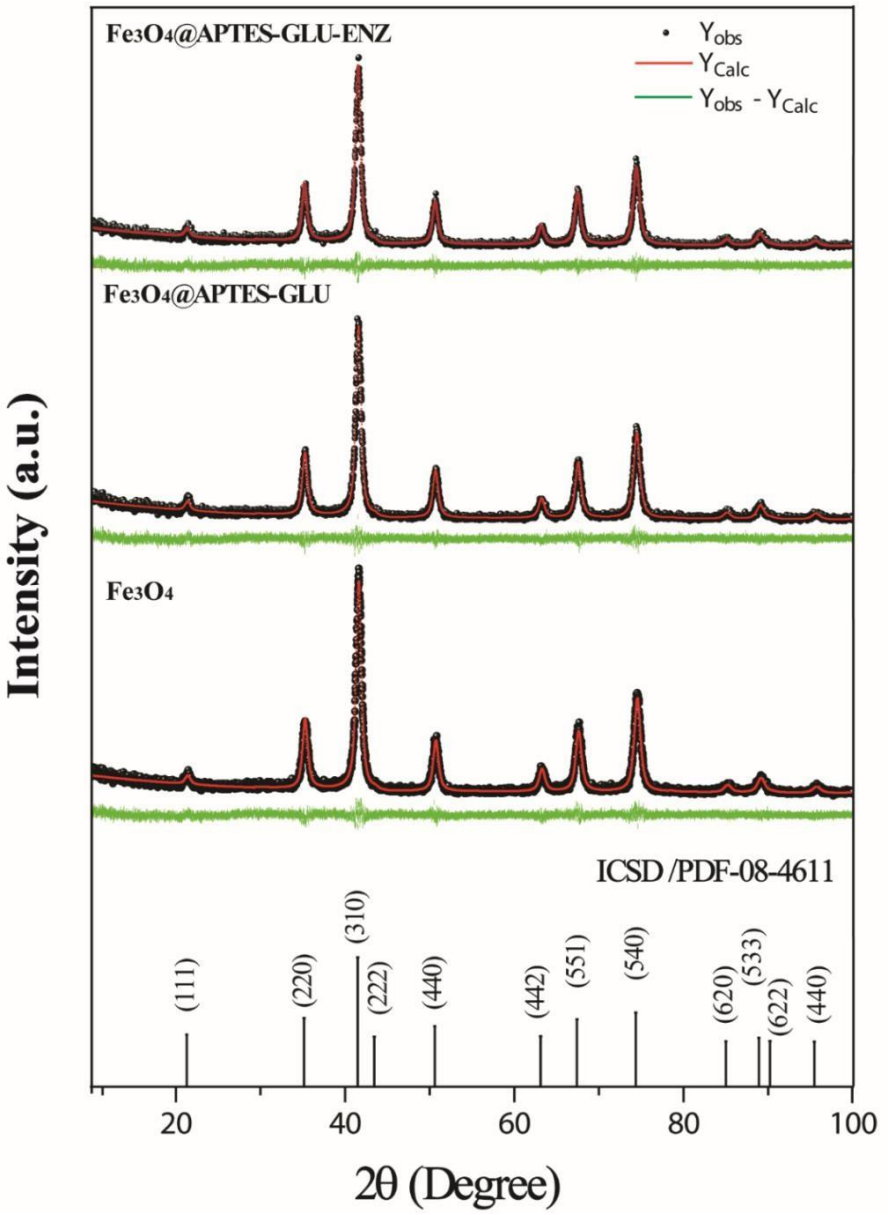

The green lines represent the relative difference between the experimental (black dots, Y_{Obs}) and the calculated (red line, Y_{Calc}) intensity obtained from the refinement. It was also possible to confirm the formation of a single phase for all samples from the refinement of the XRPD data. The

diffraction patterns showed that all peaks at 2θ of 21.5°, 29.9°, 35.3°, 41.7°, 54.1°, 56.8° and 62.5° were corresponding to (111), (220), (311), (400), (422), (511) and (440) Bragg reflection, respectively. They are indexed to the inverse spinel of Fe_3O_4 with spatial group Fd3M (ICSD/PDF-08-4611). Rietveld method [92] was used to characterize the core (Fe_3O_4) of the nanohybrid system and the obtained data were summarized in Table 2.

Table 2. Structural parameter obtained from Rietvield refinement.

Samples	**Average crystallite sizes (nm)**	**Lattice parameter (Å), *a=b=c***	**R_{WP} (%)**	***S***
Fe_3O_4 Fe_3O_4@APTES	13.2±0.2	8.358658	14.01	0.92
Fe_3O_4@APTES-GLU-PF	14.3±0.2	8.364770	14.68	0.91
	13.9±0.2	8.367538	14.53	0.90

The refinement is concluded when the parameters no longer suffer variation and the minimizing function reached the minimum value [94]. It is possible to follow the convergence function from some indices calculated in the end of each refinement cycle. In this sense, the R_{WP} (weighted residual error) and S (quality factor ‘‘goodness of fit’’) are present in the Tab. 1. These indexes provide information about the quality of refinement and the profile of diffractogram. The low values found for the R_{WP} and the proximity of S of one value show that the refinement was satisfactory. The average crystallite size was calculated from the Scherer´s equation, which relates the crystallite size with the half-width of the diffraction peak [80]. The values found for the samples Fe_3O_4, Fe_3O_4@APTES and Fe_3O_4@APTES- GLU-PF, were 13.2, 14.3 and 13.9 (±0.2) nm, respectively. The results for the crystallite size presented approximate values and this indicates, that the ultrasound treatment used for anchoring of the APTES and the enzymes immobilization process were not sufficient to promote any change in the crystal structure. The values found for the crystallite (below 15 nm) suggest the possibility of SPM phenomena for all samples [95]. These results also indicate that the ultrasound technique, combined with the co-precipitation method, are able to synthesize SPM magnetite with high purity and crystallinity.

Magnetization curves were obtained to investigate the magnetic properties of the samples. The Langevin function was used to make a prediction about the average particle size and magnetization. The values obtained of saturation magnetization M_S were 68.9, 66.9, and 62.3 emu/g for the samples Fe_3O_4, Fe_3O_4@APTESGLU and Fe_3O_4@APTES-GLU-PF, respectively. The magnetic curves show a continue decrease of the M_S as a function of the amount of no-magnetic weight. Despite this, the values obtained of M_S for the hybrid catalyst indicate that it has a high

magnetic response. Figure 22 shows the magnetic curves obtained at 300 K for the samples Fe_3O_4, Fe_3O_4@APTES-GLU and Fe_3O_4@APTES-GLU-PF

Figure 22. Magnetization curve for the samples Fe_3O_4 (a), Fe_3O_4@APTES-GLU (b) and Fe_3O_4@APTES-GLU-PF (c).

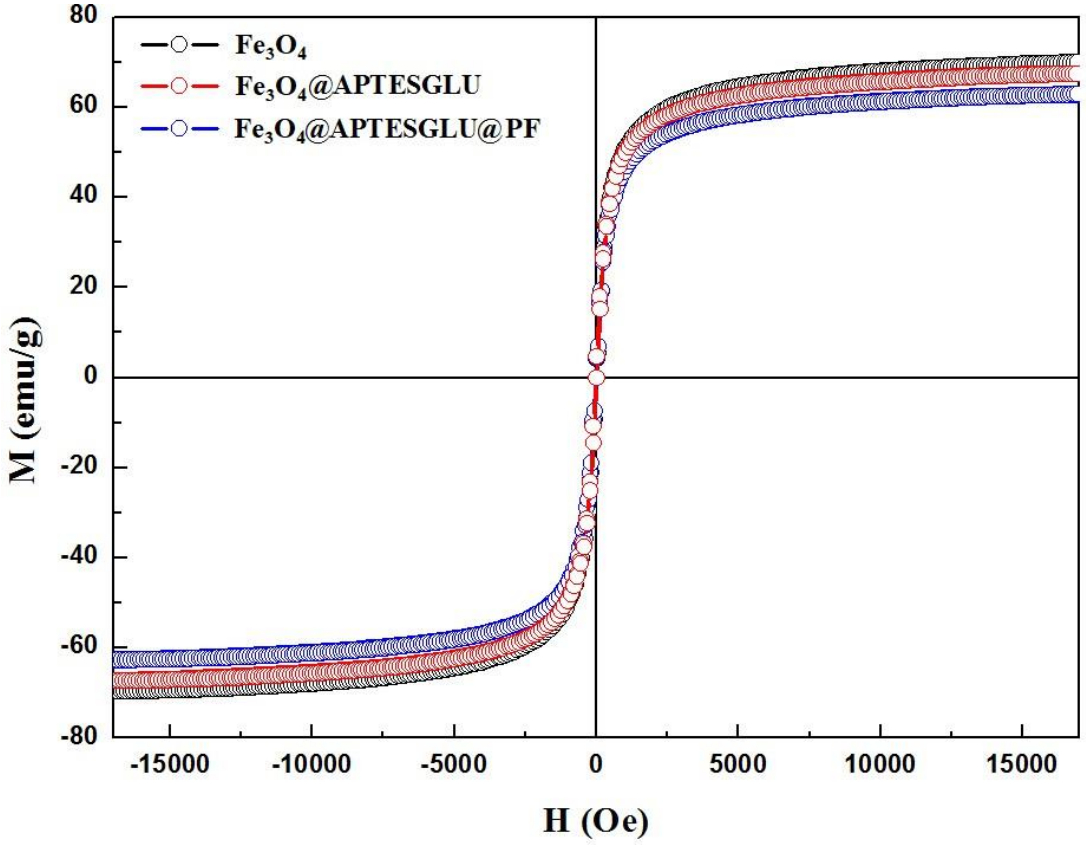

The magnetic nanoparticles have the natural tendency to aggregate due to the dipole-dipole attraction among the particles and this behavior can be intensified under magnetic field. In this case, the presence of SPM phenomena is very important for the preservation of necessary volume/surface ratio of the catalyst. Figure 22 shows that the magnetic moment of the particles rises quickly with the increase of the externally applied magnetic field (H). Besides that, no hysteresis in magnetic curves measured at 300 K has been observed (Fig. 22). This may be indicative of SPM behavior for all the samples. Furthermore, the values found for the particle size from the Langevin function for all samples were very close and around of 10 nm. These values are in concordance with those obtained from XRPD data. The TEM images were carried out in order to provide information about of the morphology, aggregation state and size of NPs (Fig. 23).

Figure 23. TEM micrographs for the samples Fe_3O_4 and Fe_3O_4@APTES-GLU-PF. (a) Atomic planes of the Fe_3O_4. (b) Spacing between planes which was indexed as (220) to the Fe_3O_4. (c) and (d) Morphology and particle size of the Fe_3O_4@APTES-GLU-PF and Histogram of the particle size distribution.

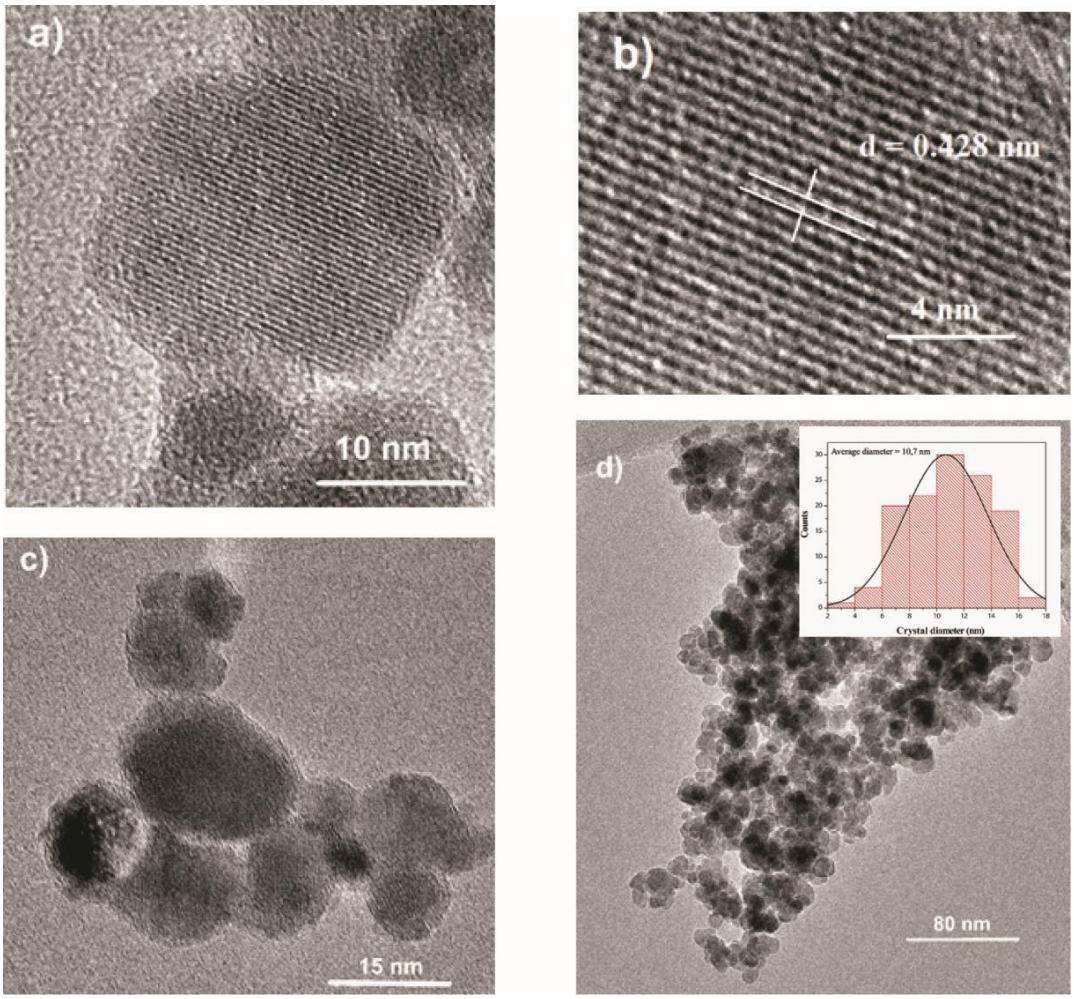

Fig. 23(a), it is possible to visualize the crystalline planes and so to evaluate the crystallinity degree of the magnetic core in the samples. Fig. 23(b) presents the measure of spacing between the atomic planes for the Fe_3O_4. The result obtained for the distance between plans was 0.428 nm and may be indexed as the plane (220) to the family of planes of Fe_3O_4. Fig. 23(c) and (d) shows the morphology and particle size of the nanohybrid catalyst (Fe_3O_4@APTES-GLU-PF) which presents globular shape. The histogram of average particle size (around 10.7 nm) for nanohybrid catalyst was determined by the measurement of 100 randomly selected particles in different regions of the expanding TEM images (Fig. 23d). The values obtained are consistent with the values obtained from the Scherrer´s equation in XRPD analysis.

TGA experiments were carried out to determine the amount of material incorporated on the magnetic nanoparticles. Figure 24 presents the results of TG and DTG curves for all samples.

Figure 24. TGA and DTG results for the samples Fe_3O_4 (a), Fe_3O_4@APTES-GLU (b) and Fe_3O_4@APTES-GLU-PF (c).

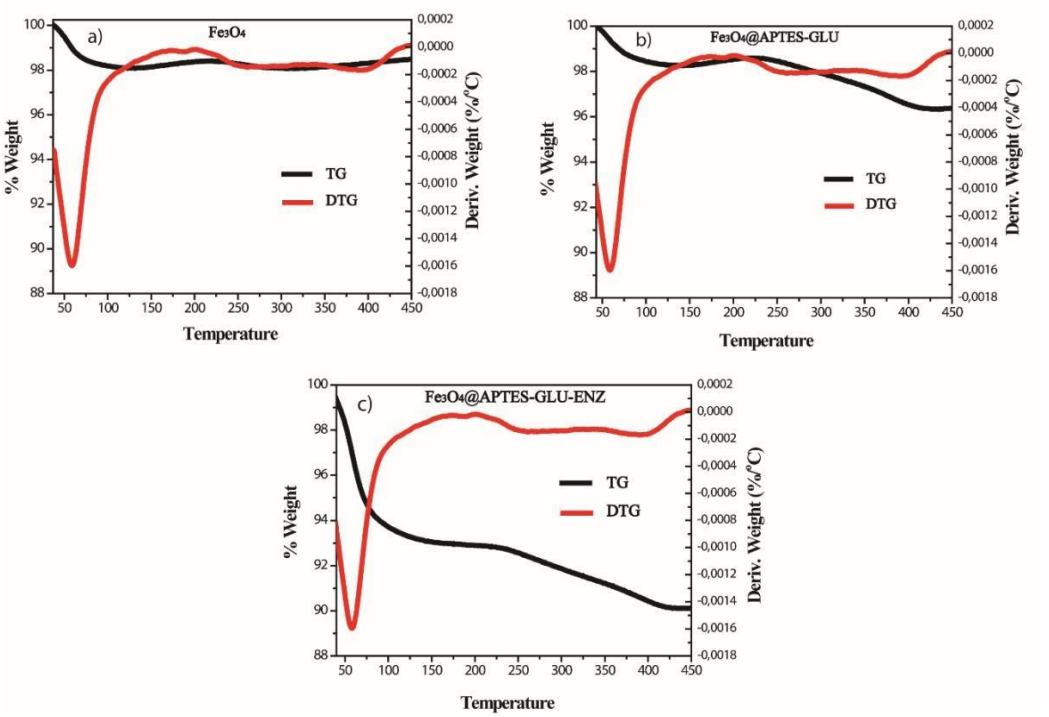

It was observed the same weight loss event at 59°C for all samples, mainly due to the presence of water physically adsorbed on the material. The TG curve from immobilized lipase on MNPs indicated that the maximum rate of weight loss (10%) occurred from 59-450ºC, probably, due to the elimination both water and complete thermal degradation of organic structure of protein. From the subtraction of the total weight loss in Fig. 24(c) by the loss of weight in Figure 24(b) it was possible to conclude that the total weight of protein immobilized was of 6 %.

4.2 Parameters of immobilization

The results obtained in the immobilization process were as follows: *IY* (%) = 66.6 ± 1.3, A_{td} (U/g) = 6.63 ± 0.1 and A_{tr} (%) = 20.5 ± 0.3. The yield of immobilization was 66.6%, showing that a large part of the enzyme was immobilized on the support. Using glutaraldehyde as immobilization agent, the enzyme may be immobilized *via* different possibilities, by ion exchange, interfacial activation and multipoint covalent attachment [89]. The activity of the derivative shows that the

detention was efficient, getting a significant activity of 6.63 U/g and 20.5% of recovered activity. This result can be explained by the distortion of the enzyme structure during the immobilization process contribute to a decrease in catalytic activity [96]. It is also possible that after the immobilization step, some protein molecules are not covalently bonded with glutaraldehyde, undergoing desorption during the washing of the carrier [97].

4.3 Stability of the enzyme preparations

It is known that the temperature is an important factor to influence the rate of an enzymatic reaction. Within certain limits, the rate of an enzymatic reaction increases with the increase of the temperature. However, from a determined temperature, the rate of the reaction decreases abruptly due to the denaturation of the enzyme and the consequent loss of its activity. Considering this fact, many researches have been carried out with the intention of minimizing this problem, associating the immobilization of enzymes with the thermal stability [43, 57]. In this sense, thermal stability assays were conducted to provide information about the best condition for the kinetic resolution reactions of the racemic alcohols. Table 3 shows the half- lives of immobilized lipase in different thermal inactivation conditions.

Table 3. Half-lives of the immobilized enzyme under different inactivation conditions. Experiments were performed as described in Section 2.

Inactivation condition	Half-lives (minutes)
pH 7 – 60 °C	≥ 420
Organic solvent (40 °C, 99% Hexane)	≥ 1050
Organic solvent (50 °C, 99% Hexane)	693

It is observed that the immobilized enzyme (Fe_3O_4@APTES-GLU-PF) has excellent stability while maintaining a temperature of 60 °C, holding 72 % of the initial activity after 7 h. This result suggests a high stability of the open form of the stabilized and immobilized enzyme on the support. The covalent attachment between the enzyme and the support may have induced some degree of rigidity, promoting the catalytic activity [99]. It is also observed that in contact with hexane, the immobilized enzyme is stable at both temperatures tested. After 1050 min at 40 °C, the immobilized enzyme retains 100% of activity and the half-life time at 50 °C was 693 min. This high stability can

be related to the strong covalent interaction between enzyme and support preventing the desorption of the supported enzyme, a very likely phenomenon using free enzyme in organic solvents [66].

4.4 Kinetic Resolution of *rac*-secondary alcohols

The kinetic resolution (KR) was first performed with *rac*-indanol in the presence of lipase from Pseudomonas fluorescens (Amano AK lipase) immobilized on magnetic nanoparticles via acetylation process.

According to the proposed mechanism, the first step consists in the formation of the intermediate acyl-enzyme by the vinyl acetate precursor. The presence of the enol formed during step 1 does not compete with the *rac*-indanol in the kinetic resolution because the equilibrium is preferably displaced to form the aldehyde, since oxygen is the most appropriate atom to accommodate the double bond. After activation of the catalytic triad of the enzyme, acetylation of the indanol occurs following the Kazlauskas rule (step 2).

The results obtained for the kinetic resolution are summarized in Table 6. The reactions were carried out under predetermined conditions in the presence of lipase from *Pseudomonas fluorescens* in the free form [66], using hexane as organic solvent, vinyl acetate as acyl donor and lipase from *Pseudomonas fluorescens* immobilized on magnetic nanoparticles (ratio 2:1 in weigh respect to *rac*-indanol). The figure 25 presents the acetylation mechanism of *rac*- indanol by lipase. Initially, KR reactions were performed at 30 °C (Table 6, entries 1-5). The maximum conversion (~50%) was achieved in 24 h of reaction with high enantioselectivity (E > 200), Table 4, entry 5. Thermal stability assays had shown the possibility of raising the temperature to reduce the total reaction time. Thus, the temperature of the reaction was raised initially to 40 °C. In this case, the maximum conversion was observed at a reaction time of 3.5 h, maintaining a high enantioselectivity (E > 200), Table 4, entry 9. Increasing the temperature to 50 °C led to a drastic decrease in the reaction time, being required only 1.75 h to reach 50% conversion with high enantioselectivity (E > 200), Table 4, entry 11.

Finally, it was conducted a study of the reuse of the enzyme system immobilized on the Fe_3O_4 SPMNPs surface at a temperature of 50 °C and reaction time of 1.75 h. The results are summarized in Table 7. During the first three cycles of reaction, the enzyme system remained with high activity and values of selectivity unchanged (Table 4, entries 1-3). In the fourth and fifth cycles, we only observed a slight decrease in selectivity (E value of 1057 to 458 and E value of 1057 to 246, respectively) and with conversion value close to 50%, (Table 5, entries 4 and 5).

Table 4. Kinetic resolution of *rac*-indanol, via acetylation, using lipase from *Pseudomonas fluorescens* immobilized on magnetic nanoparticles (Fe_3O_4@APTES-GLU-PF).[a]

Entry	Temperature (°C)	Time (h)	*e.e.*$_s$ (%)[b]	*e.e.*$_p$(%)[b]	*c* (%)[c]	E[d]
1	30	2	7	>99	7	213
2	30	4	22	>99	18	247
3	30	6	33	>99	25	275
4	30	8	44	>99	31	307
5	30	24	33	>99	48	684
6	40	1	44	>99	31	307
7	40	2	75	>99	43	451
8	40	3	91	>99	48	637
9	40	3.5	98	>99	50	922
10	50	1.5	90	>99	48	618
11	50	1.75	99	>99	50	1057

[a] Conditions: 5 equiv. of vinyl acetate and immobilized lipase: *rac*-indanol (2:1) at 250 rpm.

[b]Determined by GC.

[c] Conversion, $c = e.e._s/(e.e._s + e.e._p)$.

[d]Enantioselectivity, $E = \ln[1 - c(1 + e.e._p)]/\ln[1 - c(1 - e.e._p)]$.

Table 5. Reuse of immobilized lipase from *Pseudomonas fluorescens* immobilized on magnetic nanoparticles (Fe_3O_4@APTES-GLU-PF).[a]

Entry	Cycle	*e.e.*$_s$ (%)[b]	*e.e.*$_p$(%)[b]	*c* (%)[c]	E[d]
1	1°	>99	>99	50	1057
2	2°	>99	>99	50	1057
3	3°	>99	>99	50	1057
4	4°	98	98	50	458
5	5°	95	97	49	246

[a] Conditions: 5 equiv. of vinyl acetate, 50° C, 1.75 h and lipase: *rac*-indanol (2:1) at 250 rpm.

[b] Determined by GC.

[c]Conversion, $c = e.e._s/(e.e._s + e.e._p)$.

[d]Enantioselectivity, $E = \ln[1 - c(1 + e.e._p)]/\ln[1 - c(1 - e.e._p)]$.

The stereocenters of the (*R*)-indanyl acetate and (*S*)-indanol were determined by optical rotation using a polarimeter and the values obtained were compared with the literature. The value of specific optical rotation of (*R*)-indanyl acetate was $[\alpha]_D^{22} = +86.5$ (c 1.0, $CHCl_3$) *e.e.* = 99% while the value given in the literature is $[\alpha]_D^{26} = +87.6$ (c 1.0, $CHCl_3$) *e.e.* > 99% [100]. For the (*S*)-indanol the value obtained was $[\alpha]_D^{22} = +31.5$ (c 1.0, $CHCl_3$) *e.e.* > 99%; and the value reported in the literature is $[\alpha]_D^{25} = +30.6$ (c 1.0, $CHCl_3$) and *e.e.* > 99% [25]. The configurations of the stereocenters of the products followed the empirical rule of Kazlauskas [60] considers that, in the acetylation of secondary alcohols using lipases, the (*R*)-acetylated product and the remaining (*S*)-alcohol were obtained.

The results obtained for the kinetic resolution of *rac*-indanol using immobilized enzyme were compared with those obtained using the free enzymes. T. S. Fonseca et al. [101] used free enzymes from Pseudomonas fluorescens for the kinetic resolution of rac-indanol in the same conditions. The authors obtained e.e.s and e.e.p of 98 and 97 % respectively, with conversion of 50% in 15 min. Although our results present a total time of 1.17 h for the kinetic resolution, the system enables its reuse until five times and reactions in higher temperatures. This set of factors might provide cost-effective benefits for the industrial processes or provide new alternatives for the production of enantiomerically pure compounds.

4.5 Kinetic Resolution of *rac*-1-phenylethanol (*rac* -1), *rac* -1-(3-bromophenyl)-1- ethanol (*rac* -2) and *rac* -1-(3-methylphenyl)-1-ethanol (*rac* -3)

In view of the results obtained in the kinetic resolution of *rac*-indanol, it was decided to extend the study of the kinetic resolution for *rac*-1-phenylethanol (*rac*-1) and the analogs containing substituents at the aromatic ring moiety, *rac*-1-(3-bromophenyl)-1-ethanol (*rac*-2) and *rac*-1-(3-methylphenyl)-1-ethanol (*rac*-3). Initially, it was performed a study of the kinetic resolution of *rac*-1, *rac*-2 and *rac*-3 in the presence of the lipase of *Pseudomonas fluorescens* in the free form, in hexane, *via* acetylation reaction, varying the temperature from 30 to 50 °C, according to the procedure described in the item 2.9. In all cases, at 40 °C, the conversions reached 50% in 2 h of reaction, leading to the respective products (*R*)-acetates and corresponding remaining (*S*)-alcohols with enantiomeric excesses values > 99% and E values > 200. Then, the performance of lipase from *Pseudomonas fluorescens* immobilized on magnetic nanoparticles (Fe_3O_4@APTES-GLU-PF) was evaluated for the kinetic resolution of *rac*-1, *rac*-2 and *rac*-3. The reactions were carried out in hexane at 40 °C, 250 rpm and using vinyl acetate as an acyl donor. Aliquots were regularly withdrawn to

monitor the reactions, which were analyzed by gas chromatography using chiral column. The results are summarized in Table 6.

Table 6. Kinetic resolution of *rac*-phenylethanol (*rac*-1), *ra*c-1-(3-bromophenyl)-1-ethanol (*rac*-2) and *rac*-1-(3-methylphenyl)-1-ethanol (*rac*-3), via acetylation, using lipase from *Pseudomonas fluorescens* immobilized on magnetic nanoparticles (Fe_3O_4@APTES-GLU-PF).[a]

Entry	Substrate	Time (h)	*e.e.*$_s$ (%)[b]	*e.e.*$_p$ (%)[b]	*c* (%)[c]	E[d]
1	*rac*-1	12	80	>99	45	>200
2	*rac*-1	24	91	>99	48	>200
3	*rac*-1	48	94	>99	49	>200
4	*rac*-2	12	61	>99	38	>200
5	*rac*-2	24	73	>99	42	>200
6	*rac*-2	48	79	>99	44	>200
7	*rac*-3	12	51	>99	34	>200
8	*rac*-3	24	69	>99	41	>200
9	*rac*-3	48	79	>99	44	>200

[a]Conditions: 5 equiv. of vinyl acetate and immobilized lipase: *rac*-alcohol (2:1) at 40° C and250 rpm.

[b]Determined by GC.

[c]Conversion, $c = e.e.s/(e.e.s + e.e.p)$.

[d]Enantioselectivity, $E = \ln[1 - c(1 + e.e.p)]/\ln[1 - c(1 - e.e.p)]$.

Lipase from *Pseudomonas fluorescens* immobilized on magnetic nanoparticles was more active against *rac*-phenylethanol (*rac*-1), since in 12 h of reaction the conversion reached a value of 45% (Table 6, entry 1) compared to values of 38% and 34% for analogs containing substituents at the aromatic ring moiety (Table 6, entries 4 and 7). In all cases, reactions were monitored for up to 48 h and conversion values showed a slight increase, culminating in 49% for *rac*-1 and 44% for both *rac*-2 and *rac*-3 (Table 6, entries 3, 6 and 9, respectively). It should be noted that the kinetic resolution of *rac*-1, *rac*-2 and *rac*-3 catalyzed by *Pseudomonas fluorescens* immobilized on magnetic nanoparticles was highly enantioselective with E values > 200. As for *rac*-indanol, the kinetic resolutions for *rac*-1, *rac*-2 and *rac*-3 led to the corresponding (*R*)-acetates and the remaining (*S*)-alcohols, following the Kazlauskas rule [76].

The stereocenters of the (*R*)-phenylethyl acetate and (*S*)-phenylethanol and analogs were determined by optical rotation using a polarimeter and the values obtained were compared with the literature. The value of specific optical rotation of (*R*)-phenylethyl acetate was $[\alpha]_D^{18}$ = +28.8 (c 0.5 $CHCl_3$); *e.e*. >99 %; while the value given in the literature is $[\alpha]_D^{25}$ =+43.0 (c 2.1 $CHCl_3$); *e.e*. 98 % [77]. For the (*S*)-phenylethanol the value obtained was $[\alpha]_D^{18}$ = -36.0 (c 0.5, $CHCl_3$); *e.e*. 94 % and the value reported in the literature is $[\alpha]_D^{20}$ = -45.4 (c 0.5, $CHCl_3$); *e.e*. 98 % [78]. The value of specific optical rotation of (*R*)-1-(3- bromophenyl)-ethyl acetate was $[\alpha]_D^{19}$= +84.6 (c 0.75, $CHCl_3$); *e.e*. >99 %, while the value given in the literature is $[\alpha]_D^{22}$= +85.0 (c 1, $CHCl_3$); *e.e*. >99 % [79]. For the (*S*)-1-(3- bromophenyl)ethanol the value obtained was $[\alpha]_D^{18}$ = -23.6 (c 0.7, $CHCl_3$); *e.e*. 79 % and the value reported in the literature is $[\alpha]_D^{24}$ = -31.7 (c 0.7, $CHCl_3$); *e.e*. 89 % [80]. The value of specific optical rotation of (*R*)-1-(3-methylphenyl)-ethyl acetate was $[\alpha]_D^{18}$= +36.6 (c 1.0, $CHCl_3$); *e.e*. >99 %, and the value given in the literature is $[\alpha]_D^{27}$= -37.8 for the (*S*)- enantiomer (c 1, $CHCl_3$); *e.e*. 85 % [81]. For the (*S*)-1-(3-methylphenyl)ethanol the value obtained was $[\alpha]_D^{19}$ = -50.2 (c 0.6, $CHCl_3$); *e.e*. 79 % and the value reported in the literature is $[\alpha]_D^{22}$ = -54.2 (c 0.6, $CHCl_3$); *e.e*. 94 %[80].

5 DESIGH OF LIPASE NANOPARTICLES BIOCATALYST AND IT USE IN THE KINETIC RESOLUTION OF MEDICAMENT PRECURSORS.

5.1 OBJECTIVES

5.1.1 General

- Developing a new nanohybrid material to be used for the kinetic resolution of *rac*-1-methyl-2-(2,6-dimethylphenoxy)ethyl acetate in different co-solvents.

5.1.2 Specifics

- Synthesizing Fe_3O_4 via co-precipitation method using ultrasound irradiation.
- Performing the surface modification of the Fe_3O_4 by APTES using ultrasound irradiation.
- Performing the surface modification of the Fe_3O_4 by PEI using ultrasound irradiation.
- Activating the terminal amino groups of Fe_3O_4@APTES and Fe_3O_4@PEI by glutaraldehyde for covalent enzyme immobilization.
- Promoting the immobilization of enzyme from *Thermomyces lanuginosus* on the magnetic supports by ionic exchange and by covalent attachment after the functionalization of the support with glutaraldehyde (GA).
- Characterization of the supports by X-ray powder diffraction (XRPD) and Vibrating Sample Magnetometer (VSM).

6 EXPERIMENTAL

6.1 Materials

The commercial TLL extract (15.83 mg of protein per mL)was obtained from Novozymes (Spain). 6 BCL agarose, 25%(v/v) glutaraldehyde solution, cetyl trimethyl ammonium bro-mide (CTAB) and p-nitrophenyl butyrate (p-NPB) were purchased from Sigma Chemical Co (St. Louis, MO, USA). The commercial preparation of TLL covalently immobilized on immobead-150 (TLL,250 U/g), branched-polyethylenimine (MW 10,000) and 3-amino-propyltriethoxysilane (>98%) were purchased from Sigma-Aldrich(St. Louis, MO, USA). $FeCl_3 \cdot 6H_2O$ and $FeSO_4 \cdot 7H_2O$ were supplied by Sigma-Aldrich and Vetec Chemistry, respectively. All others reagents and solvents used were of analytical grade.

6.2 Synthesis of Fe_3O_4 and functionalization with APTES

Metallic salts containing Fe^{2+}/Fe^{3+} were dissolved and mixed in Milli-Qwater in the molar ratio of 1:2 to form the spinel phase Fe_3O_4. Briefly, 5.82 mmol of $FeCl_2 \cdot 4H_2O$ and 10.57 mmol of $FeCl_3 \cdot 6H_2O$ were dissolved in a 50 mL of Milli-Q water. The aqueous mixture remained under vigorous ultrasound stirring when 10 mL of a solution of NH_4OH was added drop wise to form the precipitate, according with the proportion 1:8 (Fe^{n+}/ammonium). The precipitate was washed several times with Milli-Q water until the residual solution became neutral, followed by drying the magnetic nanoparticles. In the functionalization procedure, 100 mg of magnetite Fe_3O_4 were suspended in a beaker using 20 mL of ethanol and 20 mL of toluene. After that, 100 μL of APTES was added. The reaction system was subjected to vigorous ultrasonic stirring for 15 min at 50 °C. Finally, the nanocomposite formed was washed several times, dried and stored in a desiccator.

6.3 Synthesis of Fe_3O_4 and functionalization with PEI

Synthesis and functionalization of Fe_3O_4 SPMNs were performed in two steps, using a probe ultrasound (Ultrasonic Disruptor) with frequency of 20 kHz and power of 750 W. Initially, two solutions were prepared. The first was an iron salts solution (Solution A) and the second one, a PEI aqueous solution (Solution B). Solution A was composed of 1.16 g of $FeSO_4 \cdot 7H_2O$ and 1.85 g of $FeCl_3 \cdot 6H_2O$ dissolved in 15 mL of deionized water, whereas, solution B was consisted of 1.0 g of PEI in 4.0 mL of deionized water. Firstly, the solution A was sonicated for 4 min, until it reaches the

temperature of 60°C. Then, 7.0 mL of concentrated NH_4OH were added, under sonication, using a burette. Thereafter, the color of solution A changed from orange to black, evidencing the formation of Fe_3O_4 SPMNs. After 4 min, solution B was added to the reaction medium, which remained for more 4 min under sonication.

To remove the excess of NH_4OH and unbounded functionalizing agent, the resultant Fe_3O_4 were washed several times with distilled water and precipitated with acetone. Then, the Fe_3O_4 were dispersed in water and centrifuged for 10 min and 3000 rpm to remove the weakly functionalized SPMNs. Finally, Fe_3O_4@PEI were dried under the vacuum. The procedure used in the reference is similar to the one for Fe_3O_4@PEI.

6.4 Activation of Fe_3O_4@APTES and Fe_3O_4@PEI with glutaraldehyde (GA)

In this procedure, 25 μL of glutaraldehyde are placed in direct contact with 10 mg of dry superparamagnetic support. The mixture was kept under agitation for 2 h at 25°C. Finally, supports were washed 3 times with phosphate buffer (25 mM and pH 7) to remove the excess of glutaraldehyde. The support was named Fe_3O_4@APTES-GA and Fe_3O_4@PEI-GA.

6.5 Characterization of the supports and biocatalysts

6.5.1 X-ray powder diffraction (XRPD)

The structural analysis and verification of single-phase nature of the samples were studied using XRPD. The measurements were carried out using Rigaku X-ray diffractometer equipped with CoKa radiation tube (λ= 1.7889 Å) operated with voltage of 30 kV and current of 15 mA. The phase identification analysis was performed by comparing powder diffractograms with standard patterns from the International center for diffraction data (ICDD). Rietveld refinement procedure [98] was performed to all diffraction patterns using the DBWS 2.25. The crystallite sizes of nanoparticles were calculated from the XRPD data using Scherrer's equation [84].

6.5.2 Magnetic characterization

The magnetic characterization at room temperature was obtained using a vibrating sample magnetometer (VSM) Lakeshore 7400, with maximum magnetic field amplitude of 17 kOe. The

VSM has been previously calibrated using a pure Ni sample. Thus, after measuring the mass of each sample, the respective magnetization is given in emu/g. 2.5.3.

6.6 Immobilization procedure

6.6.1 Covalent immobilization of lipase on Fe_3O_4@APTES-GA or Fe_3O_4@PEI-GA

The TLL was immobilized on Fe3O4@APTES-GA or Fe3O4@PEI-GA in batch mode, producing the biocatalysts Fe3O4@APTES-GA-TLL or Fe3O4@PEI-GA-TLL. For this purpose, the support (100 mg) was suspended in 10 mL of 25 mM sodium phosphate buffer at pH7 solution containing the lipase (enzyme load: 3 mg/g support) and 0.01% (v/v) CTAB at pH 7.0 [27]. The immobilization process was carried out at 25◦C for 1 h under constant agitation. The magnetic NPs containing immobilized TLL were removed by magnetic separation and washed with 25 mM sodium phosphate buffer at pH 7.0. The amount of TLL immobilized on the previously activated supports was determined by measuring the initial and final concentration of TLL in the supernatant of the immobilization suspension. The immobilization procedures in SPMN were schematized in Fig. 1.

6.6.2 Ionic immobilization of lipase on Fe_3O_4@APTES or Fe_3O_4@PEI

The immobilization procedure was performed by contacting 100 mg of Fe_3O_4@APTES or Fe_3O_4@PEI with 10 mL of enzyme solution (enzyme load: 3 mg/g support) in 5 mM sodium phosphate buffer at pH 7.0 (immobilization by means of ionic exchange) in batch mode, producing the biocatalyst Fe_3O_4@APTES-TLL or Fe_3O_4@PEI-TLL. The immobilization process was similar to that described in the previous section (Fig. 1).

7 RESULTS AND DISCUSSION

7.1 Characterization of the nanohybrid biocatalyst

Lipase from *Thermomyces lanuginosus* (TLL) was immobilized on Fe_3O_4@APTES support and used for the kinetic resolution of *rac*-1-methyl-2-(2,6-dimethylphenoxy)ethyl acetate in different co-solvents (acetonitrile, isopropanol, ethyl ether and tetrahydrofuran) (Fig. 26). The production of enantiomerically enriched chiral alcohols have high added value and are used as building blocks in the synthesis of various biologically active compounds. Specifically, the chiral alcohol 1-(2,6-dimethylphenoxy)propan-2-ol, when submitted to other reactions with exchange of the hydroxyl group by an amino group, leads to the formation of enantiomerically pure drug (*R*)-Mexiletine[(2R)-1-(2,6-dimethylphenoxy)propan-2-amine]. Mexiletine in its racemic form is an antiarrhythmic agent, but in enantiomerically (*R*)- enriched form is a compound able to block the sodium channels and has its activity enhanced [107].

Figure 25. General scheme for the use of lipase from *Thermomyces lanuginosus* for the kinetic resolution of *rac*-1-methyl-2-(2,6-dimethylphenoxy)ethyl acetate.

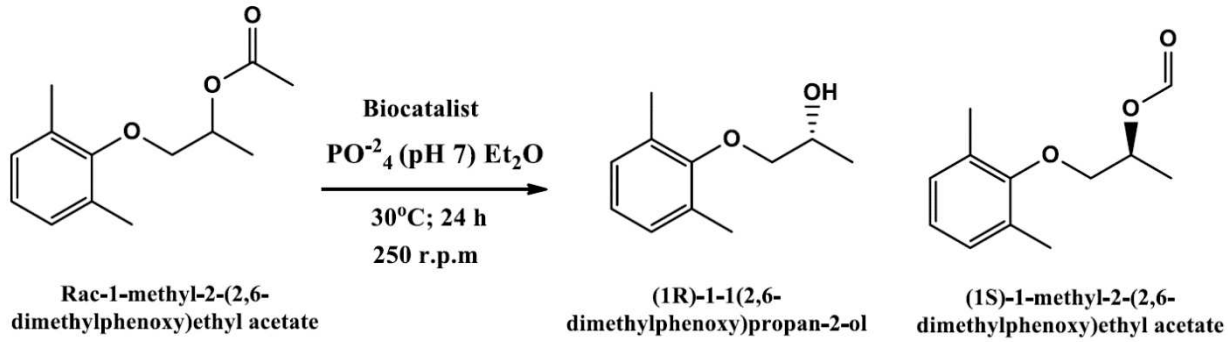

Source: Author

Two parallels methods to immobilize the lipase were performed: the first one by ionic exchange and the second one by covalent attachment after the functionalization of the support with glutaraldehyde (GA). The results were compared with those obtained with the immobilization of the same enzyme using Fe_3O_4@PEI as support. Figure 25 presents the immobilization procedures of TLL by ionic exchange or by covalent attachment in Fe_3O_4 recovered with branched-polyethylenimine (PEI) and APTES. Figure 26 presents the general procedure for ionic and covalent immobilization of TLL enzyme on magnetic NPs supports.

Figure 26. The immobilization procedures of TLL by ionic exchange or by covalent attachment in Fe_3O_4 recovered with PEI or APTES.

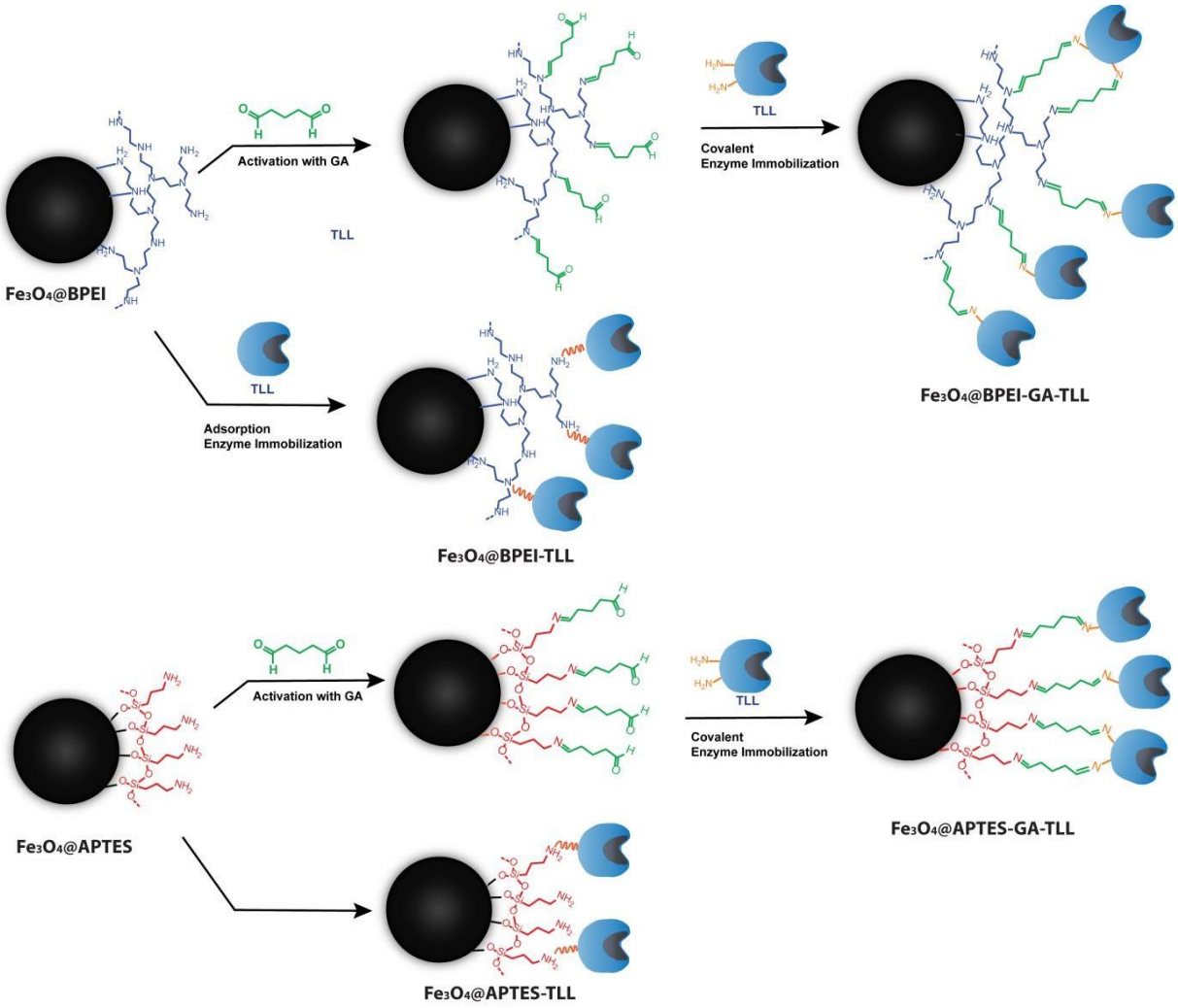

Source [4]

7.2 XRPD analysis

XRPD analyses were used to confirm the formation of crystalline phase and to verify the structural parameters of the magnetic nanoparticles. Figure 27 presents the XRPD results obtained for the investigated samples.

Figure 27. XRPD results for the investigated samples.

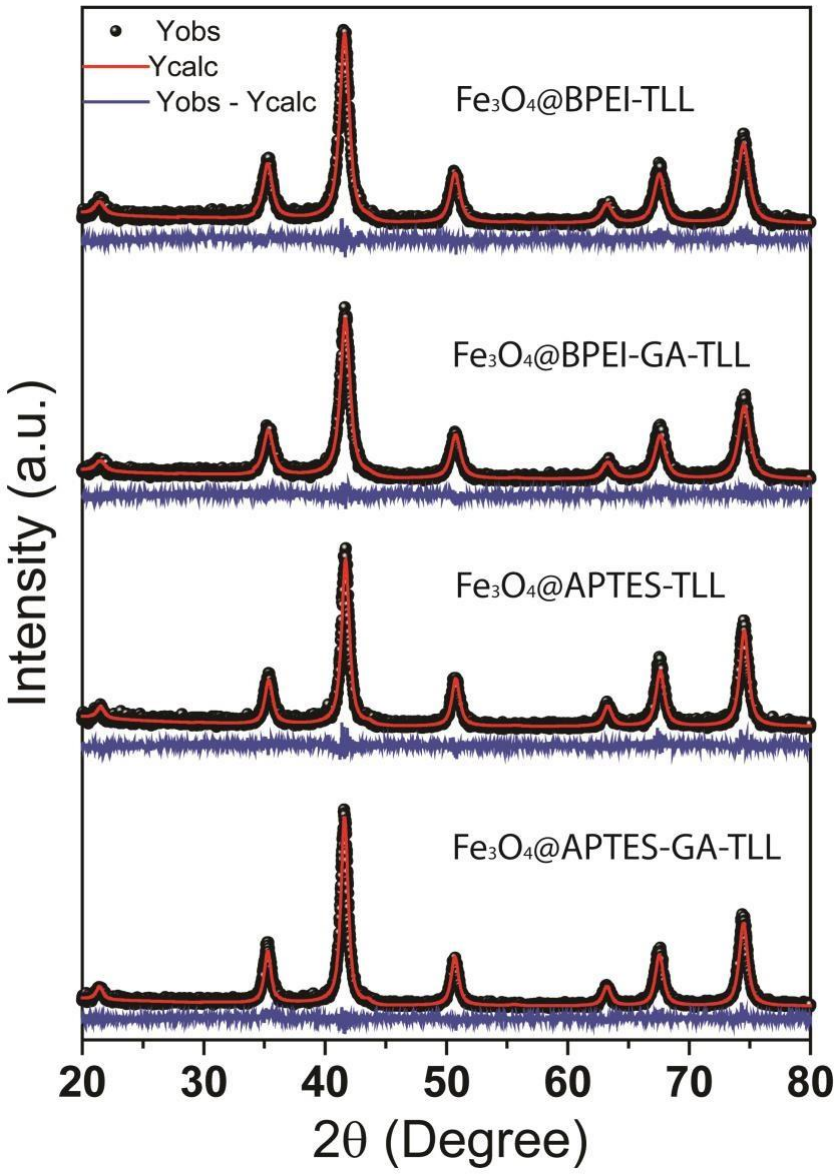

In particular, the blue line represents the relative difference between the experimental (Y_{Obs}, black dots) and the calculated (Y_{Calc}, red line) intensities obtained through the refinement. By comparison with the Inorganic Crystal Structure Database (ICSD) and the refinement, it was possible to confirm the formation of a single phase of Fe_3O_4(ICSD/PDF-08-4611) for all samples. The indexation of the peak with the diffraction patterns also showed the formation of inverse spinel ferrite with spatial group Fd3M. The values obtained from Rietveld method were summarized in Table 7.

Table 7. Structural parameters obtained from Rietvield refinement.

Sample	XRPD				VSM
	Lattice parameters (a) (Å)	R_{wp} (%)	S	Average crystallite size (nm)	Ms (emu/g)
Fe_3O_4@APTES-GA-TLL	8.367 (1)	15.7	0.93	15 ± 0.31	63.4
Fe_3O_4@APTES-TLL	8.369 (4)	18.9	0.92	15 ± 0.29	65.5
Fe_3O_4@PEI-TLL	8.365 (5)	15.2	0.91	11 ± 0.18	60.5
Fe_3O_4@PEI-GA-TLL	8.366 (2)	14.8	0.93	10 ± 0.17	56.0
Fe_3O_4	8.358 (2)	13.58	1.00	12.1 ± 0.20	56.7

The refinement converged satisfactorily to weighted profile R-factor (R_{wp}) and S(∼1) values [109]. The average crystallite size was calculated from Scherrer´s equation, which relates the crystallite size with the half-width of the diffraction peak [84,84]. The samples presented values below of 15 nm, indicating the presence of SPM phenomena [99]. It is possible to observe that the samples covered with PEI obtained small crystallite size. During co- precipitation procedure, a process of nucleation followed of the growth of crystal occurs. The insertion of PEI right after the precipitation should prevent the continuity of the crystal growth, providing magnetic nanoparticles with reduced size.

7.3 Magnetic measurement

The VSM analysis was performed to investigate the magnetic properties of the samples. Figure 28 presents the magnetization curves at room temperature obtained for the produced samples.

.**Figure 28.** Magnetic curver for all samples.

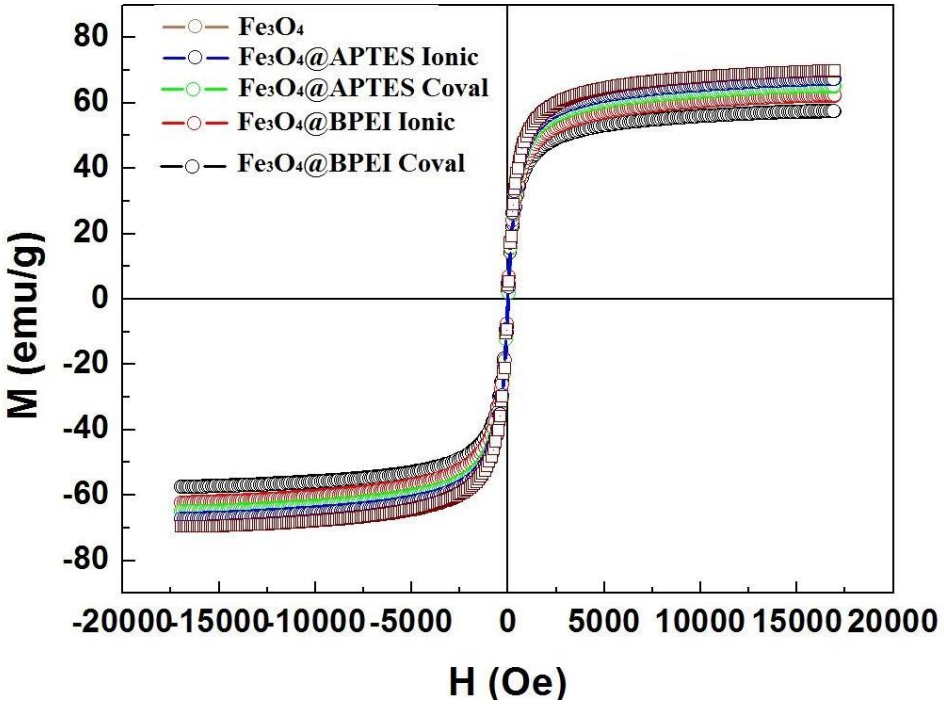

In particular, the values of saturation magnetization (M_S) for the Fe_3O_4@PEI-GA-TLL, Fe_3O_4@PEI-TLL, Fe_3O_4@APTES-GA-TLL and Fe_3O_4@APTES-TLL and Fe_3O_4 were 56.0, 60.5, 63.40, 65.5 and 56.7 emu/g, respectively. The increase of M_S values indicates the decrease of total mass of the functionalized agent anchored on the nanoparticle surface for the immobilized samples. In general, the magnetic curves show a greater amount of mass for the samples covered with PEI. As higher the amount of anchored mass, greater the number of amino groups available for enzyme immobilization. However, the sample Fe_3O_4, which were not functionalized or immobilized, presented a second lowest value of MS. This increase in the M_S values after functionalization were already reported in the literature [110,111] and is due to the increasing of crystallization of the nanoparticle surface, which is a consequence of the bond between Fe atoms at the surface and amine groups of PEI and APTES [110,112]. The room temperature M_S values obtained for all samples are smaller than the one reported bulk Fe_3O_4, which is of 70 emu/g [113]. This result confirms the surface modification process of magnetite. Moreover, according to the magnetic curves obtained at 300 K, it is verified that the curves do not present hysteresis, i.e., coercive field and remanent magnetization equal to zero, a signature of the SPM behavior of the samples.

7.4 Kinetic resolution of *rac*-1-methyl-2-(2,6-dimethylphenoxy)ethyl acetate

The nanohybrid biocatalysts were used for the kinetic resolution of of *rac*-1-methyl-2-(2,6-dimethylphenoxy)ethyl acetate. The results obtained for the kinetic resolution in different solvent are present in table 8.

Table 8. Enzymatic kinetic resolution carried out with *rac*-1-methyl-2-(2,6- dimethylphenoxy)ethyl acetate.

Entry	Biocatalyst	Co-solvent	$e.e._p$(%)	c (%)	E
2	Fe_3O_4@APTES-GA-TLL	Ethyl ether	99	10	221
3	Fe_3O_4@PEI-GA-TLL	Ethyl ether	99	34	327
4	Fe_3O_4@APTES-TLL	Ethyl ether	99	16	238
5	Fe_3O_4@PEI-TLL	Ethyl ether	99	50	1057
6	IMOBED 150-TLL	Ethyl ether	99	50	1057
7	Fe_3O_4@APTES-TLL	-	99	3	205
8	Fe_3O_4@PEI-TLL	-	99	6	211
9	Fe_3O_4@APTES-GA-TLL	Acetonitrile	99	17	13
10	Fe_3O_4@PEI-GA-TLL	Acetonitrile	99	17	242
11	Fe_3O_4@APTES-TLL	Acetonitrile	99	15	237
12	Fe_3O_4@PEI-TLL	Acetonitrile	99	34	328
13	Fe_3O_4@PEI-GA-TLL	IPA	68	17	6
14	Fe_3O_4@PEI-TLL	IPA	99	11	223
15	Fe_3O_4@PEI-TLL	THF	99	50	1057

For the Fe_3O_4@PEI-TLL, the conversion values were 50%, the enantiomeric excess of the product was >99% and the enantiospecificity was 1057 using tetrahydrofuran (THF) or ethyl ether as co-solvents (Table 9, entry 5 and 15). These results were same as those obtained with the commercial biocatalyst IMOBED 150-TLL (Table 8, entry 6). The other biocatalysts present conversion values between 3 and 34% and enantiomeric excess of the product of >99%, with enantiospecificity >200, excepting the Fe_3O_4@PEI-GA-TLL in the presence of isopropanol (IPA) which had low enantiomeric excess of the product (68%) and low enantiospecificity (6), and Fe_3O_4@APTES-GA-TLL in presence of acetonitrile which had low enantiospecificity (13). The hydrolysis reaction in an

aqueous medium occurred only in the presence of the biocatalysts immobilization by ionic adsorption (Fe_3O_4@APTES-TLL and Fe_3O_4@PEI-TLL). These reactions led to high values of enantiomeric excess of the product >99%, but with low reaction rates that drove to low conversion value (3–6%) and enantiospecificity above 200, Table 8 entries 7 and 8, respectively. All the five prepared biocatalysts were evaluated in the kinetic resolution of the *rac*-1-methyl- 2-(2,6-dimethylphenoxy)ethyl acetate (at 30◦C during 24 h) in presence of four different co- solvents (acetonitrile, isopropanol, ethyl ether and tetrahydrofuran) and without co-solvent. However, for the cases where there was no reaction, the results were not shown in Table 8. The Fe_3O_4@PEI-TLL was the only biocatalyst that presented catalytic activity in the five conditions of reaction (with and without co-solvent).

8 INTRODUCTION TO DRUG DELIVERY

8.1 Cancer

Cancer is major public health problem worldwide and one of the leading causes of death in developed countries with approximately 9.6 million deaths in 2018 [114]. The term cancer refers to the uncontrolled growth and spread of abnormal cells in the body due to the production of growth signals by the cell and its insensitivity to anti-growth signals [115]. The constant multiplication of the cells, in turn, occurs along with the formation of new blood vessels for the tumor irrigation, and all these events can be triggered by external and internal factors acting in a correlated way [13, 14].

External causes are mainly due to the exposure to risk factors present in the environment, such as food, pesticide exposure, infections, radiation, pollution and lifestyle. In this case, it is possible to relate the appearance of the disease, with the intensity and duration of exposure of the cells to the causative agents of cancer [118]. Internal factors, in turn, are related to the heredity or the ability of the body to react to external aggressions [117]. In this sense, it is possible to perceive how the dietary habits of the developed countries, together with the high exposure to the risk factors, have promoted an increase in the number of cancers in these countries. In US, for example, cancer accounts for one quarter of the deaths. On the other hand, although developed countries have the highest incidence of the disease, they are not those with the highest number of deaths. Figure 29 shows the map of countries by cancer. Lighter colors correspond with lower mortality-to-incidence ratio MIR. In general, cancer MIR was higher in middle/low-in-come countries. Western Europe, Oceania and North America have the lowest MIR. This is due mainly to greater access to diagnostic and treatment compared with the least developed countries [119].

Figure 29. Color-coded map of age-adjusted MIR for all cancer types.

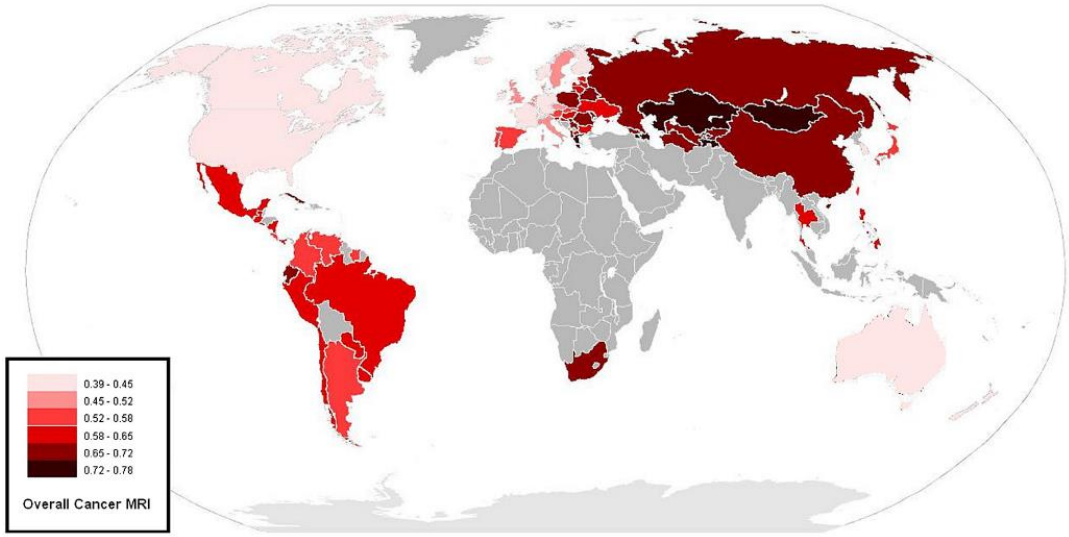

Source [119].

There are many forms of diagnosis and treatment for the cancer. The most common forms of treatment include surgery [17, 18], radiotherapy [122], and chemotherapy [123]. Oncologic surgery refers to the removal of tumors and tissues, and may vary widely for each case, being applied in a curative or palliative way. The treatment may be considered curative, when it is indicated for the removal of solid tumors and surrounding tissues during the early stage of the disease. The removal of the tumor is considered effective, when there is no metastasis, ie the spread of the cancerous cells beyond where it was started [124]. Metastasis can occur when cancer cells travel through the bloodstream or lymphatic vessels to other areas of the body. The removal of the surrounding tissue, in turn, occurs according to a safety margin and may vary according to the location and histological type of the tumor.

Radiation therapy consists of exposing the cancer cells to a pre-calculated dose of ionizing radiation [125]. The efficiency of this technique depends on some factors, especially for the degree of differentiation and sensitivity of the tumor to radiation. When the tumor shows a similar degree of sensitivity to the normal tissues in its vicinity, radiotherapy is not indicated because it causes damage to both tissues [125].

Chemotherapy consists of the use of chemotherapeutics for the destruction of neoplastic cells, preserving the normal ones [126]. Most anti-neoplastic agents end up acting on the non- specific way, acting on normal and malignant cells indiscriminately [127]. In general, these chemotherapeutics act on rapidly multiplying cells, damaging normal cells of the capillaries, gastrointestinal and the

digestive system. This unwanted action results in the appearance of side effects such as hair loss, nausea and compromised immune system. For a greater efficiency of this technique, it is necessary once again that the diagnosis and the treatment be initiated in the early stages of the disease [128]. For example, when the chemotherapy uses high concentrations of chemotherapeutic drugs, it can destroy up to 99.9% of cancer cells during each cycle of therapy. This means that the repetitive action can lead to the complete destruction of a tumor of about 1 g (109 cells) in a few cycles. However, in advanced stages of the disease, for tumors with mass over 100 g (1011 cells), there would be still large tumor cells in the body.

For a drug to achieve the desired effects, it must arrive at its destination with concentration and speed capable of producing the minimum of side effects and achieve maximum therapeutic action [129]. There are numerous systems available for administering of drugs in the body, whether through the use of traditional methods or those that use controlled drug delivery. Conventional methods for administering drugs consist in the application of injections, tablets, capsules, oral formulations containing solutions or suspensions, creams and ointments, among others [4]. The administration of parenteral drugs, in turn, it is highly invasive with ephemeral effects and consists of the intradermal, subcutaneous, intramuscular and intravenous administration. The oral administration has been widely used due to it ease ingestion, versatility to accommodate many types of drugs and the pain avoidance [130]. However, this modality of administration have some restrictions such as the use of proteins and peptides and due to their low absorption by the digestive tract [131]. On the other hand, utopic use has localized and superficial effects. In any case, the choice of the form of administration will depend on the purpose to be achieved. It is important to note, that traditional drug delivery methods rapidly release drugs into the body, resulting in rapid fluctuation of the concentration of substance in a short period of time [4]. In this case, super- dosage peaks may occur resulting in toxic effects to the patients. In addition, repeated administration of the drug is often necessary in order to keep the drug in the therapeutic concentration. Figure 30 shows the drug release kinetics in traditional methods, compared to an ideal situation with controlled delivery.

Figure 30. Drug levels in the plasma released from traditional release system, a combination of multiple oral capsules or injection dosing (blue dashed curve), and controlled release system (red continuous curve)

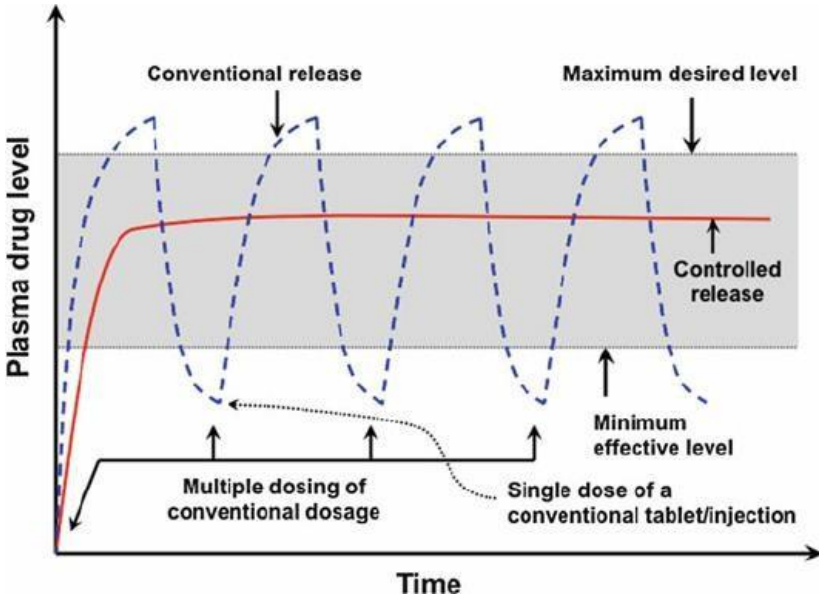

Source [132]

In the traditional method of drug administration, the chemotherapeutic agent reaches and rapidly decreases its maximum concentration, requiring repeated doses to be in the ideal concentration (blue dotted line). In the vectored delivery method, the concentration of the drug remains constant throughout the delivery process (Fig. 30).

In the case of antineoplastic[1] drugs used in cancer chemotherapy, other issues still need to be considered. In addition to the lack of chemotherapeutics specificity in their antineoplastic action, the great majority of them have high cytotoxicity [4]. Doxorubicin for example, is a drug widely used in chemotherapy, acting from the inhibition of DNA and RNA biosynthesis by the cell. Despite the proven success in the treating of numerous types of cancers, it has toxic side effects such as cardiotoxicity, myelosuppression, mucositis, and alopecia, limiting it clinical application, due to it nonspecific distribution to healthy normal tissues [133].

Another important feature for a neoplastic agent is its bioavailability, ie the drugs must be able to overcome the barriers of the immune system to reach the target in sufficient concentration to take effect [4]. In general, about 40% of the pharmacologically active molecules discovered are rejected, mainly due to the reduced solubility and bioavailability.

In addition to bioavailability, some antineoplastic drugs have low solubility in blood plasma. Paclitaxel, for example, is among the first clinically successful chemotherapeutic agent

approved by the Food and Drug Administration (FDA). This substance is an anticancer drug widely used for the treatment of various forms of cancers, such as solid tumors of breast, brain, ovary and lung. Due to its low solubility in water, its administration requires that they be solubilized by two substances: Cremophor and ethanol [134]. However, the use of Cremophor have presented adverse effects on the body [134]. On the other hand, researchers have showed that the use of paclitaxel formulations encapsulated in nanoparticles have a 13- fold greater efficiency than the use of solubilized free drug. In this case, the development of a controlled drug delivery system has proven to be an important strategy for cancer therapy, but for this to happen, its needed to understand how occurs the interaction of the drugs with specific receptors at the site of action.

8.2 Drug delivery

Nanomedicine aims at the development of controlled release systems of drugs to a specific target and in the appropriate concentration (intelligent drug), in order to increase the effectiveness of the treatment and reduces side effects [135]. These systems offer numerous advantages when compared to the traditional methods of drug administration such as dose reduction, selectivity in relation to the biological target, controlled release avoiding super dosage peaks and reduced side effects [136]. In addition, the miniaturization of drug carriers at the nanoscale improves the drug stability, the solubility and absorption, facilitating the delivery of the drug to the various barriers in the body, such as the blood-brain barrier [4].

The use of nanocapsules may also prevent foreign body reactions, increasing local and systemic tolerance, and preserving healthy cells around the tumor, minimizing secondary side effects. Besides that, the controlled drug delivery can help to overcome multidrug resistance, which occurs mainly, when the cancer is in advanced stages. For all of these reasons, these controlled liberation systems have been widely used for the treatment of numerous diseases, including cancer [137].

At the beginning of the 20th century, the German hematologist Paul Ehrlich developed the concept of Magic Bullet [138]. He noted that only some tissues were blushed after an intravenous injection of dyes into the rabbits. This led him to believe that cells should have specific receptors capable of binding to some substances. These cell recognition structures, he called sidechains, and would be produced by cells from the recognition of a foreign body or toxin. He imagined that the excess side chains (antitoxins) would be dumped into the bloodstream in order to constitute the defense mechanism of the body. The works of Ehrlich was pioneering and fundamental to laying the foundations of the immunology as a science by intuitively introducing concepts such as antigen and antibodies [138].

Today, its known that cells have structures for the recognition of substances necessary for their operation. These substances are commonly proteins, whose it presence is often high in cancer cells, or in other cells, in response to the presence of cancerous tumors [139]. The understanding of this mechanism can be a strategy for the fight against numerous diseases, from the development of intelligent systems for the vectorization of drugs.

A drug delivery system must be biocompatible or present low cytotoxicity in relation to the desired benefit. It is called biocompatible, when the cells do not present a toxic response when in contact with the drug, such as allergic reactions, irritations, inflammations, mutagenic or carcinogenic background [11, 12]. When this does not occur, the system has some toxicity. The evaluation of the toxicity of a medicinal product should consider the benefits that will be brought to the patient, in relation to the possible toxicological effects, ie, the benefits must overcome the possible side effects. One way of assessing the cytotoxicity of a material is to add it into a culture of cells grown in the laboratory (in vitro test) and compare the cell growth over time, in relation to another group of cells growing without the presence of the material. $HeLa^2$ cells are the oldest and most commonly used human cell line for this test [142].

For the cytotoxicity essays of drugs nanocarriers, it is still necessary to introduce a fluorescent agent that can be incorporated into the nanoparticles. This incorporation can occur via surface reactions or through the drug encapsulation or its dispersion in the nanocarrier matrix. Dyes adsorbed to the surface, however, may be prone to desorption or even alter the biological response [143]. Another important feature of a carrier system, especially for intravenous applications, it is their solubility in the blood plasma. An insoluble nanocarrier system represents a serious risk of clogging of blood vessels.

One of the most used ways to target a drug is to encapsulate it by biocompatible substances that have some affinity with the cellular receptors, in order to guarantee their absorption. The two major mechanisms of drug release are by diffusion or erosion. In the first case, the active ingredient flows through the walls of the carrier system by means of a concentration gradient. The other way is to release the drug from the degradation of the carrier system, which may occur by the action of enzymes, by the defense mechanisms of the organism or by the very nature of the carrier [14, 15]. In all cases, there are numerous formulations available such as the use of liposomes, polymer nanoparticles, cyclodextrins, dendrimers, among many others. Liposomes are small, biocompatible and biodegradable stable lipid vesicles consisting of phospholipids separated by an internal aqueous compartment, with sizes ranging from 50 to 1000 nm. In addition, they can be differentiated also by the composition, electrical charge of the surface and structure. Another characteristic of liposomes is that they are spontaneously organized when hydrated in aqueous medium [146]. These

compartments, in turn, can encapsulate hydrophobic drugs inside them in order to be carried, as in the case of some antineoplastic drugs. The hydrophilic drugs can be encapsulated in both the retained aqueous volume and the bilayer interface, thus being protected from extraliposomal reactions that may alter the properties of encapsulated drugs. The main routes of administration of the liposomes are intravenous, intraperitoneal, ophthalmic and subcutaneous [146].

8.3 Polymeric nanoparticles

The development of an efficient mechanism for the controlled delivery of a medicament depends on the selection of an appropriate carrier agent capable of controlling the release of the drug, maintaining the therapeutic action for a longer period. Among the many options, polymers are more versatile and promising carrier agents to perform such function. In this session, its will focus on the use of polymers to synthesize nanocarriers for the antineoplastic drugs.

Polymer nanoparticles have a diameter of less than 1 micron and differ in nanocapsules and nanospheres. The term nanocapsules, refers to a polymeric shell disposed around an oily core (reservoir systems). The oily core, in turn, may serve as a delivery medium for hydrophobic drugs. On the other hand, nanospheres are systems where the drug are homogeneously dispersed or solubilized within the polymer matrix (monolithic systems). In this case, it is not possible to identify a differentiated nucleus, which can be solid or liquid (Fig. 31).

Figure 31. Difference between nanocapsule and nanosphere for drug release

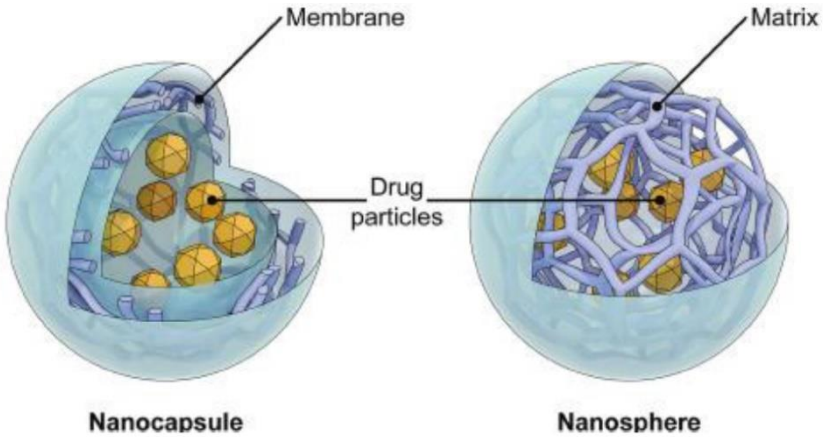

Source [147].A polymer is a substance with high weight molecule, composed of repeated structural units called monomers, bounded by covalent chemical bonds. Polymers which are formed

from a single type of monomers are called homopolymers. For example, the polystyrene (PS), is an aromatic polymer obtained from the polymerization reaction of styrene monomers (Fig. 32).

Figure 32. Polymerization reaction of styrene for the polystyrene formation.

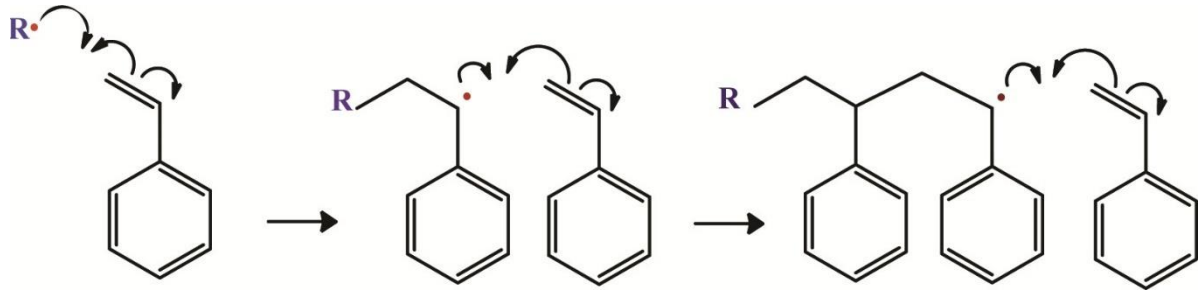

Source: Author

PS is hardly biodegradable, facilitating its use also in the food, medical product and devices industry. It is also used for disposable trays, plates, bowls and cups, for food storage and transport, but also for containers of non-food articles such as cosmetics, pharmaceuticals and cleaning agents [148]. Due to its physical inertness, biocompatibility and its ability to form stable colloids in biological fluid, PS nanoparticles has been also used as nanocarrier of hydrophobic drugs. Cornelia Loos et. al, for example, carried out internalization tests of PS nanoparticles with and without surface modified in cancer cells [18]. The studies have shown that both, macrophages and THP-1 cells rapidly internalized PS-COOH and PS-NH_2 nanoparticles with size of 110 nm. They also show that the uptake of 100 nm particles was 2.3-fold greater than that of 50 nm particles.

The drug release technology has progressed over the last six decades, since the first sustained release formulation in 1952 by Smith Kline & French [149]. The first generation of drug delivery was devoted to the production of oral and controlled release system for transdermal patches, besides of the establishment of mechanisms for controlled release, including dissolution, diffusion, osmosis, and ion exchange-based mechanisms. During the 2nd generation, it was introduced the concept of "smart" polymer and hydrogels. These systems were able to release drugs by changes in environmental factors, such as pH, temperature, or glucose. The last years of second generation was dedicated to the development nanotechnology-based carrier systems. Now, we are living the 3nd generation with the modulated delivery systems and, with the possibility to delivery the drugs for long-terms [149].

The future of drug delivery depends on the development of new technologies. In this sense, the recent advances in polymer chemistry have allowed the improvement of polymerization

techniques that allow the synthesis of polymers with defined structure, size distribution, and tunable properties.

8.4 Miniemulsion

In the last decades, the miniemulsion technique has been developed for the synthesis of materials in nanoscale [150]. This technique greatly enhances the possibilities for preparing hybrid nanomaterials by encapsulating molecular compounds, liquids, or solid material. The miniemulsion consists on the mixing of two immiscible systems (water and oil), forming stable droplets finely dispersed in a second continuous phase [151].

According to Landsfester et. al, emulsions are dispersed systems with liquid droplets (dispersed phase) in another non-miscible liquid (continuous phase) [152]. These systems are generally very unstable and the tendency is for their destabilization and consequent breakdown of the emulsion due to degradation by molecular diffusion (Ostwald ripening) or coalescences of small dispersed droplets. To prevent this from happening and to form a stable system of small particles (miniemulsion), it is necessary to introduce a surfactant to the dispersed phase. In 1962, Higuchi and Misra studied the rate of growth of large droplets and the dissolution of small droplets in an emulsion [153]. According to the authors, the ripening rate of Ostwald depends on some factors such as the size of the droplets, the polydispersity, and the solubility of the dispersed phase in the continuous phase. In this case, the more hydrophobic the dispersed phase, the slower the exchange of liquid mass between the droplets. Thus, the use of a third "ultra-hydrophobic" agent can ensure additional stability or complete stabilization of the system.

The formation of a miniemulsions begins with the homogenization of the dispersed phase with the continuous phase, to form a system with small droplets with narrow range of size distribution. These very small droplets are formed by application of high shear forces which can be produced by the use of ultrasound radiation [150]. The discovery of ultrasound occurred in 1880 by studying the Curie piezoelectric effect. In 1894, Thornycroft and Barnaby found that in the propulsion of missiles launched by the destroyer, a source of vibration was generated causing implosion of the bubbles and/or cavities in the water. This vibration is currently known as cavitations [154]. Like any sound wave, it is transmitted as a series of compression and rarefaction cycles affecting the molecules of the liquid. When the negative pressure of the rarefaction cycle exceeds the attractive forces between the molecules of the liquid, a cavity is originated. This void in the liquid phase takes a small amount of vapor from the solution. There are many thousands of such bubbles in the liquid. Some of the mare relatively stable, but others expand further to an unstable size. This causes a violent collapse and

generate temperatures about 5000 K and pressures of the order of 2000 atm [155]. These small droplets formed in the miniemulsion, might be used as a nanoreactor for polymerization reaction and as a vehicle for hydrophobic drugs. The miniemulsion technique has a great influence on the preparation of (functional) polymeric nanoparticles [143]. Figure 33 presents an example of a miniemulsion polymerization process consisting of an aqueous surfactant solution (majority phase) and a monomer phase (organic phase).

Figure 33. Miniemulsion polymerization process.

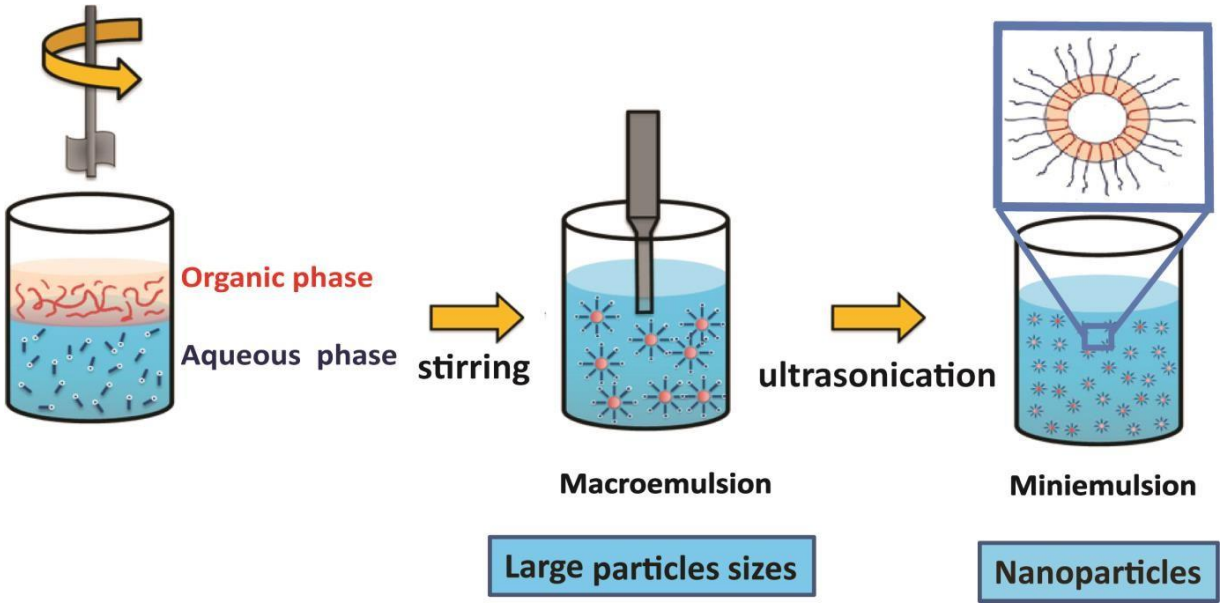

Source: adapted from “Solar Paint: From Synthesis to Printing” [156].

Initially, the mixture remains under mechanical stirring for homogenization. After a few minutes, the system is placed under vigorous ultrasonic irradiation for the formation of nanoparticles.

8.5 Target drug delivery via folate receptors

There are many different types of cancers, depending on the site of occurrence and cell. This disease is classified according to normal cell type that originated it. This is what can be called the primary classification. In this case, the most common sites for cancer to develop include ovarian, skin, lungs, breasts, prostate, colon and rectum cancer. According American Cancer Society, ovarian cancer is the fifth cause of cancer-related death in women with 22,440 new cases in 2017 only in the U.S [114]. The prognosis of cancer patients depends on time of the accuracy of finding the primary and any dormant metastasis sites. Disease-related mortality can be significantly reduced in many cases, when metastatic sites are found and treated during the early stage. Breast cancer, for example, has a survival rate of 95% when treated in zero and I stage, falling to 85% in II stage and only 20% for IV stage tumors [157]. In this case, the sooner the diagnosis and treatment of the disease occur, the greater the chances of cure.

An ideal drug delivery system should be able to concentrate the release of the chemotherapeutic agent into the focus of the disease (vectorized system). The most important approach is based on the fact that some solid metastatic tumors exhibit increased permeability of blood vessels in the tumor region compared to healthy cells. This phenomenon is known as enhanced permeability and retention (EPR effect) [115]. This increased permeability, associated with increased vascularization of the tumor region and with the decreased lymphatic drainage, it is a strategy for delivering antineoplastic agents. The EPR effect may favor the accumulation of polymer-based carrier systems when they meet certain requirements, such as being small enough to pass through the gaps of the tumor vascular system and large enough to avoid it escape of tumor (50-150 nm). It should also have high bioavailability in order to remain for a long time in circulation, allowing repeated action of accumulation in the tumor region [115]. Figure 34 shows how accumulation of macromolecules in solid tumors occurs due to the EPR effect.

Figure 34. Schematic representation of accumulation of macromolecules in solid tumors due to the EPR effect (red dots, LMW drug; blue line, macromolecule; nanoparticles are supposed to accumulate in the same way as macromolecules).

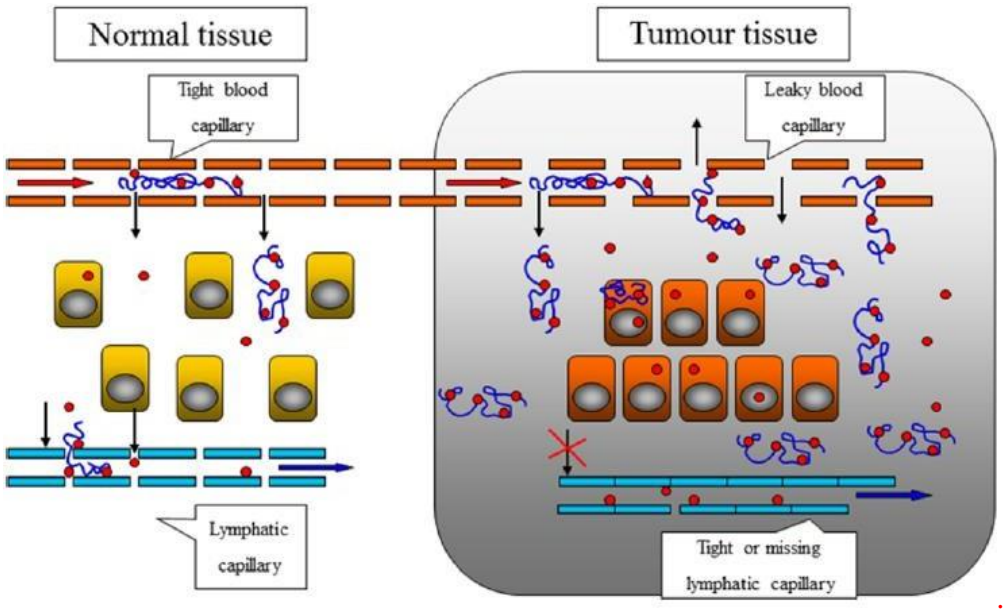

Source [158]

Now, that the transporter system is in the tumor region, the delivery of the drug can occur of two ways: passive or active. On passive delivery, the drug is released in the region external to the tumor, and, as discussed earlier, this can occur due to several factors, such as the degradation rate of the polymers or due to a concentration gradient, among others. In the active release, the delivery can occur directly inside the cancer cells, but for this, it is necessary that the carrier system has some affinity with the cancerous cells, and this can occur, due to the presence of specific ligands in the carrier such as proteins, glycoproteins or lipoproteins. Another way of achieving a binding of the carrier system to tumors can be through ligands that bind strongly to a cell wall receptor such as saccharides, lectins, antibodies and antibody fragments, peptides, enzymes or enzyme inhibitors. Figure 36 presents an example of active drug release.

Figure 35. Example of active drug target of chemical ingredient into the cancer cell. Active targeting of drug delivery system to tumor cells and subsequent mechanisms of intracellular drug release.

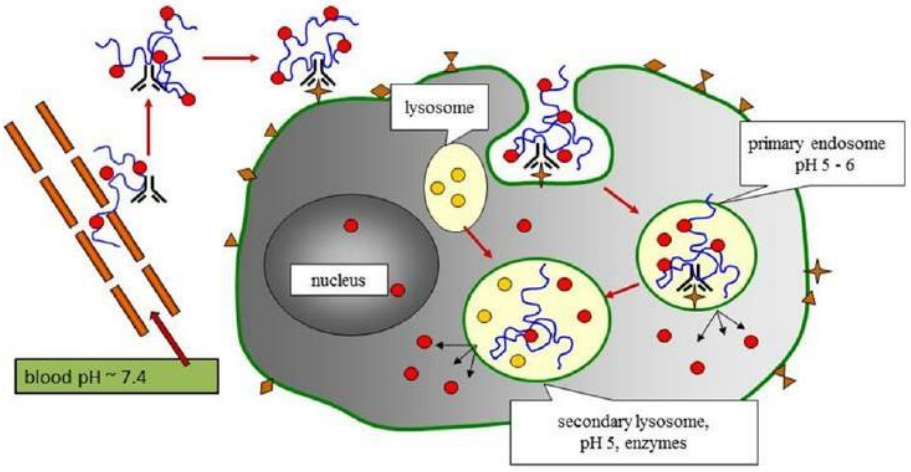

Source [115].

After the extravasation and potential accumulation of drug delivery system (DDS) in the tumor due to the EPR effect, the targeting moiety selectively binds the DDS to a specific receptor on the cancer cell membrane. The conjugate then enters the cell via pinocytosis (endocytosis), and the drug is released from the system after carrier degradation (in the case of nanoparticles), disassembly (micelles) or pH-sensitive hydrolysis in primary endosomes, redox reactions in the cytoplasm, or by enzymolysis in secondary lysosomes for systems with covalently bound drugs

The uncontrolled growth of cells in cancer requires a huge amount of vital nutrients such as the Folic acid (FA). FA is a vitamin B complex, essential for the synthesis of deoxyribonucleic (DNA) and ribonucleic (RNA) acids, being a fundamental element in erythropoiesis. Besides that, the FA is also indispensable in regulating the normal development of nerve cells, preventing congenital neural tube defects, and promoting normal human growth and development [159]. FA has a strong specific interaction with folate receptors (FR+) overexpressed on surface of some types of cancer cells such as ovarian, choriocarcinomas, meningiomas, uterine sarcomas, osteosarcomas, non-Hodgkin's, lymphomas, promyelocytic leukemias, among others [3]. It is reported that it is often overexpressed in more than 90% in ovarian carcinomas [18, 19] and absent in most normal tissues, with exception of choroid plexus, placenta, lung, thyroid and kidney [161]. Nevertheless, what might be one of the dramatic aspects of the disease may be just its vulnerable point. In the last years, the FA has been widely used to improve the drug delivery from its conjugation with polymers and drugs [20, 23].

The Pluronic F127 is a amphiphilic triblock co-polymer composed of a central hydrophobic chain of poly(ethylene oxide) (PEO) blocks and hydrophobic poly(propylene oxide) (PPO) blocks arranged in triblock structure: PEO-PPO-PEO [164]. In aqueous solutions beyond their critical micelle concentration (CMC), the F127 copolymers can self-assemble into nanomicelles with size varying from 10 nm to 100 nm that serves as a cavity for the encapsulation of high concentration of hydrophobic agents for cancer therapy [24, 23] (Fig. 36).

Figure 36. Structure and arrangement of F127 polymer in water.

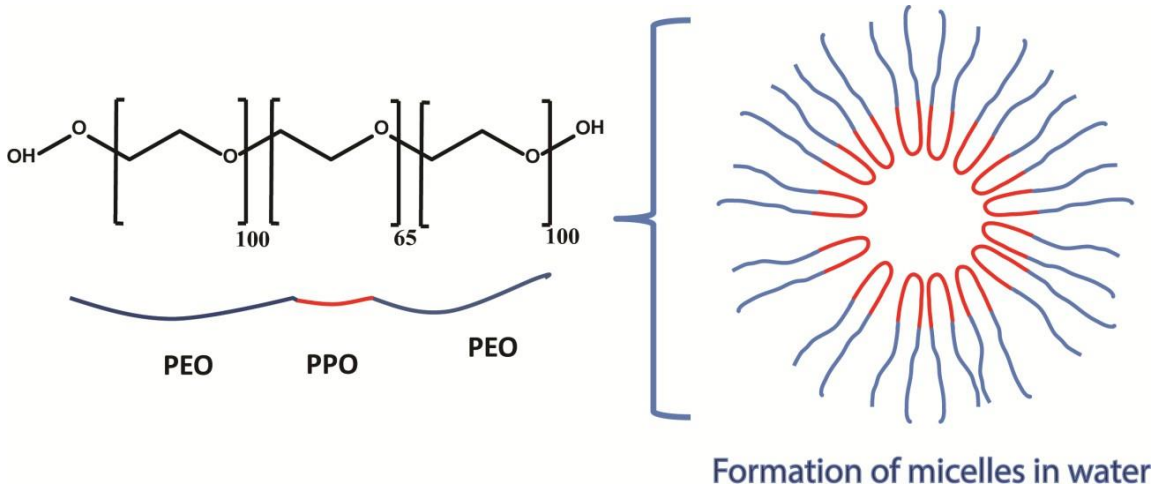

Source: Author

Studies have showed, for example, that doxorubicin molecules has been successfully encapsulated in Pluronic F127 micelles and used in Phase II study with patients with advanced esophageal carcinoma. In addition, micelles with size less than 120 nm has presented prolonged circulation in blood, easy extravasation to tumor tissues in vivo and accumulation in tumors due to EPR effect [129]. Besides that, the hydrophilic PEO corona prevents aggregation and protein adsorption, increasing its bioavailability [167]. In addition, when in aqueous medium, the F127 polymer tends to form micelles exposing its polystyrene (PEG) chains. The time of circulation in the body is one of the most important characteristics of a nanocarrier and the most used method to achieved it is by using a surface coating such as PEG[168].

Studies have shown that the PEGylation may improve the half-life of particle circulation by preventing reticuloendothelial emptying and particle accumulation at the site of the tumor [169]. Although the triblock co-polymer are non-degradable, small molecules with molecular weight less than 15 KDa are usually filtered by the kidney and eliminated by urine [25-27]. Nevertheless, its therapeutic effect can be improved from its conjugation with FA. The functionalization with FA may

promote cellular uptake and, at the same time, to improve the biocompatibility of the overall nanosystem.

Despite the advantages of using FA as a target agent, studies have reported that liposomes with FA directly attached to lipid headgroup, did not efficiently bind to FR+ cancer cells. On the other hand, when polyethylene glycol (PEG) is used as a spacer group the uptake by cancer cells might reach more than 200 000 particles/cell [172]. In this way, a nanocarrier based on folate-modified F127 can be a strategy for the drug delivery improvement. Wei Zhang et. al synthesized F127-FA and the co-polymer was mixed with P123 co-polymer to form P123/F127 micelles [173]. The system was used for encapsulation of drug Paclitaxel (FPF-PTX) and to promote drug delivery to overcoming multidrug resistance (MDR) tumor following intravenous administration. The results were compared with those obtained when the FA was not attached to the polymer (PF-PTX). According to authors, the cellular uptake of system was found to be higher than that of PF-PTX due to the folate receptor-mediated endocytosis effect.

In this context, STNPs for the controlled delivery cancer were synthesized by miniemulsion polymerization reaction, using modified F127-FA as surfactant. Samples were synthesized increasing the amount of F127-FA in the aqueous phase, in order to increase the uptake by cells.

9 STYRENE NANOPARTICLES FOR DRUG DELIVERY

9.1 OBJECTIVES

9.1.1 General

- Synthesizing of STNPs for the controlled cancer drug delivery via folate receptors.

9.1.2 Specifics

- Synthesizing a series of the STNPs from the variation of the surfactant concentration.
- Performing the morphological characterizations of the STNPs obtained by Scanning Electron Microscopy (SEM) and particle size by Dynamic Light Scattering (DLS).
- Modification of the F127 co-polymer by inclusion of FA.
- Characterization of F127-FA by Nuclear Magnetic Resonance (NMR), Gel Permeation Chromatography (GPC) and Critical Micellar Concentration (CMC) measurements.
- Synthesis of STNPs using several proportions of F127-FA as surfactant.
- Performing the cytotoxicity essays.
- Evaluating the cells uptake by confocal microscopy.

10 EXPERIMENTAL

10.1 Materials

All reagents were commercial products with analytical grade without further purification. The chemical reagents for this work were styrene (Merck), F127 (Aldrich), N,N- Carbonyldiimidazole (CDI) (Aldrich), 1,2-ethylenediamine (Aldrich), dry acetonitrile (Aldrich), N-Hydroxysuccinimide (NHS) (Aldrich), N,N'-Dicyclohexylcarbodiimide (DCC) (Aldrich), Triethylamine (Et_3N) (Aldrich), Folic Acid (FA) (Aldrich), hexadecane (HD) (Aldrich99%), 2,20-azobis(2-methylbutyronitrile) (V59). Milli-Q ultrapure water was used during the experiments.

10.2 Methods

10.2.1 Dynamic light scattering (DLS)

The average size of the capsules was measured by DLS using a PSS Nicomp Particle Sizer 380. The capsule dispersion was diluted 10x by Milli-Q water. The scattered light was detected at 90°, while the temperature was maintained at 25°C.

10.2.2 ξ-potential

The ξ-potential of capsules was measured diluting to a solid content of 10^{-9}% by Milli-Q ultrapure water in a Zeta Sizer Nano Series (Malvern Instruments, U.K.) at 25°C.

10.2.3 Scanning electron microscopy (SEM)

SEM measurements were carried out by using a LEO (Zeiss) 1530 Gemini device (Oberkochen, Germany). The samples were diluted to a solid content of 0.01% with Milli-Q ultrapure water, where 15 mL of the diluted sample were placed on the silica wafer and dried at room temperature overnight.

10.2.4 Gel Permeation Chromatography (GPC)

GPC measurements of unmodified and modified HES capsules were performed in DMF with a flow rate of 1mL.min^{-1} using a PSS Security Agilent Technologies 1260 Infinity instrument with an autosampler and a PSS GRAM 0.8x30cm column at 60°C with a particle size of 10µm and pore sizes of 10,000, 1,000 and 100Å. RI-detector G1362A RID was used for detection and poly(styrene) was used for Calibration. Standard of the pure polymers, PetOx and PEG, and SDS were also analyzed as a negative control.

10.2.5 Nuclear magnetic resonance (NMR) spectroscopy

1H NMR spectrums of functionalized capsules are measured at 300 MHz on a Bruker Avance 300 Spectrometer, by using deuterated water as solvent.

10.2.6 Cell uptake

HeLa cells were kept in DMEM (Invitrogen) supplemented with 10% FCS (Invitrogen), 100 units mL^{-1} penicillin, 100 mg mL^{-1} streptomycin (Invitrogen) and 2 mM L^{-1} glutamine (Invitrogen). Cells were grown in a humidified incubator at 378°C and 5% CO_2. For the incubation, adherent cells were seeded at a density of 50,000 cells cm^2 on the first day. On the second day, fluorescent labeled nanoparticles were added at a concentration of 75 mg mL^{-1} to the media. The adherent cells were trypsinized. Cells were then washed with PBS, centrifuged and the pellet was re-suspended in PBS for FACS analysis.

10.2.7 Synthesis of styrene nanoparticles by miniemulsion

Styrene nanoparticles were prepared by miniemulsion polymerization with incorporation of fluorescent dye according modified method [99]. The organic phase was prepared by dissolving of 3 mL of styrene, 0.05 g of initiator (V59), 162 mL of hydrophobe (hexadecane) and 1.5 mg of Body by dye in 12 mL in the aqueous solution containing F127 as surfactant (aqueous phase). A series of different concentration of F127 solutions were prepared in order to study it influence on the particle size and ξ-potential. The mixture remained under magnetic stirring by 1h/500 rpm to pre-emulsification. After that, the mixture was ultrasonicated in an ice-cooled bath at 70% amplitude (Branson sonifier W450 digital, ½ tip) for 180 s, with a pulse of 30s on and 10s off, to the

miniemulsion formations. Finally, the miniemulsion was heated in oil bath at 71ºC during 20 h on magnetic stirring, for styrol polymerization. The product obtained was filtrated and dialyzed during 3 days using dialysis membrane of 1000 DK and stored in freezer.

10.2.8 Synthesis of carbonildimidazol activated polymer F127 (F127-CDI)

12.7 g of the F127-CDI was performed according Zhang, W., et al [173] multifunctional pluronic P123/F127 mixed polymeric micelles loaded with paclitaxel for the treatment of multidrug resistant tumors. 12.6 g of co-polymer F127 was first dried in a vacuum oven at 40 oC to eliminate the water. After that, the F127 was dissolved in dry acetonitrile (15 mL) and added dropwise to an excess amount of CDI (1.62 g, 10 mmol) in dry acetonitrile (15 mL) at room temperature. The mixture was kept stirring overnight under nitrogen atmosphere. The obtained solution was concentrated by evaporation under reduced pressure and the F127-CDI system was precipitated with excess of cold ethyl ether. This process was repeated three times to remove unreacted CDI. Finally, the F127-CDI was dried under a vacuum dehydration and collected as white powder.

10.2.9 Synthesis of amino-terminated co-polymer F127 (F127-NH_2)

The F127-CDI (12.7 g, 1 mmol) was dissolved in dry acetonitrile (15 mL) and added dropwise to 10 mL of 1,2-ethylenediamine at room temperature. The mixture was allowed to react overnight. The unreacted ethylenediamine was removed by evaporation under reduced pressure and the crude product was poured into an excess amount of cold ether to obtain the white precipitate. This process was repeated three times, and the F127-NH_2 was dried under a vacuum dehydration and collected as white powder.

10.2.10 Synthesis of folate-conjugated co-polymer F127 (F127-FA)

In this procedure, F127-NH_2 (1 g, 0.079 mmol), FA (105 mg, 0.237 mmol), NHS (60 mg, 0.522 mmol) and DCC (108 mg, 0.522 mmol) were dissolved in 10 mL of DMSO in the presence of 0.1 mL Et_3N. The mixture was stirred in a nitrogen atmosphere at room temperature in the dark overnight. At the end, the mixture was further purified by dialysis against deionized water for 3 days, followed by lyophilization. The yellow powder obtained was stored in refrigerator.

10.2.11 Synthesis of STNPs by miniemulsion polymerization using F127-FA as surfactant

STNPs were prepared by miniemulsion polymerization for the controlled cancer drugs delivery via folate receptor. For this purpose, FA was covalently linked to the F127 and the polymer was used as surfactant during the polymerization reaction of styrene. During the experimental procedure, it was observed that when the concentration of surfactant is 6.5 % (w/v) in the aqueous phase, small particles with good size distribution are formed. In this sense, this concentration was chosen for the synthesis of STNPS using F127-FA as surfactant (aqueous phase). In order to evaluate the influence of the FA on the uptake of STNPs in cell, four samples were prepared increasing the percentage of FA in the aqueous phase (ST@F127 – FA 1 %, ST@F127 – FA 3 %, ST@F127 – FA 5 % and ST@F127 – FA 10 %). All particles were synthesized with incorporation of fluorescent dye.

11 RESULTS AND DISCUSSION

Hydrophilic STNPs were synthesized and used for the delivery of hydrophobic drug into the cancer cells. For this purpose, a series of samples were synthesized by miniemulsion polymerization procedure using different concentration of surfactant in the aqueous phase. All synthesis conditions were kept constant in order to evaluate the influence of the surfactant concentration on the particle size, electronic change of the particle and morphology. The hydrophobic initiator V59 was introduced into the organic phase to prevent nucleation of hydrophilic monomers in the water phase.

During the miniemulsion process, the droplets were stabilized using a surfactant and co-stabilized from an ultra-hydrophobe to suppress the diffusional degradation. The costabilizer creates osmotic pressure within the droplets, counteracting the Laplace pressure that is responsible for diffusional degradation (Ostwald ripening). In this case, the contents of the droplets remain unchanged, ie it does not interact with the external medium or with other droplets, constituting each system as an individual nanoreactors. In this work, the hydrophobe (hexadecane) was used as a co-stabilizer [150]. The summarized results for the particle size and ξ-potential obtained from the mixture of different concentration solution of F127 and the organic phase are presented in Table 09. The variation of the particle size in relation to the concentration of the surfactant in aqueous solution is shown in Figure 37.

Table 09. Relation between the percentage of F127 in 12 mL of water (aqueous phase), particle size and ξ-potential**.** Fixed constant the organic phase in 3 mL.

% F127	***r* (nm)**	**ξ (mV)**
0.5%	396.2±184.6	-
1.0%	268.8±85.5	-6.50±5.98
1.8%	191.0±49.0	-6.50±4.42
2.5%	185.5±47.7	-7.35±6.04
3.5%	148.5±39.1	-6.62±4.28
4.5%	116.0±28.0	-5.92±5.92
5.5%	108.0±28.0	-
6.5%	89.6±19.01	-6.56±4.70
7.5%	90.9±19.40	-5.47±5.54
9.5%	79.7±23.40	-5.15±4.99
11.5%	80.9±28.90	-5.41±5.95

Figure 37. Relation between percentage of F127 in solution and particle size.

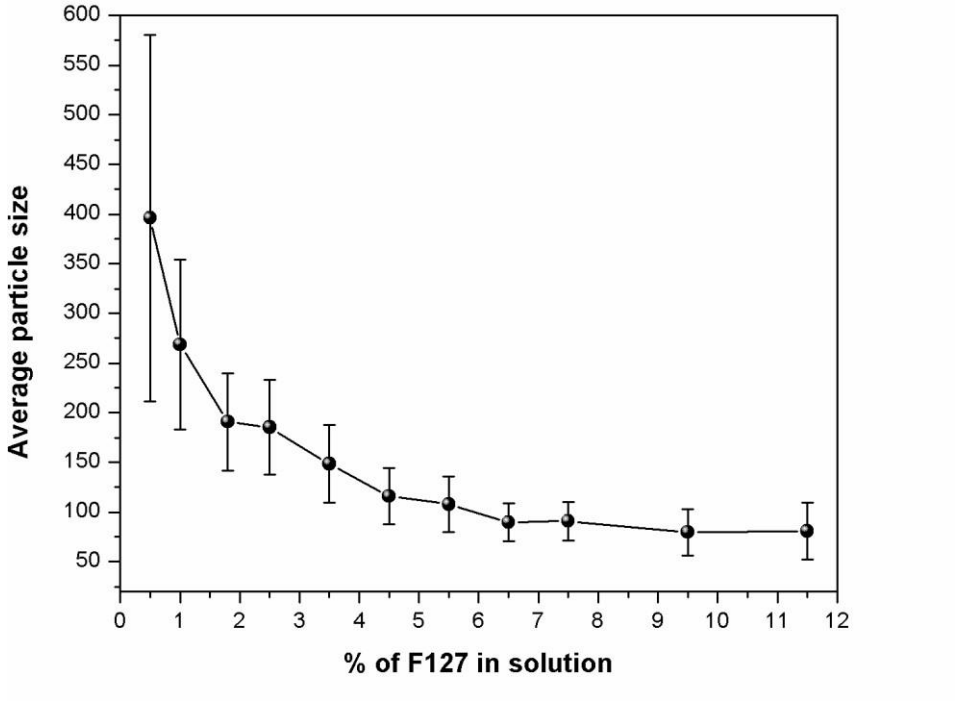

The ξ-potential measurements showed stability fort all particles in solution (Table 1). The size of the particles was measures by DLS and showed that the increase of the percentage of surfactant in the aqueous phase promoted a decrease of the particle size until reaching the minimum value around 88 nm. For the biological applications is important to synthesize particles with small enough size to allow them to uptake by cells and this critical size if below of 100 nm [174]. Although the smaller particle sizes are obtained with concentrations above 7.5%, these highly concentrated solutions present a difficulty in their purification. Therefore, the particles synthesized at 6.5% concentration were chosen for the biological tests. For the biological test, the particles were synthesized using BODIPY dye dissolved in the organic phase. The use of fluorescent dye its necessary for fluorescent cells detection by cyflow. Before irradiation with UV light, the BODIPY dye exhibits its normal fluorescence properties: excitation at 488 nm and emission at 510 nm. SEM images were carried out to provide information about the size and morphology of the ST@F127 nanoparticle (Fig. 38a and b).

Figure 38. SEM images of STNPs synthesized from a solution with 6.5% of F127 in the aqueous phase.

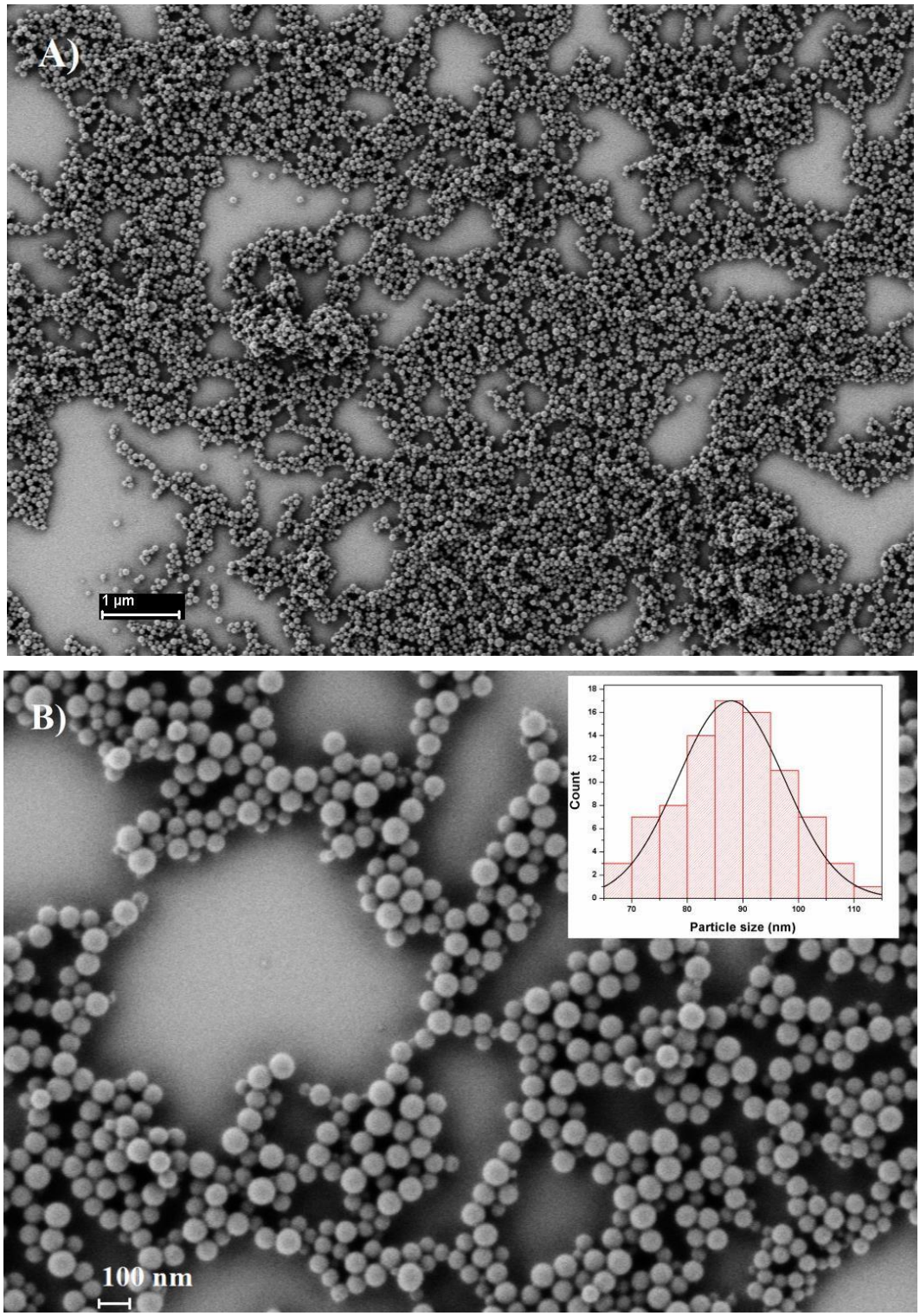

The SEM image shows particles with spherical shape and close size distribution with values below of 100 nm. The values for the particles size are in good agreement with those obtained from DLS measurements.

11.1 Synthesis of folate-conjugated co-polymer F127

In this study, it is aimed the development of STNPS for drug delivery via FA target. The linkage between the polymer F127 and the FA occurred in three major steps. Initially, the terminal hydroxyl groups of the polymer (R1) were activated with CDI (Fig. 39). CDI is a carbonylating agent with acylimidazdole groups which react with –OH from de F127 to form imidazole carbamate active intermediates.

Figure 39. Mechanism reaction for the synthesis of F127-FA.

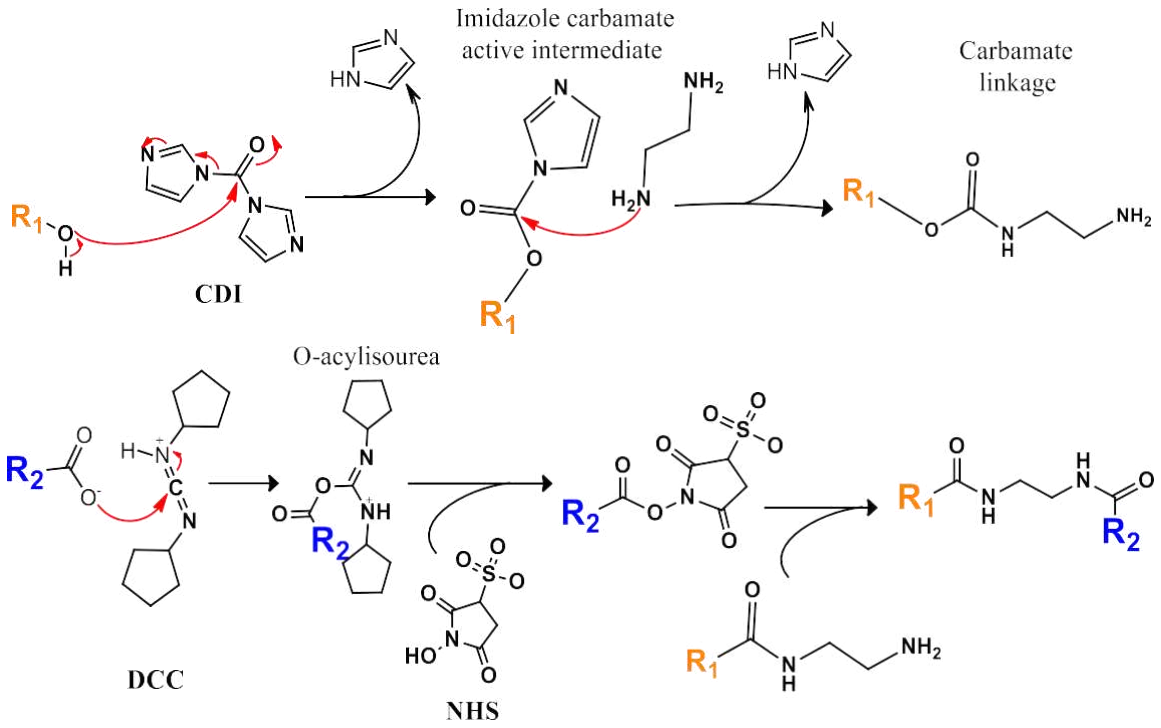

Source [175]

These intermediates in turn, react with amino groups from ethylenediamine to form carbamate linkages releasing imidazole. Finally, the primary amines of F127-NH_2 are crosslinked to carboxyl groups from FA (R2) using a carbodiimide crosslinker (DCC). In this process, DDC reacts with carboxylic acid groups to form an active O-acylisourea intermediate that is easily displaced by nucleophilic attack from primary amino groups in the reaction mixture. The NHS was included to

improve efficiency or create dry-stable (amine-reactive) intermediates. The NHS ester formed from DCC/NHS coupled is more stable than O-acylisourea allowing more efficient conjugation to primary amines.

The chemical structures of the polymer were characterized by H^1 NMR. Figure 40 presents the H^1 NMR spectra of F127-CDI (A), F127-NH_2 (B) and F127-FA (C)**.**

Figure 40. H^1 NMR spectra of (A) F127-CDI, (B) F127-NH_2 and (C) F127-FA**.**

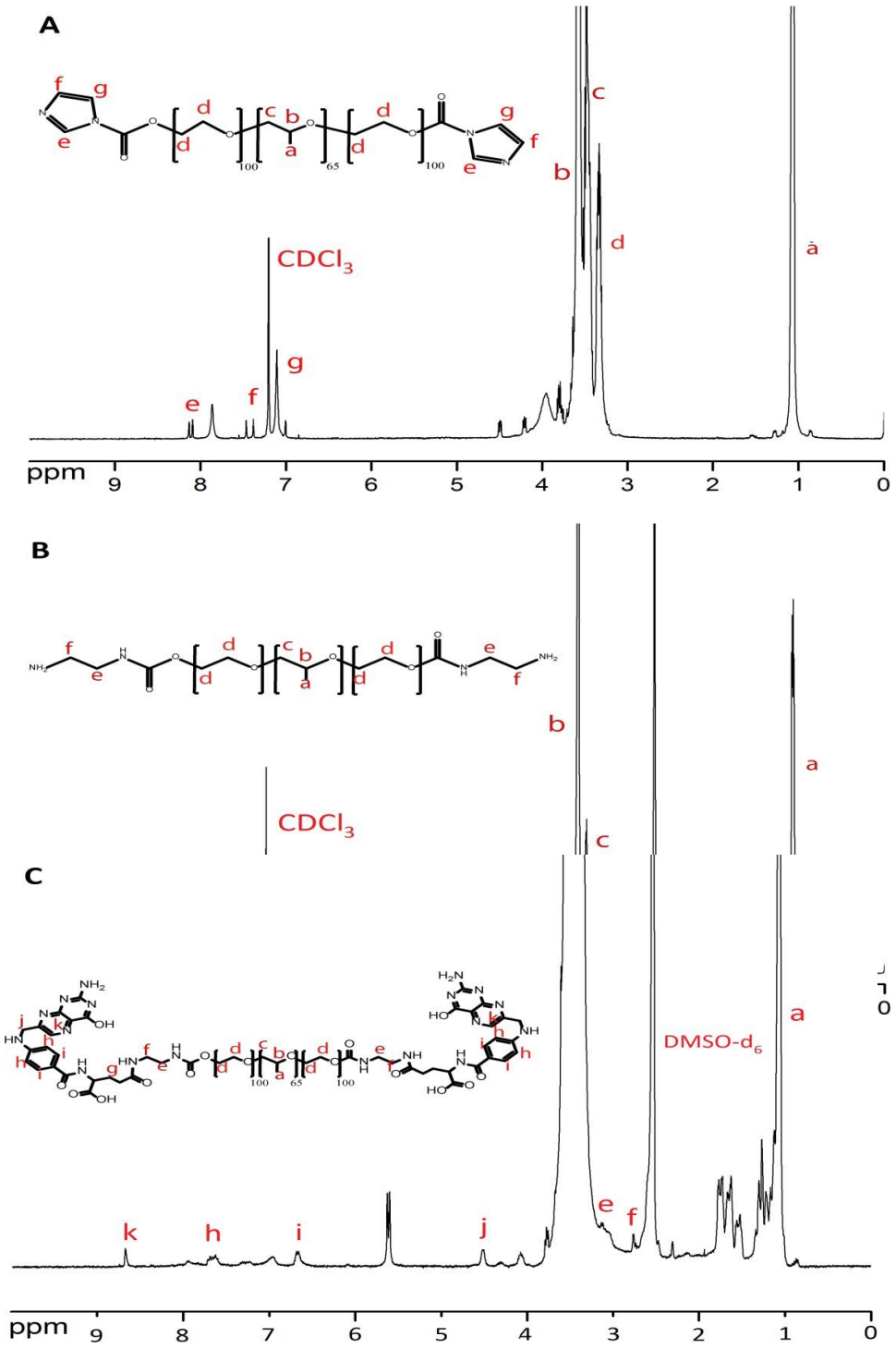

The H^1 NRM spectrum showed the typical peaks a, b, c and d from F127 at δ (ppm) = 1.02 (d, 3H x 65, -CH_3 of PPO), 3.30 - 3.50 (m, 3H x 65, 4H x 200, -CH_2CHO of PPO and -CH_2CH_2O- of PEO), respectively. The presence of the new peaks "g", "f", "e" at 8.2 (s,1H x 2), 7.4 (s, 1H x 2, 7.1) (s, 1H x 2) characterize the synthesis of the F127-CDI. The ^1H NMR spectrum of F127-NH_2 presented the peaks at δ (ppm) = 1.02 (d, 3H x 65, -CH3 of PPO), 3.30-3.50 (m, 3H x 65, 4H x 200, -CH_2CHO of PPO and -CH_2CH_2O- of PEO), 2.80 (t, 2H x 2, -CH_2N), 3.20 (q, 2H x 2, $CNCH_2$-). Besides that, Figure 4 presented ^1H NMR spectrum (400 MHz, DMSO-d6, ppm) of F127-FA at δ (ppm) = 2.28 (m, 2H, C22-H2 of FA), 4.45 (d, 2H, C9-H2 of FA), 6.60 (d, 2H, aromatic protons of FA), 7.59 (d, 2H, aromatic protons of FA), 8.62 (s, 1H, C7-H of FA) In order to provide evidence on the synthesis of F127-FA and not only obtaining a mixture of substances, others measures were performed. Figure 41 presents the results from GPC measurements for the F127-FA sample. As the FA has a fluorescence behavior [176], the GPC measurements were coupled to UV spectrometer.

Figure 41. Gel Permeation Chromatography- GPC analysis of the F127-FA.

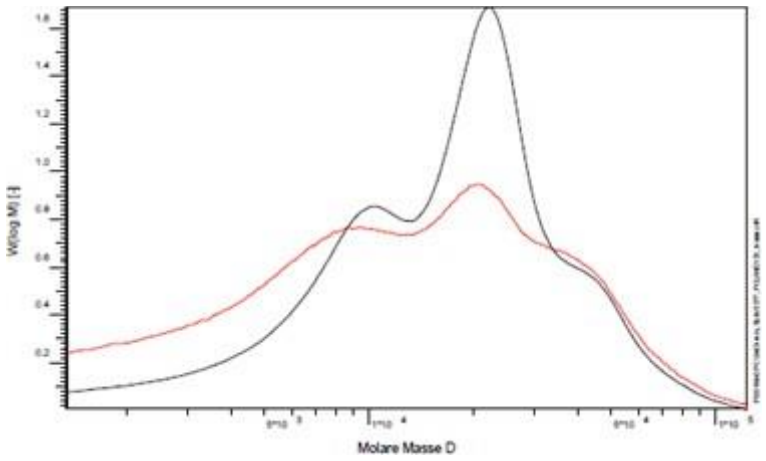

If there was only a physical mixture between F127 and FA, we would obtain separate signals for GPC analysis, considering that the mass of the polymer is thirteen times greater than the mass of the FA. However, the UV emission point of the FA is occurring in the same range of the weight distribution of the polymer. This means that the polymer should be covalently bonded to the FA, forming a single compound. Critical micellar concentration (CMC) measurements were carried out for the samples F127 and F127-FA, obtaining values of 0.44867 and 1.08120 g/L, respectively. The increase of CMC for the F127-FA is due to the presence of FA in the molecule, which has low solubility in water. All these measures together prove that F127-FA has been successfully obtained.

11.2 STNPs synthesis by miniemulsion using F127-FA as a compound of the aqueous phase

In order to study the influence of the FA as a target agent for cancer cells, the F127-FA synthesized was mixed with F127 in the aqueous phase. The proportion of F127-FA in the solution was increased in 1, 3, 5 and 10%. In this case, the synthesized STNPs were ST@F127-FA 1%, ST@F127-FA 3%, ST@F127-FA 5% and ST@F127-FA 10%. It was not possible continue increase the proportion of F127-FA in the surfactant solution, due to it low solubility in water. The results to the average particle size obtained from DLS and ξ-potential measurements are presented in Table 10.

Table 10. Average particle size and ξ-potential obtained for the samples ST@F127-FA 1%, ST@F127-FA 3%, ST@F127-FA 5% and ST@F127-FA 10%.

% FA in 6.5 % (w/v)	***r* (nm)**	**ξ (mV)**
0%	89,6±19,1	-5.93±6.93
1%	87,9±15,6	-4.09±5.70
3%	96,8±31,9	-4.36±5.36
5%	101,1±26,7	-4.16±6.77
10%	111,8±43,4	-0.954±2.85

The SEM images were carried out for all samples in order to provide information about average particle size and morphology. The results are presented in Figure 42.

Figure 42. SEM images for the samples ST@F127-FA 1% (A), ST@F127-FA 3% (B), ST@F127-FA 5% (C) and ST@F127-FA 10% (D).

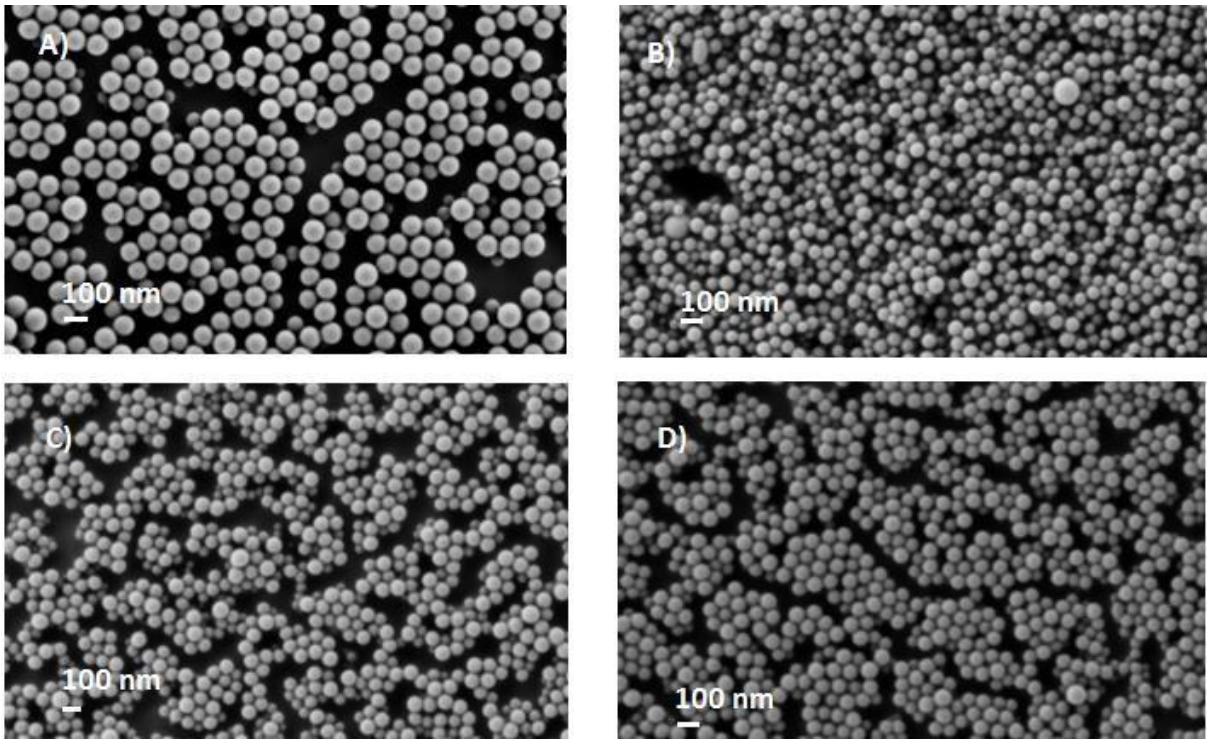

Source: Author

The SEM imagens show particles with good size distribution and spherical shape. The obtaining of particles sizes below of 100 nm is an important condition for biological applications due to the size dependent uptake by cells. The values for the particles size are in good agreement with those obtained from DLS measurements.

11.3 Cytotoxicity and cellular uptake of STNPs

A series of ST nanoparticles were synthesized via miniemulsion polymerization reaction using the polymers F127 as surfactant. In order to study the influence of the FA as target agent, the polymer F127 was modified and new samples were prepared increasing the proportion of the F127-FA in the aqueous phase. The cellular uptake analyses were carried out to evaluate the potential use of these nanoparticles for biological applications. The samples were added to culture of HeLa cells and incubated for 24 h. After that, they were washed with PBS buffer solution the cellular uptake was determined using a fluorescence activated cell sorter (FACS) (Becton Dickinson, Heidelberg, Germany) equipped with an argon ion laser. The results are presented in the figure 43.

Figure 43. FACS measurements of HeLa cells incubated for 24 h for the particles ST@F127, ST@F127-FA 1%, St@F127-FA 3%, ST@F127-FA 5% and ST@F127-FA 10% nanoparticles. Percentage of fluorescent cells (A). Intensity of fluorescence (B).

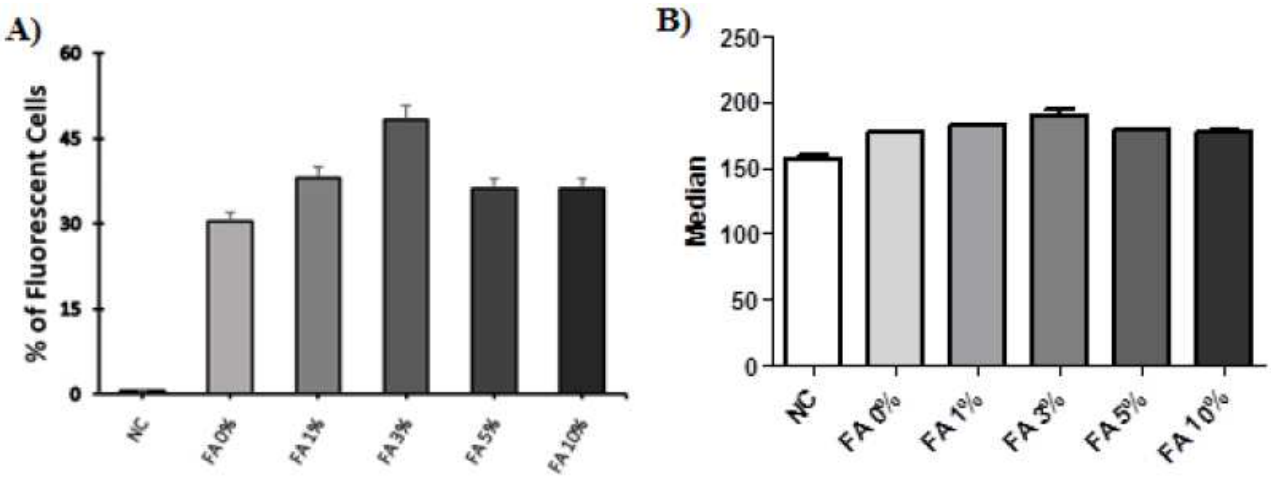

NC*: Negative Control

Figure 43 (B) shows the intensity of the fluorescence for all particles and these values are presents in terms of the median in the *Y* axes. The high values found indicate that the detected fluorescence is probably due to particles located within the cells and not just incorporated into the surface. Figure 43 (A) shows an increase of the uptake by cells for all particles with FA incorporated. The ideal condition was found when the concentration of the F127-FA in the aqueous phase was of 3 % (w/w). The particle ST@F127-FA 3 % for example, obtained an increase of 49.51 % in the uptake by HeLa cells. The confocal fluorescence images are presented in figure 44.

Figure 44. Confocal fluorescent microscopy of HeLa cells after the uptake of amino functionalized particles (green). Negative Control (A), ST@F127-FA 0 % (B), ST@F127-FA 1 % (C), ST@F127-FA 3 % (D), ST@F127-FA 5 % and ST@F127-FA 10 % (E).

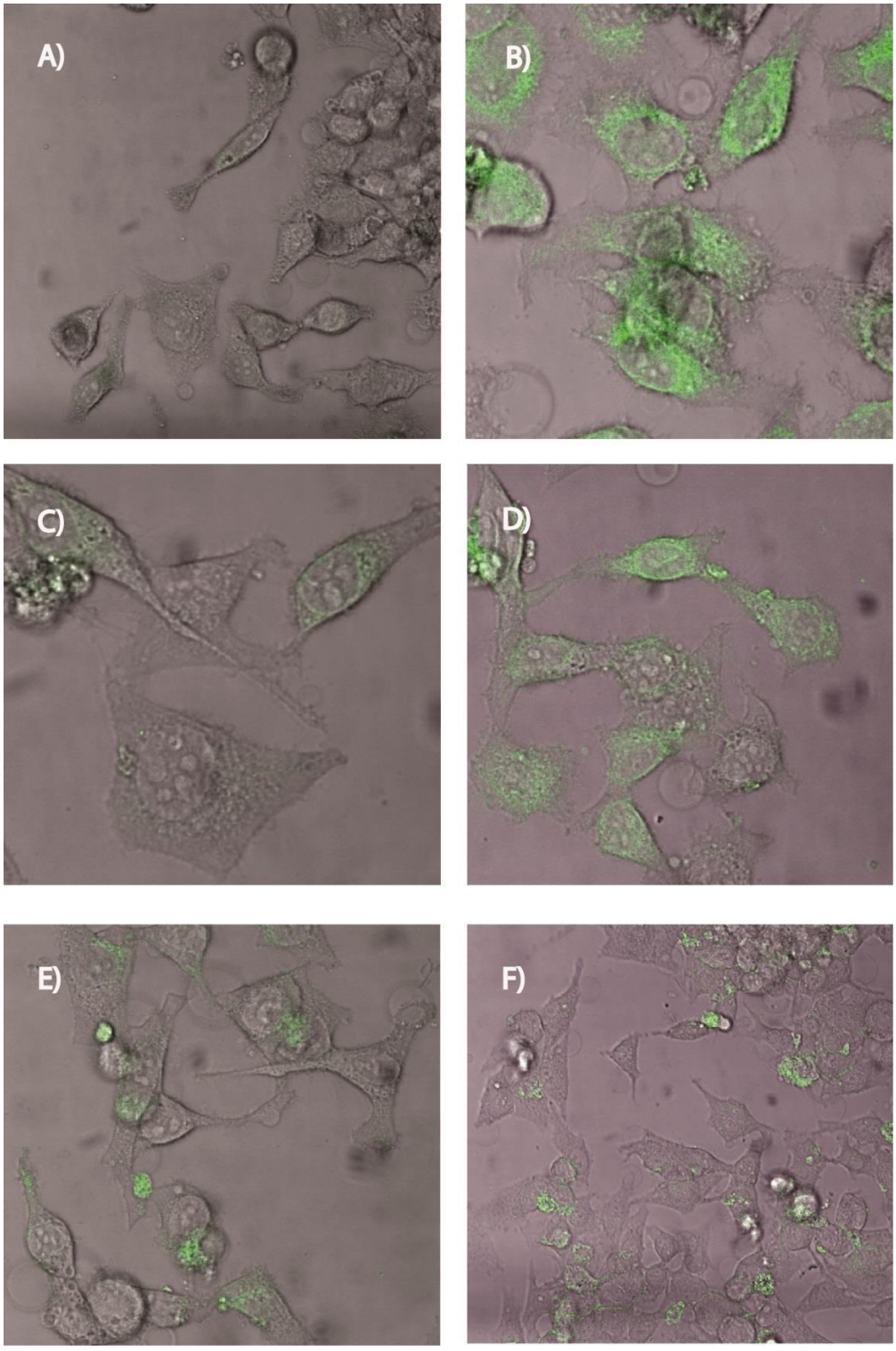

12 GENERAL CONCLUSIONS AND PERSPECTIVES

Chapter 2 and 3 presented the results for the kinetic resolution of some drug precursors using enzymes immobilized on magnetic nanoparticles. Chapter 2 reported a strategy to develop a nanohybrid material used as a heterogeneous catalyst composed by a lipase from *Pseudomonas fluorescens* immobilized on Fe_3O_4 SPMNPs. The nanohybrid catalyst was used for the first time to the kinetic resolution of secondary alcohols as *rac*-indanol, *rac*-1- phenylethanol, *rac*-1-(3-bromophenyl)-1-ethanol and *rac*-1-(3-methylphenyl)-1-ethanol. The immobilization of the enzyme on this support occurred via covalent attachment and produced a thermostable catalyst, even in the presence of organic solvent. The synthesized nanocomposite proved to be very efficient for the kinetic resolution of rac-indanol at high temperature (1.75 h/50 °C) in hexane. Besides that, reproducible results were observed, over five reuse cycles, in terms of enantioselectivity (E > 200), conversion (49-50%) and enantiomeric excess values (95% to > 99 %). The kinetic resolution of rac-1-phenylethanol reached a conversion value of 49% after 48 h of reaction with high selectivity (E > 200). Analogs with substituents at the meta-position at the aromatic ring as *rac*-1-(3-bromophenyl)-1-ethanol and *rac*-1-(3-methylphenyl)-1-ethanol reacted more slowly in comparison to *rac*-1-phenylethanol, with a conversion value of 44% after 48 h of reaction, although with high selectivity (E > 200). It should be noted that the magnetic properties of the core of support (Fe_3O_4) enable to be easily prepared and removed from the reaction medium by applying an external magnetic field. Lipase from *Pseudomonas fluorescens* immobilized on magnetic nanoparticles proved to be a robust biocatalyst in the kinetic resolution of *rac*-secondary alcohols with potential application in heterogeneous catalysis. Besides that, the enzyme immobilization process improved the physical properties such as the thermal stability and mechanical resistance. The results obtained for the kinetic resolution of *rac*-indanol, *rac*-1- phenylethanol (*rac*-1), *rac*-1-(3-bromophenyl)-1-ethanol (*rac*-2) and *rac*-1-(3-methylphenyl)- 1-ethanol (*rac*-3) were published in "Journal of Alloys and Compounds" entitled: Novel nanohybrid biocatalyst: application in kinetic resolution of secondary alcohols (See section of published articles).

Chapter 3 presents the results for the kinetic resolution of *rac*-1-methyl-2-(2,6-dimethylphenoxy)ethyl acetate in different co-solvents, using lipases from *Thermomyces lanuginosus* (TLL) immobilized on different support. These results were obtained in cooperation with the Chemical Engineering Department of the UFC and published in the "Biochemical Engineering Journal" titled: Design of a lipase-nano particle biocatalyst and its use in the kinetic resolution of medicament precursors. In this work, the enzyme was immobilized on Fe_3O_4@APTES and

Fe_3O_4@PEI using two methods: the first one by ionic exchange and the second one by covalent attachment after the functionalization of the support with glutaraldehyde (GA). The samples covered with PEI have a greater amount of mass compared to the APTES samples. However, as higher the amount of anchored mass, greater the amount of amino groups available for enzyme immobilization. Therefore, the samples functionalized with PEI presented greater amount of immobilized enzymes. The interaction between the sup-port and the lipase is stronger when the immobilization takes place by covalent bonds rather than by ionic adsorption. Therefore, the strong attraction of covalent bonds and the branched structure of PEI may cause distortions in the protein structure and affect the catalytic activity of the biocatalyst. In general, the activation of the support by glutaraldehyde produced more stable and resistant biocatalyst to the most severe conditions, but with lower catalytic activity. The preparations presented good stability without an expressive loss of catalytic activity, which shows the potential application of the TLL immobilized on superparamagnetic nanoparticles as heterogeneous biocatalyst to replace chemical catalysts.

All the biocatalyst presented low cost of production and superior physical properties in comparison with the free enzymes. In addition, their magnetic properties provide a great ease of removal of the medium compared to the non-magnetic commercial models. These magnetic nanobiocatalysts may constitute an important strategy to the pharmaceutical industry for the synthesis of drug precursors. Future prospects for these biocatalysts are the production of an automatic system for kinetic resolution of racemic mixtures.

Chapter 5 presents the results for the synthesis of ST nanocarriers for hydrophobic anticancer drugs. The F127 polymer was modified by the inclusion of FA and used as a surfactant during the miniemulsion polymerization process. The cytotoxicity assays were carried out and showed that the particles had no toxicity and could be used for biological purpose. The *in vitro* tests showed that the F127-FA improved the uptake of STNPs by HeLa cells and this indicate that the system ST@F127-FA may be used to increase the uptake by cancer cells and improve the drug delivery of hydrophobic drugs. Despite these preliminary results, it has not yet been possible to significantly increase the uptake of the ST@ F127-FA systems by the cells as compared to the unmodified polymer. This is mainly due to the impossibility to increase the amount of F127-FA in proportion to F127 in the aqueous phase. However, this can be solved by choosing a more soluble water polymer than F127. The future perspective for this work includes increasing F127-FA in the aqueous phase and testing with other cell cultures.

Other contributions:

Articles:

- Nanocrystal growth, magnetic and electrochemical properties of NiZn ferrite. Journal: Journal of Alloys and Compounds [178].
- Superparamagnetic nanoparticles with spinel structure: A review of synthesis and biomedical applications [179].

Book chapter:

- Bimagnetic Core/Shell Nanoparticles: Current Status and Future Possibilities. Springer (2017).

Patente deposited:

- Development of a process for immobilization and stabilization of *Pseudomonas fluorescens* lipase in magnetic nanoparticles $Ni_{0,5}Zn_{0,5}Fe_2O_4$. Main author: Nathalia S. Rios.

REFERENCES

[1] MAGDOLENOVA, Zuzana et al. Mechanisms of genotoxicity. A review of in vitro and in vivo studies with engineered nanoparticles. **Nanotoxicology**, v. 8, n. 3, p. 233-278, 2014.

[2] SHARMA, K. S. et al. Synthesis and characterization of monodispersed water dispersible Fe3O4 nanoparticles and in vitro studies on human breast carcinoma cell line under hyperthermia condition. **Scientific reports**, v. 8, n. 1, p. 14766, 2018.

[3] XIONG, Xiang Yuan et al. Novel folated Pluronic/poly (lactic acid) nanoparticles for targeted delivery of paclitaxel. **RSC advances**, v. 6, n. 58, p. 52729-52738, 2016.C. Ding and Z. Li, "A review of drug release mechanisms from nanocarrier systems," *Mater. Sci. Eng. C*, vol. 76, pp. 1440–1453, 2017.

[4] SALAM, Hasna Abdul; SIVARAJ, Rajeshwari; VENCKATESH, R. J. M. L. Green synthesis and characterization of zinc oxide nanoparticles from Ocimum basilicum L. var. purpurascens Benth.-Lamiaceae leaf extract. **Materials letters**, v. 131, p. 16-18, 2014.

[5] GALVÃO, Wesley S. et al. Super-paramagnetic nanoparticles with spinel structure: a review of synthesis and biomedical applications. **solid state phenomena**, v. 241, p. 139-176, 2016. S. Gandhi and I. Roy, "Doxorubicin-loaded casein nanoparticles for drug delivery: Preparation, characterization and in vitro evaluation," *Int. J. Biol. Macromol.*, vol. 121, pp. 6–12, 2019.

[6] DE SOLORZANO, Isabel Ortiz et al. Cleavable and thermo-responsive hybrid nanoparticles for on-demand drug delivery. **Journal of colloid and interface science**, v. 533, p. 171-181, 2019.

[7] USOV, N. A.; NESMEYANOV, M. S.; TARASOV, V. P. Magnetic vortices as efficient nano heaters in magnetic nanoparticle hyperthermia. **Scientific reports**, v. 8, n. 1, p. 1224, 2018.

[8] NAGESETTI, Abhignyan et al. Erratum: Multiferroic coreshell magnetoelectric nanoparticles as NMR sensitive nanoprobes for cancer cell detection. **Scientific reports**, v. 7, 2017.

[9] BASINI, M. et al. Tailoring the magnetic core of organic-coated iron oxides nanoparticles to influence their contrast efficiency for Magnetic Resonance Imaging. **Journal of Alloys and Compounds**, v. 770, p. 58-66, 2019.

[10] FATHI, Farzaneh; RASHIDI, Mohammad-Reza; OMIDI, Yadollah. Ultra-sensitive detection by metal nanoparticles-mediated enhanced SPR biosensors. **Talanta**, v. 192, p. 118-127, 2019.

[11] XIA, Ni et al. The detection of mercury ion using DNA as sensors based on fluorescence resonance energy transfer. **Talanta**, v. 192, p. 500-507, 2019.

[12] ARGUDO, Pablo G. et al. Fluorinated CdSe/ZnS quantum dots: Interactions with cell membrane. **Colloids and Surfaces B: Biointerfaces**, v. 173, p. 148-154, 2019.

[13] ZENG, Zhuotong et al. Interaction of tetramer protein with carbon nanotubes. **Applied Surface Science**, v. 464, p. 30-35, 2019.

[14] REZNICKOVA, A. et al. PEGylated gold nanoparticles: Stability, cytotoxicity and antibacterial activity. **Colloids and Surfaces A: Physicochemical and Engineering Aspects**, v. 560, p. 26-34, 2019.

[15] OUELLETTE R. J. and RAWN, J. D. "8 - Stereochemistry," R. J. Ouellette and J. D. B. T.-O. C. (Second E. Rawn, Eds. Academic Press, 2018, pp. 213–253.

[16] J. D'Angelo and M. B. Smith, "Chapter 6 - Stereochemistry," J. D'Angelo and M. B. B. T.-H.R. Smith, Eds. Boston: Elsevier, 2015, pp. 63–66.

[17] EZQUERRA-ROMANO, I. Ivan et al. Ketamine for the treatment of addiction: evidence and potential mechanisms. **Neuropharmacology**, v. 142, p. 72-82, 2018.

[18] JACQUES, Jean et al. **Enantiomers, racemates, and resolutions**. New York: Wiley, 1981.

[19] FLACK, H. D. Louis Pasteur's discovery of molecular chirality and spontaneous resolution in 1848, together with a complete review of his crystallographic and chemical work. **Acta Crystallographica Section A: Foundations of Crystallography**, v. 65, n. 5, p. 371-389, 2009.

[20] MAIER, Norbert M.; FRANCO, Pilar; LINDNER, Wolfgang. Separation of enantiomers: needs, challenges, perspectives. **Journal of Chromatography A**, v. 906, n. 1-2, p. 3-33, 2001.

[21] SILBERBERG, Martin Stuart. Principles of general chemistry. **(No Title)**, 2007.

[22] LIMA, Vera Lucia Eifler. Os fármacos e a quiralidade: uma breve abordagem. **Química Nova**, v. 20, p. 657-663, 1997.

[23] NEWBRONNER, Elizabeth; ATKIN, Karl. The changing health of Thalidomide survivors as they age: A scoping review. **Disability and Health Journal**, v. 11, n. 2, p. 184-191, 2018.

[24] NGUYEN, Lien Ai; HE, Hua; PHAM-HUY, Chuong. Chiral drugs: an overview. **International journal of biomedical science: IJBS**, v. 2, n. 2, p. 85, 2006.

[25] SINGH, Nirmal; SHARMA, Lalit. Enantioseparation of D-and L-isomers of chiral drugs for improving their bioavailability: Some techniques including micellization with gemini surfactants. **Indian J. Pharm. Educ**, v. 52, p. 334-341, 2018.

[26] NOWAK, Richard. Single-isomer levalbuterol: a review of the acute data. **Current Allergy and Asthma Reports**, v. 3, n. 2, p. 172-178, 2003.

[27] LANDONI, M. F.; SORACI, A. Pharmacology of chiral compounds 2-arylpropionic acid derivatives. **Current drug metabolism**, v. 2, n. 1, p. 37-51, 2001.

[28] WALDECK, Bertil. Three-dimensional pharmacology, a subject ranging from ignorance to overstatements. **Pharmacology & toxicology**, v. 93, n. 5, p. 203-210, 2003.

[29] ECHIZEN, H.; MANZ, M.; EICHELBAUM, M. Electrophysiologic effects of dextro-and levo-verapamil on sinus node and AV node function in humans. **Journal of Cardiovascular Pharmacology**, v. 12, n. 5, p. 543-546, 1988.

[30] SATOH, Keisuke; YANAGISAWA, Teruyuki; TAIRA, Norio. Coronary vasodilator and cardiac effects of optical isomers of verapamil in the dog. **Journal of cardiovascular pharmacology**, v. 2, n. 3, p. 309-318, 1980.

[31] DRAYER, Dennis E. Pharmacodynamic and pharmacokinetic differences between drug enantiomers in humans: an overview. **Clinical Pharmacology & Therapeutics**, v. 40, n. 2, p. 125-133, 1986.

[32] OLSEN, George D. et al. Clinical eftects and pharmacokinetics of racemic methadone and its optical isomers. **Clinical Pharmacology & Therapeutics**, v. 21, n. 2, p. 147-157, 1977.

[33] CIRIANI, Marina; OLIVEIRA, Rudi; AFONSO, Carlos AM. Semi-continuous and continuous processes for enantiomeric separation. **Green Chemistry**, v. 24, n. 11, p. 4328-4362, 2022.

[34] HANCU, Gabriel; MODROIU, Adriana. Chiral switch: Between therapeutical benefit and marketing strategy. **Pharmaceuticals**, v. 15, n. 2, p. 240, 2022.

[35] BURKE, D.; HENDERSON, D. J. Chirality: a blueprint for the future. **British Journal of Anaesthesia**, v. 88, n. 4, p. 563-576, 2002.

[36] HOYOS, Pilar; PACE, Vittorio; ALCÁNTARA, Andrés R. Chiral building blocks for drugs synthesis via biotransformations. **Asymmetric Synthesis of Drugs and Natural Products; Nag, A., Ed**, p. 346-448, 2018.

[37] OU, Ling et al. Chemoenzymatic deracemization of chiral secondary alcohols: process optimization for production of (R)-1-indanol and (R)-1-phenylethanol. **Organic Process Research & Development**, v. 12, n. 2, p. 192-195, 2008.

[38] BOUZEMI, Nassima; ARIBI-ZOUIOUECHE, Louisa; FIAUD, Jean-Claude. Combined lipase-catalyzed resolution/Mitsunobu esterification for the production of enantiomerically enriched arylalkyl carbinols. **Tetrahedron: Asymmetry**, v. 17, n. 5, p. 797-800, 2006.

[39] LEE, Sang Hwi et al. Stereoselective amination of chiral benzylic ethers using chlorosulfonyl isocyanate: total synthesis of (+)-sertraline. **The Journal of Organic Chemistry**, v. 76, n. 24, p. 10011-10019, 2011.

[40] DE SOUSA FONSECA, Thiago et al. Chemoenzymatic synthesis of rasagiline mesylate using lipases. **Applied Catalysis A: General**, v. 492, p. 76-82, 2015.

[41] FERNANDEZ, Marcos et al. An effective novel delivery strategy of rasagiline for Parkinson's disease. **International journal of pharmaceutics**, v. 419, n. 1-2, p. 271-280, 2011.

[42] HOY, Sheridan M.; KEATING, Gillian M. Rasagiline: a review of its use in the treatment of idiopathic Parkinson's disease. **Drugs**, v. 72, n. 5, p. 643-669, 2012.

[43] CHAUDHURI, K. Ray; HEALY, Daniel G.; SCHAPIRA, Anthony HV. Non-motor symptoms of Parkinson's disease: diagnosis and management. **The Lancet Neurology**, v. 5, n. 3, p. 235-245, 2006.

[44] PIENAAR, Ilse S.; CHINNERY, Patrick F. Existing and emerging mitochondrial-targeting therapies for altering Parkinson's disease severity and progression. **Pharmacology & therapeutics**, v. 137, n. 1, p. 1-21, 2013.

[45] SHULMAN, L. M. et al. Non-recognition of depression and other non-motor symptoms in Parkinson's disease. **Parkinsonism & related disorders**, v. 8, n. 3, p. 193-197, 2002.

[46] RODRÍGUEZ-VIOLANTE, Mayela et al. Who can diagnose Parkinson's disease first? Role of pre-motor symptoms. **Archives of medical research**, v. 48, n. 3, p. 221-227, 2017.

[47] RABEY, J. M. et al. Rasagiline mesylate, a new MAO-B inhibitor for the treatment of Parkinson's disease: a double-blind study as adjunctive therapy to levodopa. **Clinical neuropharmacology**, v. 23, n. 6, p. 324-330, 2000.

[48] "3rd BBBB-Bosphorus International Conference on Pharmaceutical Sciences," *Eur. J. Pharm.Sci.*, vol. 38, no. 1, Supplement, pp. S1–S220, 2009.

[49] AHMED, Marwa; KELLY, Tamsin; GHANEM, Ashraf. Applications of enzymatic and non-enzymatic methods to access enantiomerically pure compounds using kinetic resolution and racemisation. **Tetrahedron**, v. 68, n. 34, p. 6781-6802, 2012.

[50] H. Caner, E. Groner, L. Levy, and I. Agranat, "Trends in the development of chiral drugs,"*Drug Discov. Today*, vol. 9, no. 3, pp. 105–110, 2004.

[51] RADZICKA, Anna; WOLFENDEN, Richard. A proficient enzyme. **Science**, v. 267, n. 5194, p. 90-93, 1995.

[52] WISNIAK, Jaime. The history of catalysis. From the beginning to Nobel prizes. **Educación química**, v. 21, n. 1, p. 60-69, 2010.

[53] ZECCHINA, Adriano; CALIFANO, Salvatore. **The development of catalysis: a history of key processes and personas in catalytic science and technology**. John Wiley & Sons, 2017.

[54] TIPTON, Keith; BOYCE, Sinéad. History of the enzyme nomenclature system. **Bioinformatics**, v. 16, n. 1, p. 34-40, 2000.

[55] BARNETT, James A. A history of research on yeasts 2: Louis Pasteur and his contemporaries, 1850–1880. **Yeast**, v. 16, n. 8, p. 755-771, 2000.

[56] LERESCHE, James E.; MEYER, Hans-Peter. Chemocatalysis and biocatalysis (biotransformation): some thoughts of a chemist and of a biotechnologist. **Organic process research & development**, v. 10, n. 3, p. 572-580, 2006.

[57] HOROWITZ, Benjamin. What are Enzymes?. **The Scientific Monthly**, v. 6, n. 3, p. 253-259, 1918.

[58] DALLA-VECCHIA, Roberto; NASCIMENTO, Maria da Graça; SOLDI, Valdir. Aplicações sintéticas de lipases imobilizadas em polímeros. **Química Nova**, v. 27, p. 623-630, 2004.

[59] PÀMIES, Oscar; BÄCKVALL, Jan-E. Chemoenzymatic dynamic kinetic resolution. **TRENDS in Biotechnology**, v. 22, n. 3, p. 130-135, 2004.

[60] PELLISSIER, Helene. Catalytic non-enzymatic kinetic resolution. **Advanced Synthesis & Catalysis**, v. 353, n. 10, p. 1613-1666, 2011.

[61] SHARPLESS, K. Barry. On the Mechanism of Asymmetric Epoxidation with Titanium—Tartrate Catalysts. **Asymmetric Synthesis: Volume 5**, v. 5, p. 247, 2012.

[62] MOORE, Walter J. Físico-Química (Tradução da 4a. edição americana). **Editora Edgard**, 1976.

[63] NAKAMURA, Kaoru; MATSUDA, Tomoko. Enzymatic kinetic resolution. **Enantiomer Separation: Fundamentals and Practical Methods**, p. 231-266, 2004.

[64] SUGAI, Takeshi; HIGASHIBAYASHI, Shuhei; HANAYA, Kengo. Recent examples of the use of biocatalysts with high accessibility and availability in natural product synthesis. **Tetrahedron**, v. 74, n. 27, p. 3469-3487, 2018.

[65] GHANEM, Ashraf. Trends in lipase-catalyzed asymmetric access to enantiomerically pure/enriched compounds. **Tetrahedron**, v. 63, n. 8, p. 1721-1754, 2007.

[66] BORNSCHEUER, Uwe T. Methods to increase enantioselectivity of lipases and esterases. **Current opinion in biotechnology**, v. 13, n. 6, p. 543-547, 2002.

[67] VERDASCO-MARTÍN, Carlos M. et al. Effect of chemical modification of Novozym 435 on its performance in the alcoholysis of camelina oil. **Biochemical Engineering Journal**, v. 111, p. 75-86, 2016.

[68] MANOEL, Evelin A. et al. Immobilization of lipases on hydrophobic supports involves the open form of the enzyme. **Enzyme and Microbial Technology**, v. 71, p. 53-57, 2015.

[69] LOZANO, Pedro. Enzymes in neoteric solvents: From one-phase to multiphase systems. **Green Chemistry**, v. 12, n. 4, p. 555-569, 2010.

[70] MANOEL, Evelin A. et al. Accurel MP 1000 as a support for the immobilization of lipase from Burkholderia cepacia: application to the kinetic resolution of myo-inositol derivatives. **Process Biochemistry**, v. 50, n. 10, p. 1557-1564, 2015.

[71] MONIRUZZAMAN, Muhammad; KAMIYA, Noriho; GOTO, Masahiro. Activation and stabilization of enzymes in ionic liquids. **Organic & biomolecular chemistry**, v. 8, n. 13, p. 2887-2899, 2010.

[72] BRADY, Leo et al. A serine protease triad forms the catalytic centre of a triacylglycerol lipase. **Nature**, v. 343, n. 6260, p. 767-770, 1990.

[73] CARTER, Paul; WELLS, James A. Dissecting the catalytic triad of a serine protease. **Nature**, v. 332, n. 6164, p. 564-568, 1988.

[74] KAZLAUSKAS, Romas J. et al. A Rule To Predict Wbicb Enantiomer of a Secondary A1cobol Reacts Faster in Reactions Catalyzed by Cbolesterol Esterase, Lipase from Pseudomonas cepacia, and Lipase from Candida rugosa. l. **NOTE TO USERS**, p. 86.

[75] GOTOR-FERNÁNDEZ, Vicente; BRIEVA, Rosario; GOTOR, Vicente. Lipases: Useful biocatalysts for the preparation of pharmaceuticals. **Journal of Molecular Catalysis B: Enzymatic**, v. 40, n. 3-4, p. 111-120, 2006.

[76] CHEN, Yi-Yu et al. Covalent immobilization of Bacillus licheniformis γ-glutamyl transpeptidase on aldehyde-functionalized magnetic nanoparticles. **International Journal of Molecular Sciences**, v. 14, n. 3, p. 4613-4628, 2013.

[77] DICOSIMO, Robert et al. Industrial use of immobilized enzymes. **Chemical Society Reviews**, v. 42, n. 15, p. 6437-6474, 2013.

[78] DE SOUSA FONSECA, Thiago et al. Chemoenzymatic synthesis of rasagiline mesylate using lipases. **Applied Catalysis A: General**, v. 492, p. 76-82, 2015.

[79] DE SOUZA, Ticiane C. et al. Cashew apple bagasse as a support for the immobilization of lipase B from Candida antarctica: Application to the chemoenzymatic production of (R)-Indanol. **Journal of Molecular Catalysis B: Enzymatic**, v. 130, p. 58-69, 2016.

[80] KEFENI, Kebede K.; MAMBA, Bhekie B.; MSAGATI, Titus AM. Application of spinel ferrite nanoparticles in water and wastewater treatment: a review. **Separation and Purification Technology**, v. 188, p. 399-422, 2017.

[81] HOLZWARTH, Uwe; GIBSON, Neil. The Scherrer equation versus the'Debye-Scherrer equation'. **Nature nanotechnology**, v. 6, n. 9, p. 534-534, 2011.

[82] E. Gupta and M. R. R. Yadav, “Hardware Implementation of a Vibrating Sample Magnetometer Circuitry,” 2014.

[83] GALVÃO, Wesley dos Santos et al. Cubic superparamagnetic nanoparticles of NiFe 2 O 4 via fast microwave heating. **Journal of nanoparticle research**, v. 16, p. 1-10, 2014.

[84] WEINSTEIN, Jason S. et al. Superparamagnetic iron oxide nanoparticles: diagnostic magnetic resonance imaging and potential therapeutic applications in neurooncology and central nervous system inflammatory pathologies, a review. **Journal of Cerebral Blood Flow & Metabolism**, v. 30, n. 1, p. 15-35, 2010.

[85] OBERDICK, Samuel D. et al. Spin canting across core/shell Fe3O4/MnxFe3− xO4 nanoparticles. **Scientific Reports**, v. 8, n. 1, p. 3425, 2018.

[86] UCHINO, Kenji. The development of piezoelectric materials and the new perspective. In: **Advanced Piezoelectric Materials**. Woodhead Publishing, 2017. p. 1-92.

[87] SUSLICK, Kenneth S. The chemical effects of ultrasound. **Scientific American**, v. 260, n. 2, p. 80-87, 1989.

[88] ZHANG, Li-Shuang et al. Improvement of the stabilization and activity of protocatechuate 3, 4-dioxygenase isolated from Rhizobium sp. LMB-1 and immobilized on Fe_3O_4 nanoparticles. **Applied biochemistry and biotechnology**, v. 183, p. 1035-1048, 2017.

[89] BHATNAGAR, Tej et al. Lipolytic activity from Halobacteria: screening and hydrolase production. **FEMS Microbiology Letters**, v. 248, n. 2, p. 133-140, 2005.

[90] RIOS, Nathalia S. et al. Strategies of covalent immobilization of a recombinant Candida antarctica lipase B on pore-expanded SBA-15 and its application in the kinetic resolution of (R, S)-Phenylethyl acetate. **Journal of Molecular Catalysis B: Enzymatic**, v. 133, p. 246-258, 2016.

[91] CHENG, Yongfeng et al. Rapid method for protein quantitation by Bradford assay after elimination of the interference of polysorbate 80. **Analytical biochemistry**, v. 494, p. 37-39, 2016.

[92] SADANA, Ajit; HENLEY, James P. Analysis of Enzyme Deactivations by a Series-Type Mechanism: Influence of Modification on the Activity and Stability of Enzymes. **Annals of the New York Academy of Sciences**, v. 501, n. 1, p. 73-79, 1987.

[93] RIETVELD, Hugo M. A profile refinement method for nuclear and magnetic structures. **Applied Crystallography**, v. 2, n. 2, p. 65-71, 1969.

[94] SAWABE, Takashi; YANO, Toyohiko. Neutron irradiation effect on site distribution of cations in non-stoichiometric magnesium aluminate spinel. **Journal of nuclear materials**, v. 373, n. 1-3, p. 328-334, 2008.

[95] SANTOS, Carla OP. Aplicações do Método de Rietveld. **Instituto de Química, Unesp**, 2006.

[96] PARK, Jongnam et al. Ultra-large-scale syntheses of monodisperse nanocrystals. **Nature materials**, v. 3, n. 12, p. 891-895, 2004.

[97] MENDES, Adriano A. et al. Multipoint covalent immobilization of lipase on chitosan hybrid hydrogels: influence of the polyelectrolyte complex type and chemical modification on the catalytic properties of the biocatalysts. **Journal of Industrial Microbiology and Biotechnology**, v. 38, n. 8, p. 1055-1066, 2011.

[98] DOS SANTOS, Jose CS et al. Evaluation of divinylsulfone activated agarose to immobilize lipases and to tune their catalytic properties. **Process Biochemistry**, v. 50, n. 6, p. 918-927, 2015.

[99] SANCHEZ, Alfredo et al. Inactivation of immobilized trypsin under dissimilar conditions produces trypsin molecules with different structures. **RSC advances**, v. 6, n. 33, p. 27329-27334, 2016.

[100] KIM, Mahn-Joo et al. Dynamic kinetic resolution of secondary alcohols by enzyme–metal combinations in ionic liquid. **Green chemistry**, v. 6, n. 9, p. 471-474, 2004.

[101] DE SOUSA FONSECA, Thiago et al. Chemoenzymatic synthesis of rasagiline mesylate using lipases. **Applied Catalysis A: General**, v. 492, p. 76-82, 2015.

[102] XIE, Wenlei; MA, Ning. Immobilized lipase on Fe3O4 nanoparticles as biocatalyst for biodiesel production. **Energy & Fuels**, v. 23, n. 3, p. 1347-1353, 2009.

[103] VISWANADH, N. et al. Chiral aziridine ring opening: facile synthesis of (R)-mexiletine and (R)-phenoxybenzamine hydrochloride. **Tetrahedron letters**, v. 56, n. 38, p. 5269-5271, 2015.

[104] BEZERRA, Rayanne M. et al. Design of a lipase-nano particle biocatalysts and its use in the kinetic resolution of medicament precursors. **Biochemical Engineering Journal**, v. 125, p. 104-115, 2017.

[105] DE MOURA, Carla Verônica Rodarte et al. Heterogeneous catalysis of babassu oil monitored by thermogravimetric analysis. **Energy & fuels**, v. 24, n. 12, p. 6527-6532, 2010.

[106] KOLEN'KO, Yury V. et al. High-temperature magnetism as a probe for structural and compositional uniformity in ligand-capped magnetite nanoparticles. **The Journal of Physical Chemistry C**, v. 118, n. 48, p. 28322-28329, 2014.

[107] KEASBERRY, Natasha A. et al. Tuning the relaxation rates of dual-mode T 1/T 2 nanoparticle contrast agents: a study into the ideal system. **Nanoscale**, v. 7, n. 38, p. 16119-16128, 2015.

[108] KUBICKOVA, S. et al. Structural disorder versus spin canting in monodisperse maghemite nanocrystals. **Applied Physics Letters**, v. 104, n. 22, 2014.

[109] WU, Shen et al. Fe3O4 magnetic nanoparticles synthesis from tailings by ultrasonic chemical co-precipitation. **Materials Letters**, v. 65, n. 12, p. 1882-1884, 2011.

[110] SIEGEL, Rebecca L.; MILLER, Kimberly D.; JEMAL, Ahmedin. Cancer statistics, 2018. CA: a cancer journal for clinicians, v. 68, n. 1, p. 7-30, 2018.

[111] ULBRICH, Karel et al. Targeted drug delivery with polymers and magnetic nanoparticles: covalent and noncovalent approaches, release control, and clinical studies. **Chemical reviews**, v. 116, n. 9, p. 5338-5431, 2016.

[112] LOWENFELS, Albert B.; MAISONNEUVE, Patrick. Chronic pancreatitis: risk factors in cancer. **The Pancreas: An Integrated Textbook of Basic Science, Medicine, and Surgery**, p. 417-420, 2018.

[113] PAZ, Márcia Fernanda Correia Jardim et al. Correlations between risk factors for breast cancer and genetic instability in cancer patients—A clinical perspective study. **Frontiers in genetics**, v. 8, p. 236, 2018.

[114] MALIK, Saima Shakil et al. Risk factors for prostate cancer: A multifactorial case-control study. **Current problems in cancer**, v. 42, n. 3, p. 337-343, 2018.

[115] BATOULI, Ali et al. The global cancer divide: Relationships between national healthcare resources and cancer outcomes in high-income vs. middle-and low-income countries. **Journal of epidemiology and global health**, v. 4, n. 2, p. 115-124, 2014.

[116] D'ANDREA, Anthony P. et al. Operations for Rectal Cancer: Low Anterior Resection—Open, Laparoscopic or Robotic, taTME, Coloanal Anastomosis. **Shackelford's Surgery of the Alimentary Tract, 2 Volume Set**, p. 2005-2034, 2019.

[117] ALBERT, Matthew R.; PLUMMER, Joseph M.; LEE, Lawrence L. Transanal Approaches to Early Rectal Cancers: Transanal Minimally Invasive Surgery. In: **Shackelford's Surgery of the Alimentary Tract, 2 Volume Set**. Elsevier, 2019. p. 1992-1996.

[118] POSSANZINI, Marco; GRECO, Carlo. Stereotactic radiotherapy in metastatic breast cancer. **The Breast**, v. 41, p. 57-66, 2018.

[119] FELIU, Jaime et al. Can we avoid the toxicity of chemotherapy in elderly cancer patients?. **Critical Reviews in Oncology/Hematology**, v. 131, p. 16-23, 2018.

[120] DISAIA, Philip J. et al. **Clinical gynecologic oncology**. Elsevier Health Sciences, 2017.

[121] ABSHIRE, Dorothy; LANG, Matthew K. The evolution of radiation therapy in treating cancer. In: **Seminars in oncology nursing**. WB Saunders, 2018. p. 151-157.

[122] TURCI, Roberta et al. Biological and environmental monitoring of hospital personnel exposed to antineoplastic agents: a review of analytical methods. **Journal of Chromatography B**, v. 789, n. 2, p. 169-209, 2003.

[123] CHEN, Yu-Li; CHANG, Ming-Cheng; CHENG, Wen-Fang. Metronomic chemotherapy and immunotherapy in cancer treatment. **Cancer letters**, v. 400, p. 282-292, 2017.

[124] FAHMY, Tarek M. et al. Targeted for drug delivery. **Materials Today**, v. 8, n. 8, p. 18-26, 2005.

[125] SASTRY, Srikonda Venkateswara; NYSHADHAM, Janaki Ram; FIX, Joseph A. Recent technological advances in oral drug delivery–a review. **Pharmaceutical science & technology today**, v. 3, n. 4, p. 138-145, 2000.

[126] SHOJAEI, Amir H. et al. Buccal mucosa as a route for systemic drug delivery: a review. **J Pharm Pharm Sci**, v. 1, n. 1, p. 15-30, 1998.

[127] BERMEJO, Marival et al. Oral controlled release dosage forms: dissolution versus diffusion. **Expert Opinion on Drug Delivery**, v. 17, n. 6, p. 791-803, 2020.

[128] JIA, Yanhui et al. Co-encapsulation of magnetic Fe3O4 nanoparticles and doxorubicin into biodegradable PLGA nanocarriers for intratumoral drug delivery. **International journal of nanomedicine**, p. 1697-1708, 2012.

[129] DU, Xiyou et al. Current development in the formulations of non-injection administration of paclitaxel. **International journal of pharmaceutics**, v. 542, n. 1-2, p. 242-252, 2018.

[130] DOANE, Tennyson L.; BURDA, Clemens. The unique role of nanoparticles in nanomedicine: imaging, drug delivery and therapy. **Chemical Society Reviews**, v. 41, n. 7, p. 2885-2911, 2012.

[131] GAO, Wei; WANG, Joseph. Synthetic micro/nanomotors in drug delivery. **Nanoscale**, v. 6, n. 18, p. 10486-10494, 2014.

[132] ELKHODIRY, Mohamed A. et al. Synergistic nanomedicine: passive, active, and ultrasound-triggered drug delivery in cancer treatment. **Journal of nanoscience and nanotechnology**, v. 16, n. 1, p. 1-18, 2016.

[133] STREBHARDT, Klaus; ULLRICH, Axel. Paul Ehrlich's magic bullet concept: 100 years of progress. **Nature Reviews Cancer**, v. 8, n. 6, p. 473-480, 2008.

[134] CHEN, Hongmin et al. Nanoparticles for improving cancer diagnosis. **Materials Science and Engineering: R: Reports**, v. 74, n. 3, p. 35-69, 2013.

[135] KAO, Chia-Tze et al. The cytotoxicity of orthodontic metal bracket immersion L. M. de Menezes, M. P. M. Freitas, and T. S. Gonçalves, "Biocompatibility of orthodontic materials: myth or reality?," *Rev. Dent. Press Ortod. e Ortop. Facial*, vol. 14, no. 2, pp. 144– 157, 2009.

[136] LUCEY, Brendan P.; NELSON-REES, Walter A.; HUTCHINS, Grover M. Henrietta Lacks, HeLa cells, and cell culture contamination. **Archives of pathology & laboratory medicine**, v. 133, n. 9, p. 1463-1467, 2009.

[137] LANDFESTER, Katharina. Miniemulsion polymerization and the structure of polymer and hybrid nanoparticles. **Angewandte Chemie International Edition**, v. 48, n. 25, p. 4488-4507, 2009.

[138] SALATIN, Sara; YARI KHOSROUSHAHI, Ahmad. Overviews on the cellular uptake mechanism of polysaccharide colloidal nanoparticles. **Journal of cellular and molecular medicine**, v. 21, n. 9, p. 1668-1686, 2017.

[139] RÖSLER, Annette; VANDERMEULEN, Guido WM; KLOK, Harm-Anton. Advanced drug delivery devices via self-assembly of amphiphilic block copolymers. **Advanced drug delivery reviews**, v. 64, p. 270-279, 2012.

[140] WONG, Chun Y.; AL-SALAMI, Hani; DASS, Crispin R. Recent advancements in oral administration of insulin-loaded liposomal drug delivery systems for diabetes mellitus. **International journal of pharmaceutics**, v. 549, n. 1-2, p. 201-217, 2018.

[141] SUFFREDINI, G.; EAST, J. E.; LEVY, Lucien M. New applications of nanotechnology for neuroimaging. **American journal of neuroradiology**, v. 35, n. 7, p. 1246-1253, 2014.

[142] LOOS, Cornelia et al. Functionalized polystyrene nanoparticles as a platform for studying bio–nano interactions. **Beilstein journal of nanotechnology**, v. 5, n. 1, p. 2403-2412, 2014.

[143] PARK, Kinam. Controlled drug delivery systems: past forward and future back. **Journal of Controlled Release**, v. 190, p. 3-8, 2014.

[144] WEISS, Clemens K.; LANDFESTER, Katharina. Miniemulsion polymerization as a means to encapsulate organic and inorganic materials. **Hybrid Latex Particles: Preparation with (Mini) emulsion Polymerization**, p. 185-236, 2010.

[145] LANDFESTER, Katharina. Encapsulation through (mini) emulsion polymerization. **Functional coatings: by polymer microencapsulation**, p. 29-66, 2006.

[146] LANDFESTER, Katharina. Miniemulsions for nanoparticle synthesis. **Colloid chemistry II**, p. 75-123, 2003.

[147] BIBETTE, Jerome et al. Emulsion science: Basic principles. An overview. 2003.

[148] RAVIKUMAR, Madhusudan et al. Ultrasonication: An advanced technology for food preservation. **International Journal of Pure & Applied Bioscience**, v. 5, n. 6, p. 363-371, 2017.

[149] MEROUANI, Slimane et al. Theoretical estimation of the temperature and pressure within collapsing acoustical bubbles. **Ultrasonics sonochemistry**, v. 21, n. 1, p. 53-59, 2014.

[150] ZHOU, Xiaojing; BELCHER, Warwick; DASTOOR, Paul. Solar paint: From synthesis to printing. **Polymers**, v. 6, n. 11, p. 2832-2844, 2014.

[151] CHEN, Hongmin et al. Nanoparticles for improving cancer diagnosis. **Materials Science and Engineering: R: Reports**, v. 74, n. 3, p. 35-69, 2013.

[152] ULBRICH, Karel et al. Targeted drug delivery with polymers and magnetic nanoparticles: covalent and noncovalent approaches, release control, and clinical studies. **Chemical reviews**, v. 116, n. 9, p. 5338-5431, 2016.

[153] LINHARES, Angélica Ozório; CESAR, Juraci Almeida. Folic acid supplementation among pregnant women in Southern Brazil: Prevalence and factors associated. **Ciência & Saúde Coletiva**, v. 22, p. 535-542, 2017.

[154] KR, KALLI. Folate receptor alpha as a tumor target in epithelial ovarian cancer. **Gynecol. Oncol**, v. 108, p. 619-626, 2008.

[155] SUDIMACK, Jennifer; LEE, Robert J. Targeted drug delivery via the folate receptor. **Advanced drug delivery reviews**, v. 41, n. 2, p. 147-162, 2000.

[156] ROGER, Emilie et al. Folic acid functionalized nanoparticles for enhanced oral drug delivery. **Molecular pharmaceutics**, v. 9, n. 7, p. 2103-2110, 2012.

[157] GABIZON, Alberto et al. Tumor cell targeting of liposome-entrapped drugs with phospholipid-anchored folic acid–PEG conjugates. **Advanced drug delivery reviews**, v. 56, n. 8, p. 1177-1192, 2004.

[158] AKASH, Muhammad Sajid Hamid; REHMAN, Kanwal. Recent progress in biomedical applications of Pluronic (PF127): Pharmaceutical perspectives. **Journal of Controlled Release**, v. 209, p. 120-138, 2015.

[159] TUDISCO, C. et al. Multifunctional magnetic nanoparticles for enhanced intracellular drug transport. **Journal of Materials Chemistry B**, v. 3, n. 20, p. 4134-4145, 2015.

[160] ESCORCIA, Freddy E. et al. Targeted nanomaterials for radiotherapy. **Nanomedicine**, v. 2, n. 6, p. 805-815, 2007.

[161] CHEN, Guo-Jing et al. Angiopep-pluronic F127-conjugated superparamagnetic iron oxide nanoparticles as nanotheranostic agents for BBB targeting. **Journal of Materials Chemistry B**, v. 2, n. 34, p. 5666-5675, 2014.

[162] WANG, Zhe et al. Mechanisms of drug release in pH-sensitive micelles for tumour targeted drug delivery system: A review. **International journal of pharmaceutics**, v. 535, n. 1-2, p. 253-260, 2018.

[163] BAHRAMI, Behdokht et al. Nanoparticles and targeted drug delivery in cancer therapy. **Immunology letters**, v. 190, p. 64-83, 2017.

[164] HUANG, Shih-Jer et al. Folate-mediated chondroitin sulfate-Pluronic® 127 nanogels as a drug carrier. **European Journal of Pharmaceutical Sciences**, v. 38, n. 1, p. 64-73, 2009.

[165] GRINDEL, J. Michael et al. Distribution, metabolism, and excretion of a novel surface-active agent, purified poloxamer 188, in rats, dogs, and humans. **Journal of pharmaceutical sciences**, v. 91, n. 9, p. 1936-1947, 2002.

[166] LOW, Philip S.; HENNE, Walter A.; DOORNEWEERD, Derek D. Discovery and development of folic-acid-based receptor targeting for imaging and therapy of cancer and inflammatory diseases. **Accounts of chemical research**, v. 41, n. 1, p. 120-129, 2008.

[167] ZHANG, Wei et al. Multifunctional Pluronic P123/F127 mixed polymeric micelles loaded with paclitaxel for the treatment of multidrug resistant tumors. **Biomaterials**, v. 32, n. 11, p. 2894-2906, 2011.

[168] DARR, Jawwad A. et al. Continuous hydrothermal synthesis of inorganic nanoparticles: applications and future directions. **Chemical reviews**, v. 117, n. 17, p. 11125-11238, 2017.

[169] NEISES, Bernhard; STEGLICH, Wolfgang. Simple method for the esterification of carboxylic acids. **Angewandte Chemie International Edition in English**, v. 17, n. 7, p. 522-524, 1978.

[170] TYAGI, Amit; PENZKOFER, Alfons. Fluorescence spectroscopic behaviour of folic acid. **Chemical physics**, v. 367, n. 2-3, p. 83-92, 2010.

[171] BERMAN, Jules. Modern classification of neoplasms: reconciling differences between morphologic and molecular approaches. **BMC cancer**, v. 5, p. 1-12, 2005.

[172] FREIRE, Rafael Melo et al. Nanocrystal growth, magnetic and electrochemical properties of NiZn ferrite. **Journal of Alloys and Compounds**, v. 738, p. 206-217, 2018.

[173] GALVÃO, Wesley S. et al. Super-paramagnetic nanoparticles with spinel structure: a review of synthesis and biomedical applications. solid state phenomena, v. 241, p. 139-176, 2016.